ELECTROMAGNETIC RADIATION FROM PARTONS AND HADRONS

By

Payal Mohanty

Enrollment No. PHYS04200704006

Variable Energy Cyclotron Centre, Kolkata

A thesis submitted to

The Board of Studies in Physical Sciences

In partial fulfillment of requirements for the Degree of

DOCTOR OF PHILOSOPHY

of

HOMI BHABHA NATIONAL INSTITUTE

March, 2012

Homi Bhabha National Institute

Recommendation of the Viva Voce Board

As members of the Viva Voce Board, we certify that we have read the dissertation prepared by **Payal Mohanty** entitled **Electromagnetic radiation from partons and hadrons** and recommend that it may be accepted as fulfilling the dissertation requirement for the degree of Doctor of Philosophy.

....Date: 27-11-12

Chairman- Prof. A. K. Chaudhuri

....Date: 27-11-2012

Convener- Prof. J. Alam

....Date: 27. 11. 2012

Member 1- Prof. S. Sarkar

....Date: 27. 11. 2012

Member 2- Prof. R. Roy

....Date:

Member 3 (External Examiner)- Prof. A. Mishra Amruta Mishra 27-11-12

Finally approval and acceptance of this dissertation is contingent upon the candidate's submission of the final copies of the dissertation to HBNI.

I hereby certify that I have read this dissertation prepared under my direction and recommend that it may be accepted as fulfilling the dissertation requirement.

Date: 27-11-2012

Place: VECC/Kolkata

STATEMENT BY AUTHOR

Payal Mohanty

DECLARATION

I, hereby declare that the investigation presented in the thesis has been carried out by me. The work is original and has not been submitted earlier as a whole or in part for a degree/diploma at this or any other Institution/University.

Payal Mohanty

Dedicated to my dear parents

Braja Kishore Mohanty

&

Pravati Mohanty

ACKNOWLEDGEMENTS

This PhD thesis is the outcome of four years of continuous hard work possible due to constant guidance, supervision, inspiration and encouragement from my supervisors, Prof. Jan-e Alam, Variable Energy Cyclotron Centre, Kolkata, India. So first of all, I would like to express my utmost gratitude to him. I would also like to thank Dr. Sourav Sarkar, Dr. Bedangdas Mohanty and Jajati K Nayak for their extensive advice, discussion, help and support which has been effectively useful in clearing up my concepts and ideas in wide range of aspects and help in enhancing my depth of understanding. I am really fortunate to get the best opportunity to work with such talented persons in such a challenging field surrounded by a good academic environment. I also take this opportunity to thank my colleagues, Santosh K Das, Sabyasachi Ghosh, Victor Roy and Haridas Pai with whom I have enjoyed working together over the years. A special thanks for my seniors, friends and juniors for their cooperation and also support. All those discussion we have done in the blackboard helped me a lot in clearing my understanding. They no longer have to ask : *is it complete?* During all the time I spent at VECC, I received support from all of them both on scientific and personal level.

And last but not the least, my thanks go to family and friends who are there always with me giving the strength to complete this thesis. Especially, I thank my husband, Dilip who is also continuing his PhD simultaneously with me. His continuous and unwavering support, and encouragement helped me a lot in the completion of the thesis. It is really wonderful to share my good experiences with him through the challenges. I would also like to mention that, without the love, consolations and blessing from my parents over phone during the time I am away from home and enthusiasm from Prachi, my younger sister, at the time of less patient, it is not possible to write forward.

This PhD thesis is supported by DAE-BRNS project Sanction No. 2005/21/5-BRNS/2455. I am also thankful to the research facilities and the financial support provided by Variable Energy Cyclotron Centre, DAE, Government of India.

Payal Mohanty

SYNOPSIS

According to *Quantum Chromodynamics (QCD)*, colored *quarks* and *anti-quarks* are the fundamental particle which always remain confined within a colorless hadrons via strong force mediated by another colored object called, *gluon*. Heavy ion collision (HIC) at relativistic energies provides an opportunity to study QCD at finite temperature and densities. Calculations based on Lattice QCD predict at high temperatures and/or densities the hadronic matter melts down to a state of *quarks*, *anti-quarks* and *gluons*. Such a deconfined state of thermal system is called *Quark Gluon Plasma (QGP)*.

Relativistic Heavy Ion Collider (RHIC) at BNL and Large Hadron Collider (LHC) at CERN are two experimental facilities where QGP may be created for a short duration of time. Collision between nuclei at ultra relativistic energies produce charged particles either in hadronic or partonic state depending on the collision energy. Interaction among these charged particle produce electromagnetic (EM) radiation - real and virtual photons (dileptons). *Electromagnetic (EM) probes - dileptons and photons* - are considered to be very efficient tool for detection of QGP, because of their nature of interaction - they do not suffer final state re-scattering, hence provide clean signature of each stages of the evolving fireball.

The hot and dense matter expected to be formed in the partonic phase after ultra-relativistic heavy ion collisions dynamically evolve in space and time due to high internal pressure. Consequently, the system cools and reverts to the hadronic matter from the partonic phase. Just after the formation, the entire energy of the system is thermal in nature and with progress of time some part of the thermal energy gets converted to the collective (flow) energy. In other words, during the expansion stage the total energy of the system is shared by the thermal as well as the collective degrees of freedom. The collective motion is sensitive to the Equation of State (EoS) of the system, hence estimation of collectivity will shed light on the nature of the system.

The collective parameters extracted using hadronic spectra have hardly any information about the interior of the matter, as the parameters of collectivity extracted from the hadronic spectra are limited to the evolution stage where the collectivity ceases to exist. In contrast to hadrons, EM probes are produced and emitted from each space time points. Therefore, estimating flow from the EM probes will shed light on the space-time evolution of the collectivity in the system. We study the evolution of collective motion, both radial and elliptic flow of the system formed in HIC at relativistic energies by using photons and lepton pairs.

The transverse momentum (p_T) distribution of photons reflect the temperature of the source as their productions from a thermal source depend on the temperature (T) of the bath through the thermal phase space factors of the participants of the reaction that produces the photon. However, the thermal phase space factor may be changed by several factors - *e.g.* the transverse kick due to flow received by low p_T photons from the low temperature hadronic phase will mingle with the high p_T photons from the partonic phase, making the task of detecting and characterizing QGP more difficult. For dilepton the situation is, however, different because in this case we have two kinematic variables - out of these two, the p_T spectra of lepton pairs is affected but the p_T integrated invariant mass (M) spectra is unaltered by the flow. From p_T integrated M distribution of lepton pairs, we infer that lepton pairs with M ($> m_\phi$) originate from the early time, providing information of partonic phase and pairs with $M < m_\rho$ are chiefly produced at late times giving information of the hadronic phase. Therefore, the study of the p_T integrated M distribution of lepton pairs can act as a *chronometer* of the heavy ion collisions. On the other hand, the p_T distribution of dilepton for different M windows can be used as *flow meter*, and a judicious selection of p_T and M windows will be very useful to characterize the QGP and the hadronic phases separately.

Radial Flow

(a) Ratio of photon to dilepton spectra: The photon and dilepton spectra produced in RHIC at relativistic energies have been studied. The initial condition have been constrained to reproduce the available experimental data. The calculations of spectra from thermal sources depend on the parameters like initial temperature (T_i), thermalization time (τ_i), chemical freeze-out temperature (T_{ch}), kinetic freeze-out temperature (T_f), etc., which are not known unambiguously. To minimize the dependence of thermal sources on these parameters, the importance of the ratio of the transverse momentum spectra of photons to dileptons has been emphasized to partially overcome some of these uncertainties. It may be mentioned here that in the limit of M $\rightarrow 0$, the lepton pairs (virtual photons) emerge as real photons. Therefore, the evaluation of the ratio of the p_T spectra of photons to dileptons for various invariant mass bins along with a judicious choice of the p_T and M windows will be very useful to extract the properties of QGP as well as that of the hadronic phase. We have extracted the radial flow from the ratio of photon to dilepton spectra. The variation of average radial flow velocity with average temperature of the system and $\langle M \rangle$ has been studied for different collision energies. Within the ambit of the present analysis it is shown that the variation of the radial velocity with invariant mass is indicative of a phase transition from the initially produced partons to hadrons.

(b) Correlation Function of lepton pairs : The correlation functions of lepton pairs have also been evaluated with the same inputs which reproduce the experimental data from HIC. It has been shown that the HBT radii extracted from the correlation functions of lepton pairs can be used to estimate the temporal and spatial dimension of the system. The M dependence of the HBT radii could be used to characterize source properties at various instances of evolution. In one of the first such calculations involving dileptons, we show that the mass dependence of radii extracted from the dilepton interferometry provide access to the development of collective flow with time.

Elliptic Flow

We study the variation of elliptic flow of thermal dileptons with transverse momentum and invariant mass of the pairs for Pb+Pb collisions at $\sqrt{s_{NN}} = 2.76$ TeV. The dilepton productions from quark gluon plasma (QGP) and hot hadrons have been considered including the spectral change of light vector mesons in the thermal bath. The space time evolution has been carried out within the framework of 2+1 dimensional ideal hydrodynamics with lattice+hadron resonance gas equation of state. We find that a judicious selection of invariant mass (M) window can be used to extract the collective properties of quark matter, hadronic matter and also get a distinct signature of medium effects on vector mesons. We observe a reduction of elliptic flow (v_2) for M beyond ϕ mass, which if observed experimentally would give the measure of v_2 of the partonic phase. We also observe that the magnitude of the elliptic flow at LHC is significantly larger than at RHIC collision condition.

List Of Publications

Refereed Journals:

1. **Elliptic Flow of Thermal Dileptons as a Probe of QCD Matter.**
   Payal Mohanty, Victor Roy, Sabyasachi Ghosh, Santosh K. Das,
   Bedangadas Mohanty, Sourav Sarkar, Jane Alam, Asis K. Chaudhuri.
   Phys. Rev. C **85** (2012) 031903 (R)
   Preprint : Nucl-th/1111.2159

2. **Evolution of Collectivity as a Signal of Quark Gluon Plasma Formation in Heavy Ion Collisions.**
   Payal Mohanty, Jan-e Alam, Bedangadas Mohanty.
   Phys. Rev. C **84** (2011) 024903.
   Preprint : Nucl-th/1008.1112.

3. **Characterizing the Partonic Phase by Dilepton Interferometry.**
   Payal Mohanty, Jan-e Alam, Bedangadas Mohanty.
   Nucl.Phys.A **862** (2011)301-303.
   Preprint : Nucl-th/1101.4120.

4. **Radial Flow from Electromagnetic Probes and Signal of Quark Gluon Plasma.**
   Payal Mohanty, Jajati K Nayak, Jan-e Alam, Satosh K Das.
   Phys. Rev. C **82** (2010) 034901.
   Preprint : Nucl-th/0910.4856

5. **Nuclear Suppression at Low energy Heavy Ion Collision.**
   Santosh K das, Jan-e Alam, Payal Mohanty, Bikash Sinha.
   Phys.Rev.C **81** (2010) 044912.
   Preprint : Nucl-th/0910.4853

6. **Dragging Heavy Quarks in Quark Gluon Plasma at the Large Hadron Collider.**

   Santosh K das, Jan-e Alam, Payal Mohanty.

   Phys. Rev. C **82** (2010) 014908.

   Preprint : Nucl-th/1003-5508

7. **Probing Quark Guon Plasma Properties by Heavy Flavors.**

   Santosh K das, Jan-e Alam, Payal Mohanty.

   Phys.Rev.C **80** (2009) 054916.

   Preprint : Nucl-th/0908.4194

Axiv Submission:

1. **Thermal Radiation from an Expanding Viscous Medium.**

   Sukanya Mitra,Payal Mohanty, Sourav Sarkar,Jan-e Alam.

   Preprint : Nucl-th/1107.2500.

Conference Proceedings in Journals:

1. **Equilibration in Quark Gluon Plasma.**

   Santosh K das, Jan-e Alam, Payal Mohanty.

   Indian J. Phys **85** (2011)1149-1153.

   Preprint : Nucl-th/ 0912.4089.

2. **Scaling Quark Gluon Plasma by HBT Interferometry with Lepton Pairs**

   Payal Mohanty, Jan-e Alam

   Proceedings of Science PoS(WPCF2011)**040**

   Preprint: Nucl-th/1202.2189

Conference Proceedings:

1. **Freeze Out Time in Ultra-Relativistic Heavy Ion Collisions.**
   Santosh K Das, Payal Mohanty, Jajati K Nayak and Jan-e Alam
   Proceedings of DAE Symp. on Nucl. Phys. (India) **52** (2007) 521

2. **Flow from Electromagnetic Radiation**
   Payal Mohanty, Jajati K Nayak, Jan-e Alam, Satosh K Das.
   Proceedings of DAE Symp. on Nucl. Phys. (India) **55** (2010) 628

3. **Dilepton Interferometry : a Tool to Charecterize Different Phases of Collision in HIC**
   Payal Mohanty, Jan-e Alam, Bedangadas Mohanty
   Proceedings of DAE Symp. on Nucl. Phys. (India) **55** (2010) 630

4. **Probing Elliptic Flow of QCD Matter by Lepton Pairs**
   Payal Mohanty, Victor Roy, Sabyasachi Ghosh, Santosh K Das, Bedangadas Mohanty, Sourav Sarkar, Jan-e Alam, Asis K Chaudhuri
   Proceedings of DAE Symp. on Nucl. Phys. (India) **56** (2011) 910

5. **Thermal Radiation from an Expanding Viscous Medium**
   Sukanya Mitra, Payal Mohanty, Sourav Sarkar, Jan-e Alam
   Proceedings of DAE Symp. on Nucl. Phys. (India) **56** (2011) 936

6. **Dilepton Interferometry at Different Collision Energies**
   Payal Mohanty, Jan-e Alam, Bedangadas Mohanty
   Proceedings of DAE Symp. on Nucl. Phys. (India) **56** (2011) 960

Notation and Conventions

In the thesis, I have used the natural units, $\hbar = c = k_B = 1$. The matric tensor used is $g^{\mu\nu} = \mathrm{diag}(1, -1, -1, -1)$. Variables in bold face denote 3-vectors. Most of the notation is introduced during the discussion and the frequently used notations are enlisted below:

$N-N$	Nucleon-Nucleon
$p-p$	proton-proton
$p-A$	proton-Nucleus with mass number A
$A-A$	Nucleus-Nucleus with mass number A
$s,\ t,\ u$	Madelstam Variables, where $s = (p_1+p_2)^2,\ t = (p_1-p_3)^2,\ u = (p_1-p_4)^2$
$\mu_B = \mu$	Baryonic chemical potential
τ	Proper time $(= \sqrt{t^2 - z^2})$
y	Particle rapidity $(= \frac{1}{2} \ln \left[\frac{E+p_z}{E-p_z}\right])$
η	Space-time rapidity $(= \tan^{-1}(t/z))$, thus $t = \tau \cosh \eta$ and $z = \tau \sinh \eta$
M	Invariant mass of lepton pairs
p_T	transverse momentum
M_T	transverse mass of lepton pair $(M_T^2 = M^2 + p_T^2)$
m_T	transverse mass of hadron with mass, m_h $(m_T^2 = m_h^2 + p_T^2)$
ϵ	Energy density
P	Thermodynamic pressure
s	Entropy density
V	Vector mesons
τ_i	Thermalization time
T_i	Thermalization temperature
T_c	Transition temperature
T_{ch}	Chemical freeze-out temperature
T_f	Thermal freeze-out temperature
d^4x	four-volume
K	average pair momentum $(= (p_1+p_2)/2)$, off-shell
q	relative pair momentum $(= p_1 - p_2)$, off-shell

Contents

Chapter 1

Introduction

Today, we are at the verge of understanding the origin of matter surrounding us. How did the surrounding visible matter, all the protons and neutrons, i.e., hadrons emerg from the quark-gluon soup which filled the microsecond old early Universe. In this context, the *Big Bang* theory is the prevailing cosmological model that explains the evolution of the Universe. It is believed that just few microsecond after the *Big Bang* [1, 2], the early Universe was in extremely hot and dense transient state of particles. For very short interval of time, the microsecond old Universe was filled with quarks and gluons, which aren't freely seen in the present world, forming a color deconfined thermalized state of matter - called *Quark Gluon Plasma(QGP)*. This state of matter may exist in the interior of compact neutron star [3, 4, 5]. However, we can recreate the condition for formation of QGP by means of colliding two heavy nuclei at relativistic energy, which we call " *Little Bang*" . With expansion, the temperature falls down and quarks will no longer remain free rather form color neutral hadrons because of asymptotic freedom [6, 7]- the unique aspect of non-Abelian guage theory which is responsible for anti-screening of color charge. The formation and evolution of the exotic hot and dense matter is described by the laws of *Quantum Chromodynamics (QCD)*.

1.1 Basic Concept of Quantum Chromo Dynamics

The dynamical theory of colored quarks and gluons that describe the color interaction is known as *Quantum Chromodynamics (QCD)* - it is a guage theory of non-commuting color symmetric group $SU(3)$. This theory is very similar to *Quantum Electrodynamics (QED)* which is a guage theory corresponding to commuting symmetry group $U(1)$. Being a gauge theory of color symmetry, QCD also contains massless guage bosons, gluons. In contrast to photon - carrier of QED interaction, which is charge-neutral, the gluon carry color charge, and consequently has self-interaction. This makes the QCD more complex compared to QED.

The dynamics of quarks and gluons is governed by *Quantum Chromodynamics* - a viable theory of strong interaction. In the frame work of QCD, Lagrangian density which describe the interactions of quarks and gluons is expressed as follows; [8, 9, 10],

$$\mathcal{L}_{QCD} = \mathcal{L}_{inv} + \mathcal{L}_{gauge} + \mathcal{L}_{ghost} \tag{1.1}$$

$\mathcal{L}_{inv}$ is the classical density, invariant under local SU(N_c) gauge transformation, with $N_c = 3$ for QCD and can be expressed as following [11];

$$\begin{aligned}
\mathcal{L}_{inv} \quad &= \sum_f \bar{\psi}_f (i\not{D} - m_f)\psi_f - \frac{1}{4}F^2 \\
&= \sum_{f=1}^{N_f} \sum_{\alpha,\beta=1}^{4} \sum_{i,j=1}^{N_c} \bar{\psi}_{f,\beta,j} \left[i\gamma^{\mu}_{\beta\alpha} D_{\mu,ji} - m_f \delta_{\beta\alpha}\delta_{ji} \right] \psi_{f.\alpha,i} \\
&- \frac{1}{4} \sum_{\mu,\nu=0}^{3} \sum_{a=1}^{N_c^2-1} F_{\mu\nu,a} F^{\mu\nu}_a
\end{aligned} \tag{1.2}$$

where $\mathcal{L}_{inv}$ is a function of fields, such as quark ($\psi_{f,\alpha,i}$), gluon ($A_{\mu,a}$); α is the Dirac index and i are the color indices for a quark field, similarly μ is the Dirac index and a is the color index for gluon field and m_f, is the mass of quark. There are N_f independent quark fields, where 'f' stands for quark flavors (see Fig. 1.1 for differnt flavors of quarks).

Quarks	Charge	Mass	Baryon Number	Isospin
u up	+ 2/3	~ 4 MeV	1/3	+1/2
d down	-1/3	~ 7 MeV	1/3	-1/2
c charm	+2/3	~ 1.5 GeV	1/3	0
s strange	-1/3	~ 135 MeV	1/3	0
t top	+2/3	~ 175 GeV	1/3	0
b bottom	-1/3	~ 5 GeV	1/3	0

Figure 1.1: Properties of six flavors of quark according to the Standard Model [12].

The $D_{\mu,ij}$ and $F_{\mu\nu,a}$ of above expression takes the form,

$$D_{\mu,ij} = \partial_\mu \delta_{ij} + igA_{\mu a}(T_a^{(F)})_{ij} \tag{1.3}$$

$$F_{\mu\nu,a} = \partial_\mu A_{\nu,a} - \partial_\nu A_{\mu,a} - gC_{abc}A_{\mu b}A_{\nu c} \tag{1.4}$$

where $F_{\mu\nu,a}$ is the non-Abelian field strength defined in terms of the gluon vector field A_a^μ, with $N_c^2 - 1$ group components a, where N_c is the "number of color". "g" is the QCD ("strong") coupling and C_{abc}; known as the structure constants of $SU(N_c)$, a,b,c=1,...,$N_c^2 - 1$ are real numbers, which define its Lie Algebra. The Lie Algebra is defined by commutator relation of the $N_c^2 - 1$; $N_c \times N_c$ matrices $(T_a^{(F)})_{ij}$ that appear in the definition of $D_{\mu,ij}$ (E. (1.3)),

$$\left[T_a^{(F)}, T_b^{(F)}\right] = iC_{abc}T_c^{(F)} \tag{1.5}$$

These commutation relations define the algebra. Here $T_a^{(F)}$ are known as the Gell Mann matrices. $D_{\mu,ij}$ - is the co-variant derivative in N_c-dimensional representation of $SU(N_c)$, which acts on the spinor quark field in Eq. 1.1, with color indices i=1, ..., N_c.

Under local guage transformation, quark fields transform as;

$$\psi'_{f,\alpha,j}(x) = U_{ij}(x)\psi_{f,\alpha,i}(x) \tag{1.6}$$

where

$$U_{ij}(x) = \left[\exp\left\{i\sum_{a=1}^{N_c^2-1}\beta_a(x)T_a^{(F)}\right\}\right]_{ij} \tag{1.7}$$

with $\beta_a(x)$ real. $U_{ij}(x)$ for each x is an element of the group SU(N_c), which acts on the local invariance that has been built into the theory. The gluon field can be expressed in terms of an $N_c \times N_c$ matrix, $A_\mu(x)$

$$[A_\mu(x)]_{ij} = \sum_{a=1}^{N_c^2-1} A_{\mu a}(x)(T_a^{(F)})_{ij}, \tag{1.8}$$

which is the form that occurs in the covariant derivative. The gluonic field is then defined to transform as

$$A'_\mu(x) = U(x)A_\mu(x)U^{-1}(x) + \frac{i}{g}[\partial_\mu U(x)]U^{-1}(x) \tag{1.9}$$

With these transformation rules, $\mathcal{L}_{inv}$ is invariant under local guage transformation. But the guage invariance of $\mathcal{L}_{inv}$ actually makes it difficult to quantize. This problem is solved by adding to $\mathcal{L}_{inv}$ a guage fixing ($\mathcal{L}_{gauge}$) and ghost densities ($\mathcal{L}_{ghost}$).

$$\mathcal{L}_{gauge} = \left\{\begin{array}{c} -\frac{\lambda}{2}\sum_{a=1}^{N_c^2-1}\left(\partial_\mu A_a^\mu\right)^2, \;\; ; \quad 1 < \lambda < \infty \\ \\ -\frac{\lambda}{2}\sum_{a=1}^{N_c^2-1}\left(n.A_a\right)^2, \;\; \lambda \to \infty \end{array}\right\} \tag{1.10}$$

where n^μ is a fixed vector. The first defines the set of "covariant" gauges, the most familiar having $\lambda = 1$, the *Feynman guage*. The second defines the "axial" or "physical" guage, since taking λ to infinity eliminates the need for ghost field. Here, picking n^μ to be lightlike, $n^2 = 0$, defines the *light-cone guage*. For $\lambda \to \infty$, a non zero value of $n.A$ leads to infinite action and for this reason the physical guage are often called "$n.A = 0$" guages. Finally, in covariant guages we must add a ghost Lagrangian [7, 13],

$$\mathcal{L}_{ghost} = (\partial_\mu \bar{c_a})(\partial^\mu\delta_{ab} - gC_{abd}A_b^\mu)c_d, \tag{1.11}$$

where $c_a(x)$ and $\bar{c_a}(x)$ are scalar ghost and antighost field. In the quantization procedure, ghost fields anti-commute, despite the fact that they are scalars. In SU(N_c) theory, the ghost field ensures that the guage fixing does not spoil the unitarity of "physical" S matrix that governs the scattering of quarks and gluons in perturbation theory.

Feynman Rules for QCD

The Feynman rules for QCD is summarized in Fig 1.2.

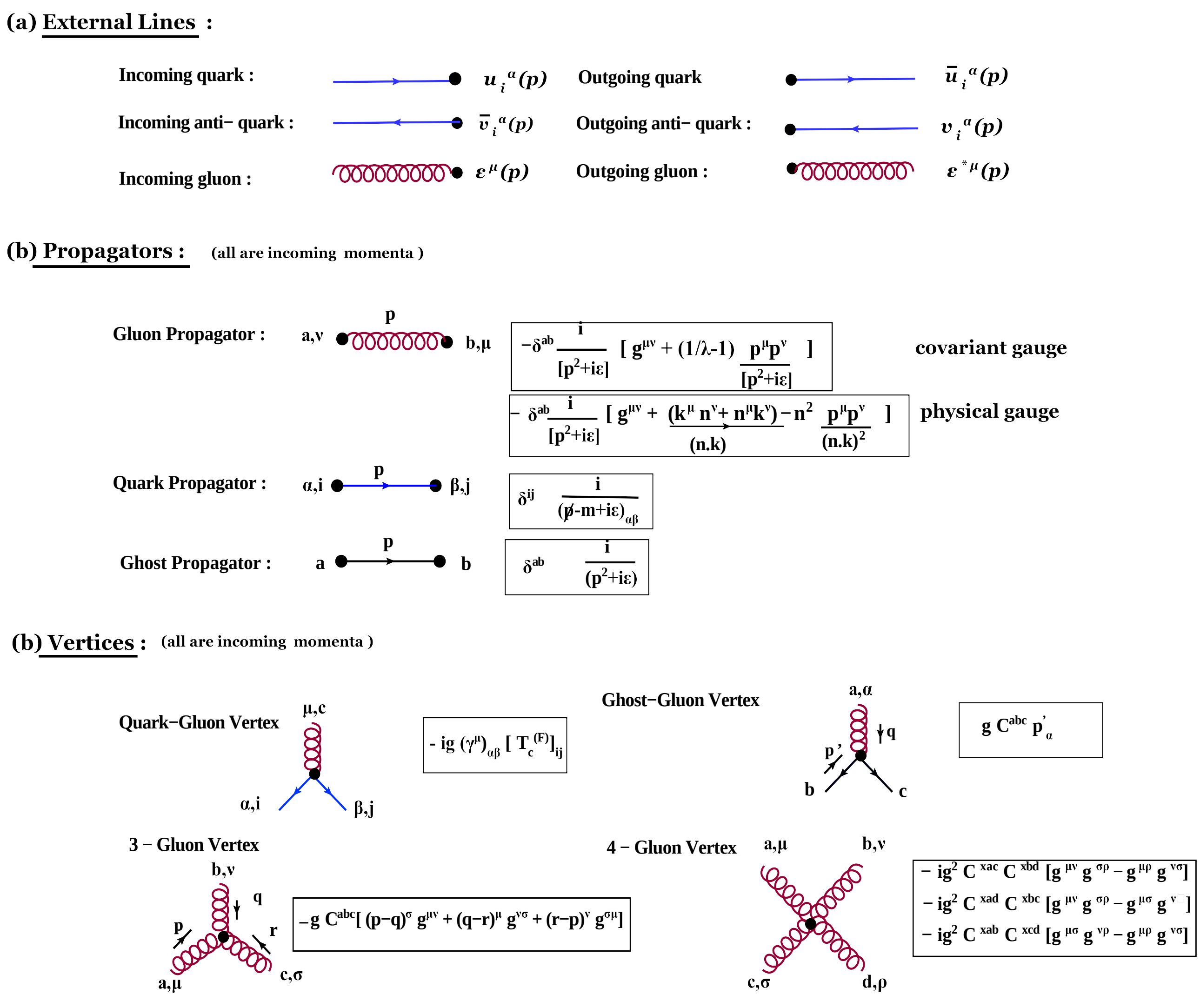

Figure 1.2: Feynman Rules for QCD in covariant guage for gluons (red curly line), quarks (blue line) and ghost field (black line).

1.1.1 Asymptotic Freedom

Many remarkable features of QCD can be traced to the underlying $SU(3)$ gauge symmetry of the strong interaction between quarks and gluons, both of which carry color charges. In the frame work of QCD, the color charge is responsible for two unique aspects of strong interaction - *asymptotic freedom* [6, 7] and *confinement* [14]. *Asymptotic freedom* refers to weakness of short distance interaction, while *confinement* of quarks follows from its strength at long distances. The extraordinary feature of QCD is its ability to accommodate both kind of behavior. Because of non-Abelian self-interaction among gluons, the color charges at short distance anti-screened due to color diffusion via gluon radiation, leading to a weakening of coupling constant. This asymptotic freedom of strong interaction opens the door for perturbation studies of the strong interaction within QCD, including renormalization.

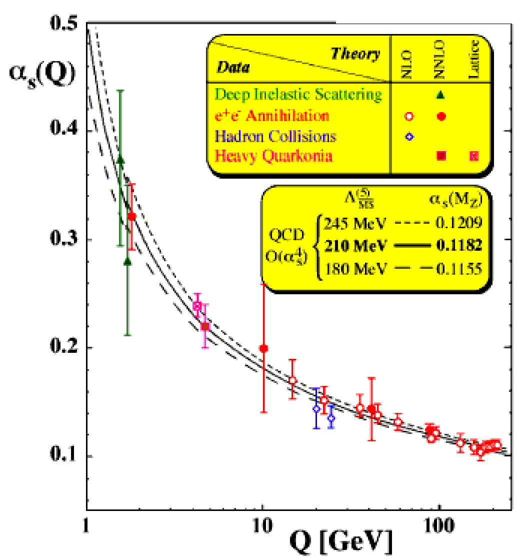

FIG. 1: QCD running coupling constant

Figure 1.3: $\alpha_s(Q^2)$ from theory and experiment. Figure taken from [15]

The effective strong coupling constant α_s depends on momentum transfer between the interacting hadrons. The QCD running coupling constant, α_s ($= g^2/4\pi$) can be written in perturbative QCD (pQCD) as [9]:

$$\alpha_s(Q^2) = \frac{12\pi}{(33 - 2n_f)\ln(Q^2/\Lambda^2)} \tag{1.12}$$

The number of participating quark flavor(n_f) is determined by the available energy characterized by Q^2. The parameter Λ has to be determined by comparing QCD predictions to experimental results and is commonly given as $\Lambda \sim 250$ MeV. $\alpha_s(Q^2)$ (shown in Fig 1.3) is therefore referred as the running coupling constant.

The Q dependence of α_s reproduces the phenomenologically determined behavior of quarks:

- For small values of Q, the interaction strength between quarks is strong (as the α_s increases) and hence they remain confined within the hadrons and not seen isolated in nature. This is known as *confinement*.
- On the other hand, for large Q which corresponds to small distance, the α_s vanishes asymptotically. Due to the weak coupling the quarks behave like free particles. This feature is known as $asymptotic freedom$.

1.1.2 Deconfinement

Just after the discovery of asymptotic freedom, Collins and Perry [3] predicted that at extreme condition of temperature and densities, asymptotic freedom leads to deconfinement. The asymptotically vanishing nature of running coupling constant in low coupling regime does not allow the quarks to remain intact inside hadronic matter rather they move freely due to anti-screening of color - the new state of deconfined thermalized colored matter is known as *Quark-Gluon Plasma (QGP)*. Fig 1.4 illustrates two different

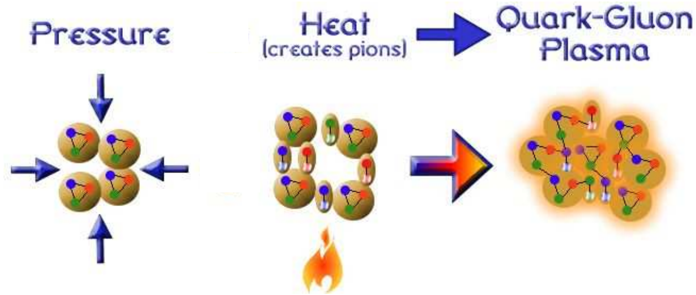

Figure 1.4: Illustration of nuclear matter melting to QGP.

scenario of creation of QGP. Firstly, by supplying heat to the hadronic system (say pion gas), they are excited and more pions formed and create a dense environment where they start overlapping at certain critical temperature (T_c) and in consequence, above T_c, the hadronic system dissolves into a new system of quarks and gluons. Secondly, when a system containing large number of baryons is compressed adiabatically, the baryons start overlapping at certain critical baryon density (or baryonic Chemical potential, μ_B), and dissolves into system of degenerate quark matter. This feature can be better understood through the QCD phase diagram, discussed in the next section.

1.1.3 QCD Phase Diagram

Fig. 1.5 shows a qualitative sketch of QCD phase diagram in temperature (T) and baryonic chemical potential (μ_B) plane. At high temperature or high baryon number density, QCD describes a world of weakly interacting quarks and gluons very different from the hadronic world in which we live. It is believed that microsecond old Universe has undergone a quark-hadron phase transition with μ_B close to zero. So the subject of phase transition from a state of matter where quarks are confined inside hadrons to one where quarks are free to move around within a large volume - the "quark-gluon plasma" (QGP), is an interesting physics issue [17, 18, 19]. The magnitude of temperature and/or

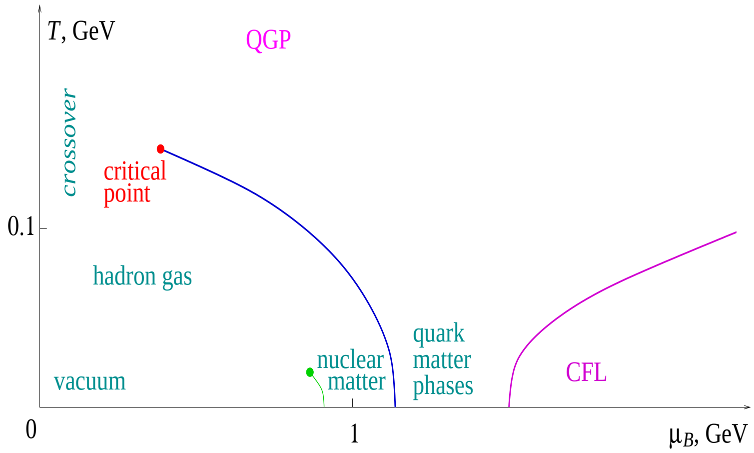

Figure 1.5: Schematic illustration of QCD phase diagram of strongly interacting matter in T -μ_B plane [16]

density required for the deconfinement can be achieved by colliding nuclei at relativistic energies. At low T and high μ_B, 1st order phase transition occurs and by decreasing μ_B and increasing temperature, at certain point the latent heat disappears and the 1st order phase transition ends. At high T and low μ_B, the transition is just a crossover.

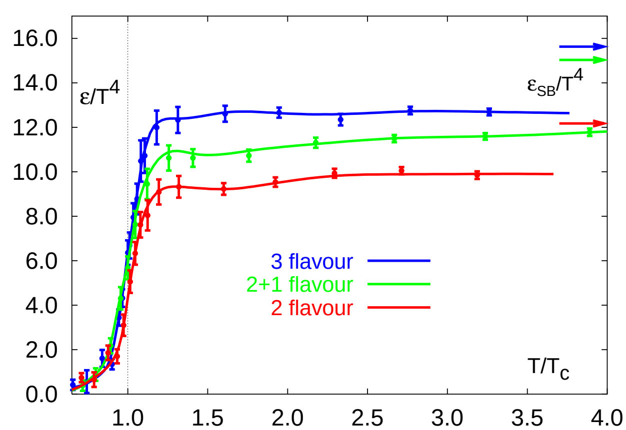

Figure 1.6: Lattice results for equation of state(EoS) for hot QCD [20].

Theoretical model based on lattice QCD(lQCD) calculation confirms the existence of a phase transition for the nuclear matter at a temperature around $T_c \sim 175$ MeV for low μ_B [21]. The point in $T - \mu_B$ plane (Fig. 1.5) where 1st order transition ends is called *critical end point*. There are rigorous experimental and theoretical [22, 23] efforts going to locate and understand the physics near critical end point.

1.2 Heavy Ion Collision (HIC)

The main motto of Nucleus-Nucleus collision at relativistic energies is to create QGP. Relativistic Heavy Ion Collider (RHIC) at BNL and Large Hadron Collider (LHC) at CERN are two such experimental facilities, where by accelerating two heavy nuclei, a large amount of energy is deposited into a very small region, creating suitable condition for formation of QGP. The transient phase lasts for very short interval of time $\sim 10^{-23}$sec. The evolution of high energy Nucleus-Nucleus collision is usually pictured in the form depicted in the Fig. 1.7. After a short equilibration time, $\tau_i \simeq 0.1-1$ fm/c, the presence of thermalized medium is assumed, and for sufficiently high energy densities, this medium would be in quark gluon plasma phase. Afterwards, as the expansion reduces the energy density, the system undergoes a phase transition and transforms to a hadronic gas phase and finally reaches freeze-out, when the final state hadrons don't interact with each other anymore.

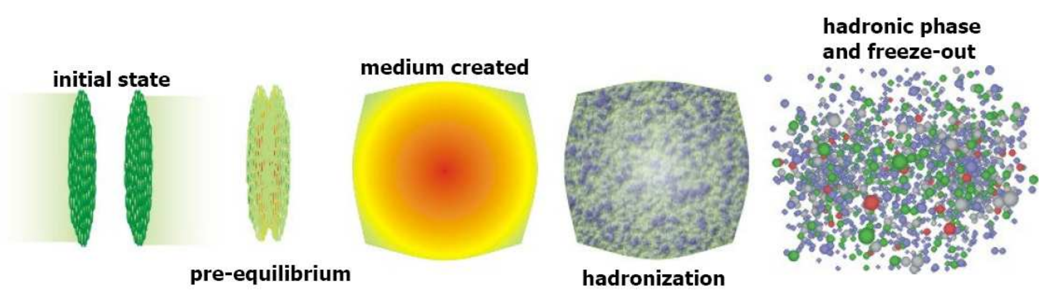

Figure 1.7: Schematic view of the space time evolution nuclear collision. Art is courtesy of S.A.Bass.

1.3 Different Stages of Collision

Within the scope of relativistic hydrodynamical model, owing to high internal pressure inside the system formed in HIC, expands and evolves through different stages of collision as illustrated in Fig. 1.8.

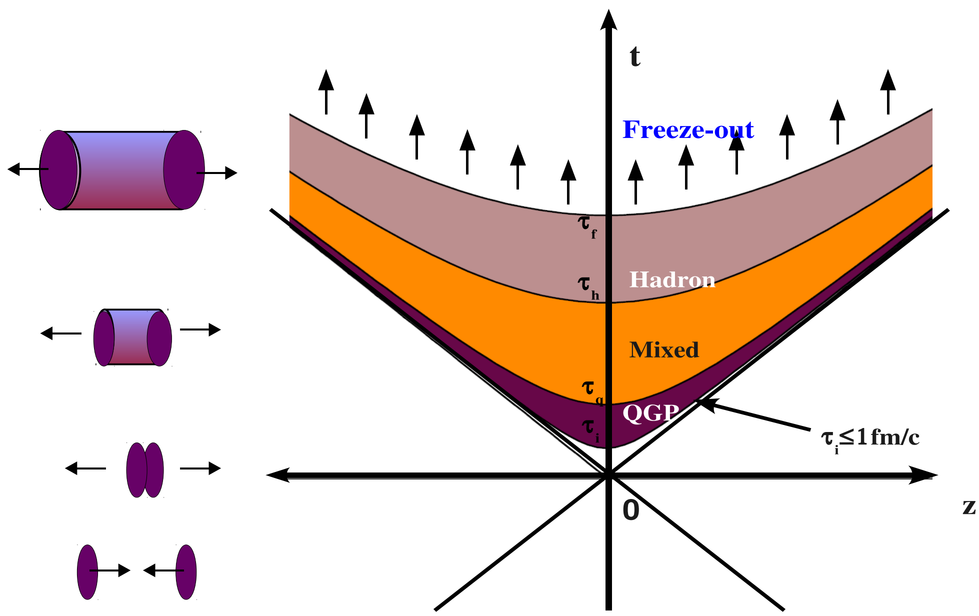

Figure 1.8: Schematic view of expanding system and the trajectories of collision of nuclei coming from z=±∞ with a velocity closer to velocity of light and collide at (z,t)=(0,0), this point is known as the collision point. The τ is the proper time defined as $\tau = \sqrt{t^2 - z^2}$.

• In the initial "pre-equilibrium' stage of collision, system is not thermalized. The secondary partons are produced predominantly by parton-parton hard scatterings occur in the overlap region of two colliding nuclei, depositing a large amount of energy in the medium. The perturbative QCD model is required to describe the processes which occur in this stage. It was predicted that the pre-equilibrium stage exists for a time duration ∼ 1 fm/c [24], after which the thermalization is reached. So this is known as thermalization time, τ_i. However, it is difficult to determine the value of τ_i theoretically.

• After a proper time τ_i, due to subsequent partonic interactions, the system may achieved thermal equilibrium and QGP is formed and the system assigned with a temperature T_i known as the initial temperature. The equilibrium distribution function of the constituents take form $f = 1/[\exp[(E - \mu_B)/T] \pm 1$, where E is the energy of the system in a co-moving frame and μ_B is the baryonic chemical potential, here the (+) sign is for fermions and (-) is for bosons. The proper time where the QGP phase ends is τ_q, thus the life time of QGP is $\tau_Q = \tau_q - \tau_i$.

• As argued previously, at high μ_B and low temperature the nature of phase transition is 1st order, where the mixed phase , i.e. coexisting phase of QGP and hadron appear at T_c. In this phase, quarks and gluons get confined into hadrons at the critical temperature T_c. Through the process of hadronization the colored particles - quarks and gluons combine to form color-neutral hadrons. The released latent heat maintains the temperature of the system at T_c by compensating the energy spent due to expansion.

This mixed phase persists until all the matter has converted to the hadronic phase. During the mixed phase, temperature remains constant but the degeneracy of the medium changes , in consequence the entropy density changes. Therefore, the system is prevented from its fast expansion and cooling due to the "softest point" defined by a minimum "$\partial\epsilon/\partial P$" in the equation of state. This leads to a maximum lifetime of the mixed phase($\tau_M = \tau_h - \tau_q$), which is expected to last for a relatively long time (τ >10 fm/c) during the softening of the equation of state.

• With further expansion and cooling, at $\tau = \tau_h$ (Fig. 1.8) and $T = T_c$ the whole system converts to hadrons. The system of hadrons may be in thermal equilibrium due to the interaction among the hadrons. However, analysis of the hadronic ratio from various experiments [25] indicate that the chemical freeze-out temperature is close to the QCD boundary (indicated in Fig. 1.5), i.e. in the hadronic phase the system may remain out of chemical equilibrium. However, the system may maintain kinetic equilibrium through elastic interactions. Still it reaches a temperature, T_f, called kinetic freeze-out temperature, when the mean free path becomes comparable to the system size. At this stage, all the distribution of particles are frozen out and free stream towards the detector.

For the present study, the evaluation of matter from QGP (initial) to the hadronic system (final) via an intermediate quark-hadron transition is studied by applying relativistic ideal hydrodynamics.

1.4 QGP and Its Signatures in Relativistic Heavy Ion Collision

The Quark Gluon Plasma (QGP) is a phase of quantum chromo dynamics which exists at high temperature and baryon density. The difference between QGP and hadronic phase of QCD is the following:

- In normal matter, the quarks are confined, each quark either ties up with an anti-quark to form mesons or joins with two other quarks to form baryons.

- In QGP, in contrast, the mesons and baryons lose their identity and they are deconfined and dissolve into a fluid of quarks and gluons.

So, QGP is thermalized deconfined state of matter, the properties of which are governed by partonic degrees of freedom showing a collective behavior. As lifetime of the transient phase is too small, therefore it is nontrivial to determine the formation of QGP by direct observations. Hence by studying signals using the particles that shower out from the collisions and reach the detectors, we diagnose the properties of QGP. Out of many attempts done to detect this novel state of matter, few such successful attempts have discussed below.

1.4.1 QGP Diagnostics Using Hadrons

QGP formed in nucleus-nucleus collision subsequently expands, cools and hadronizes into hot hadronic gas. The final state hadrons are the most abundant and dominant source of information about the early stage of collisions; however, hadrons suffer from the final-state interaction, which partially mask the early information. Still then, collectivity of hadrons, especially the elliptic flow of hadrons provides information about the initial stage of the collision.

Elliptic Flow

The elliptic flow is described as one of the most important observations measured at the Relativistic Heavy Ion Collider (RHIC). It is one of the strongest evidences for the discovery of hot partonic system. It describes the azimuthal momentum space anisotropy of particle emission from non-central heavy-ion collisions in the plane transverse to the beam direction. Elliptic flow is the second harmonic coefficient of an azimuthal Fourier decomposition of the momentum distribution.

$$E\frac{dN}{d^3P} = E\frac{dN}{2\pi p_T dp_T dy}\left(1 + \sum_{n=1}^{\infty} 2v_n \cos[n(\phi - \psi_r)]\right) \tag{1.13}$$

where ϕ is the azimuthal angle of the particle and ψ_r is the angle subtended by the reaction plane containing the beam axis and impact parameter with x-direction. Most of the studies with elliptic flow [26, 27, 28, 29, 30] have dealt with the hadrons. Since the spatial anisotropy is largest at the beginning of the evolution, elliptic flow is especially sensitive to the early stages of system evolution.

Interferometry and Space Time Evolution

The only known way to obtain experimental information of the space-time structure of the particle emitting source is through two-particle intensity interferometry [31, 32]. The method of two-particle intensity interferometry, originally developed by Hanbury Brown and Twiss (HBT) [33] to measure angular distances of stars and other stellar objects, utilizes particle intensities and the exploitation of quantum statistical effects to access spatial information of the emitting source. In high energy physics, for the first time this method was introduced independently by Goldhaber, Goldhaber, Lee and Pais (GGLP) [34] in 1960 in hadron sector in order to study space-time structure of identical pion produced in particle interaction. The heavy-ion community refers to any intensity interferometric measurement of correlations among identical particles as "HBT interferometry". The HBT radii extracted from the Bose Einstein correlation functions provide the spatial and temporal information from heavy-ion collisions. By studying both dynamics and geometry of the system, one can examine the fireball medium and check whether condition for the creation of QGP is reached or not.

1.4.2 QGP Diagnostics Using Hard Probes: Jet Quenching

When two protons collide at high energies, pairs of their constituent quarks or gluons may collide with each other and scatter back to back, quickly breaking up again into "jets" (Fig 1.9) or spray of particles such as pions and kaons.

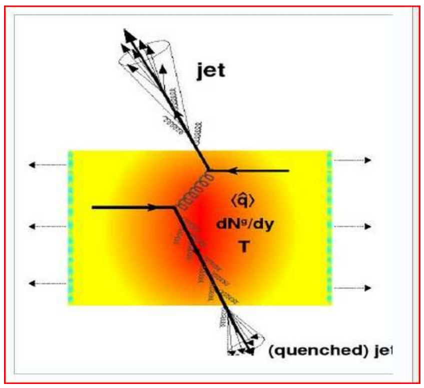

Figure 1.9: Schematic presentation of production of jets back-to-back

Jets are fundamental to QCD and they have been seen in high energy physics experiments since 1980's in pp collision [35]. The fireball created in heavy ion collision is bigger in volume compared to that of form in p-p collision. Moreover, the possibility of the creation of a very hot and dense system in A-A collision is more compared to p-p collision. Therefore when a jet is created in early collision it will propagate through this hot matter. While propagating through the QGP, the high energy partons or jets will dissipate energy due to its interaction with the medium. The magnitude of the dissipation will depend on the density and temperature of the medium. The energy loss of the jets in the QGP is measured through the nuclear suppression factor, R_{AA} , and is found to be very useful quantity to extract the properties of QGP. This suppression of high energy partons in HIC is commonly known as "jet quenching" [36, 37]. Experimentally, the quantity R_{AA} being the quotient of observed jet yield in A + A collisions and $N_{bin}\times$ yield in p + p collisions shows a strong damping with increasing A, which indicates significant interaction of the jets with the hot and dense medium formed in HIC. This suppression has been used to extract the transport coefficients of the hot medium [38].

1.4.3 QGP Diagnostics Using Electromagnetic Probes: Real Photons and Dileptons

Electromagnetic(EM) probes [39, 40, 41, 42, 43, 44, 45, 46] are represented as - real photons and dileptons, have large mean free-path($\lambda \sim 1/n\sigma$) compared to the size of the system formed in HIC. Once produced they are not distorted by the final state interaction and escape from the medium carrying undistorted information from the point of production straight to the detector. Hence they can probe the entire space-time history and emerge out copiously from each stages of collision and thus considered as penetrating probes. Depending on the process through which photons/dileptons produce, they are categorized (see Fig. 3.1) as;

1. *Prompt :* The EM radiations produced by hard scattering of the partons inside the nucleons of incoming nuclei in the initial stage of collision, before the thermalization sets in, are known as prompt photons and dileptons (Drell Yan). This contribution may be evaluated by using pQCD.

2. *Thermal :* EM radiations which are emitted from the thermalized systems of quarks and gluons or hadronic gas.

3. *Decay:* EM radiations produced from the decays of hadrons after the fireball freezes-out are known as decay photons or dileptons. They build up substantial

backgrounds and complicate the extraction of information of the thermal system.

Out of different sources, our interest lies in the thermal photons and dileptons since they are expected to render information about the formation of QGP. Thus one has to subtract out the non-thermal sources to understand the properties of the QGP. However, it is not possible experimentally to distinguish between different sources. Thus, theoretical models and calculations can be used in great advantage to identify different sources of direct photons and their relative importance and characteristics in the spectrum. The hard photons and dileptons are well understood in the framework of pQCD and decay contributions can be filtered out experimentally using different subtraction method, like invariant mass analysis, mixed event analysis, internal conversion method etc. Calculation based on theory tells the hard photons dominate the high p_T part of the invariant momentum spectra and decay photon populate the low p_T part and rest over thermal contribution shines in the intermediate domain of the p_T spectra $\sim$ 1-3 GeV. As photons from hadronic phase dominate the spectra in low $p_T(<\ 1\mathrm{GeV})$, so there is a small window in the spectra, i.e. $p_T \sim 2-3\mathrm{GeV}$, which may help in learning the properties of QGP.

However, photons appear to be a more restrictive probe since they are characterized only by their momentum whereas the dileptons have two kinematic variable , p_T and invariant mass(M) to play with. A soft photon (low p_T) in one frame of reference can be hard (high p_T) in another frame, whereas the p_T integrated invariant mass distribution of dileptons is independent of any frame. In addition to it the p_T spectra is affected by the flow, however, the p_T integrated M spectra remain unaltered by the flow in the system. Also in the M spectra of dileptons, above ϕ peak dileptons from QGP dominates over its hadronic counterpart. All these suggests that a judicious choice of p_T and M windows will be very useful to characterize the QGP and hadronic phase separately.

1.4.4 QGP Diagnostics Through J/Ψ Suppression

Matsui and Satz [47] proposed that J/Ψ yield in the relativistic heavy ion collision is suppressed compared to the p-p, p-A interaction appropriately scaled if QGP is formed because the binding potential becomes short range due to the color Debye screening in the QCD plasma. J/Ψ particles are the bound state of $c\bar{c}$ pair. Since charm quark is heavy ($m_c \sim 1.5$ Gev), they are likely to be produced in the initial hard parton scattering. In p-p or p-A collisions, the produced J/Ψ's would simply escape the collision region and be detected through their decay channels. However in nucleus- nucleus collision, the J/Ψ need to pass through the extended hot and dense matter. Further in the hot QGP environment, the quark and gluon move freely and due to Debye screening of color charges the string tension vanishes. In consequence, the interaction between the $c\bar{c}$ quarks is weakened to a point in which J/Ψ can dissociate resulting suppression of J/ψ yield compared to p-p or p-A collision [47]. The probability of forming a c quark ($\sim \exp(-m_c/T)$)is less than that of lighter quark (u,d,s) ($\sim \exp(-m_q/T)$, q for light quark). Hence when charm and anti-charm quarks travel through the plasma until the system cools down, then due to the plenty of abundance of u, d, s quarks and anti-quarks there is high possibility that the c and $\bar{c}$ can hadronize by combining with the light quarks and antiquarks forming open charm particles $D^+(c\bar{d}),\ D^0(c\bar{u}),\ D^-(\bar{c}d),\ \bar{D}^0(\bar{c}u),\ D_s(c\bar{s}),\ \bar{D}_s(\bar{c}s)$, which will result in the suppression of J/ψ in QGP. Recent calculations based on lQCD show J/ψ does not melt when temperature $T \simeq 1.6T_c$ [48]. Experimental data from SPS and RHIC shows similar J/ψ suppression pattern, the reason for which this happens is yet to be settled [49].

1.4.5 QGP Diagnostics Through Strangeness Enhancement

Rafelski & Müller proposed that the strangeness abundance [50], along with strange anti-baryon yields offers an opportunity to identify formation of the deconfined quark gluon matter, and the exploration of its properties. The basic idea was to look at the abundance of strange and (especially) multi-strange particles in AA collisions and compare with the corresponding results from pp and pA collisions (all scaled by the number of participants, N_{part} or the multiplicity, $dN/d\eta$). The appropriate observable is the enhancement E of strange particle Y [51],

$$E_Y = \frac{\langle N_{part}^{p-A} \rangle \langle N_Y^{A-A} \rangle}{\langle N_{part}^{A-A} \rangle \langle N_Y^{p-A} \rangle} \tag{1.14}$$

where $N_{part}(N_Y)$ is the number of participants (strange particles, Y). It is expected that $E_Y > 1$ and increases with strangeness content of the particle. The reasons given in [50] is that strangeness-producing processes in a QGP,

$$q\bar{q} \leftrightarrow s\bar{s} \qquad gg \leftrightarrow s\bar{s} \tag{1.15}$$

should equilibrate faster than the corresponding processes in a hadron gas (HG):

$$\pi^- \pi^+ \leftrightarrow KK \qquad \pi N \leftrightarrow \Lambda K \tag{1.16}$$

This can be seen relatively quickly by computing the average momentum exchange $\langle Q \rangle$ needed for these processes ($\langle Q \rangle \sim 2m_s$ for Eq.. 1.15 , $\langle Q \rangle \sim 2m_K$ for Eq.. 1.16. In a thermally equilibrated medium the equilibration time depends on $\langle Q \rangle / T$). The greater degeneracy of massless quarks and gluons with respect to pions and nucleons makes the difference of thermalization times for the two phases even larger. Hence, the strangeness abundance should reach chemical equilibrium (where the strangeness relative to light quark abundance depends only on mass difference and temperature, not on initial conditions) much faster in a quark gluon plasma than in a hadron gas. Since the initial strangeness abundance in collisions is zero, the number of strange particles in a system of a certain lifetime with a phase transition should be parametrically higher than for a similar system where the transition did not occur.

In summary, strangeness particle abundance in a collision where a QGP is produced (a high-energy AA collision) should be enhanced w.r.t. a collision where hadronic dynamics is at play (a pp or pA collision, or an AA collision where hadronic dynamics dominates). The enhancement should also grow with the hadrons strangeness content. The onset of this enhancement could signal the appearance of a phase transition, or more generally a change in the degrees of freedom of the system.

1.5 Motivation of This Study

The Relativistic Heavy Ion Collision (RHIC) has initiated an new era in the study of QCD matter at extreme conditions. The main motivation of RHIC is to study the Quark - Hadron phase transition (which is discussed in Sec. 1.1.3), as it is believed that the early universe also has undergone such kind of transition. Various key observable signals for the study of the transient state, and its properties have been discussed in the Sec. 1.4. Out of the several attempts done in this direction, electromagnetic radiations, thermal photons and dileptons in particular, is one of the most efficient probes due to its nature of interaction. They are produced from each stages of collision and carry the information of interior of the system formed. The interactions among the quarks and gluons help in achieving the local thermal equilibrium. Collective motion is generated due to the pressure gradient which results in expansion of the system. Thus owing to high internal pressure built after the collision and subsequent expansion, system cools and QGP revert to hadronic phase at a temperature T_c. In this work, relativistic hydrodynamics has been used to describe the space time evolution of the system. The basics equations and assumptions of relativistic hydrodynamics is described in the Chapter- 2. In this analyses, we neglect the effect of dissipation and concentrate on discussion about the ideal hydrodynamical model. All the ingredients of the ideal hydrodynamic model like, EoS, initial conditions and freeze-out criteria etc. (discussed in Section 2.3) are useful to match the measured single particle spectra of hadrons at freeze-out surface. As the main focus of the thesis is on the production of EM radiation, the various sources of such radiations and the formulation of the single particle spectra of thermal photons and dileptons are presented in Chapter- 3. With the help of basic ingredients of ideal hydrodynamics depicted in Chapter- 2, invariant momentum distributions of photons and dileptons are evaluated and compared with the available experimental data. The calculation of invaraint moemtum spectra of photons and dileptons depend on the quantities like, initial temperature (T_i), thermalization time (τ_i), chemical freeze-out temperature ($T_{\rm ch}$), kinetic freeze-out temperature (T_f) etc, which are not known unambiguously. To minimize the dependence of thermal sources on these parameters the importance of the ratio of the transverse momentum spectra of photon to dilepton has been considered (Chapter- 4) in order to overcome the above mentioned uncertainties. The procedure of extraction radial flow velocity from the ratio is explained in Chapter- 4. Using the single particle spectra of leptopn pairs, the two particle correlation for the lepton pairs has been evaluated and shown that HBT interferometry with lepton pair must be used as an efficient to study the evaluation of radial flow (Chapter- 5). The variation of source size with invariant mass of lepton pairs may be useful to characterize different phase of collision . The collectivity in the system may be manifested in the form of radial as well as elliptic flow. The evaluation of both quantities may be performed by using thermal photons and dileptons as they bestow information of the evolution of the collectivity of the system. For qualitative extraction of radial flow velocity, two different procedures are followed , i.e. firstly, from ratio of p_T spectra of photon to dilepton and secondly, from HBT interferometry of lepton pairs are constrained to the experimental data. The elliptic flow of thermal dilepton is discussed in Chapter- 6. Finally, I have summarized the work in Chapter- 7.

Chapter 2

Expansion Dynamics of Heavy Ion Collision

"*In high energy physics we have concentrated on experiments in which we distribute higher and higher amount of energy in to a region of smaller and smaller dimension. In order to study the question of "vacuum' we must turn to different direction; we should investigate the bulk phenomena by distributing high energy over large volume*".

-T. D. Lee [52]

2.1 Introduction

The main objective of the relativistic heavy ion collision is to create a nuclear matter at extreme condition of temperature and density which is primarily governed by partonic degree of freedom. By increasing energies, the relevant degrees of freedom changes.

Over the years, several attempts have been made in this direction. The nuclear beam energies have been increasing starting from beam kinetic energies of few MeV/nucleon on fixed target experiments to, at present, collider energies with few thousand GeV/nucleon (See Table. 2.1). In collider, both the projectile and the target accelerated leading to much higher energies available for particle production compared to fixed target facilities. Physicist at Relativistic Heavy Ion Collider (RHIC) at BNL and Large Hadron collider (LHC) at CERN create the condition for formation of QGP by accelerating two heavy nuclei (Au+Au at RHIC and Pb+Pb at LHC) at very high energy. At such high energies, the relevant degrees of freedom for the system produced are quarks and gluons rather than hadrons.

Table 2.1: Different Experiments with their colliding system and energies are tabulated.

Experiment	Colliding System	Colliding Energy($\sqrt{s_{NN}}$)
SIS	Au + Au	2.24 GeV
AGS	Au + Au	4.86 GeV
SPS	Pb + Pb	17.3 GeV
RHIC	Au + Au	200 GeV
LHC	Pb + Pb	5500 Gev

In central nucleus-nucleus collisions, the inelastic nucleon-nucleon collisions largely contribute to production of new particles. The effect of such inelastic collision in nucleus - nucleus reaction is additive in nature, resulting larger deposition of energy in the vicinity of center of mass. As the larger fraction of energy is squeezed in a small region for a short duration of time, the energy density in this region is very high [24]. The energy density produced in this small region is an order of magnitude greater than that of normal nuclear matter in equilibrium, may favor the environment for creation of QGP.

2.2 Relativistic Hydrodynamics

Ideally, one can not describe heavy ion experimental data from the first principle, i.e., quantum chromodynamics (QCD) due to its complexity which mainly arises from non-linearity of interactions of gluons, strong coupling, dynamical many body system and color confinement. One promising strategy to connect the first principle with phenomena is to introduce hydrodynamics as a phenomenological theory. Relativistic hydrodynamics [53, 54, 55, 56] is interesting because it is simple and general. It is simple because the information on the system is encoded in its thermodynamic properties, i.e., its equation of state. Hydrodynamics is also general, in the sense that it relies on only one assumption, unfortunately a very strong one: local thermodynamic equilibrium. No other assumption is made concerning the nature of the particles and fields, their interactions, the classical/quantum nature of the phenomena involved. The validity of ideal hydrodynamics demands the mean free path of a particle between two collisions(λ) is much smaller than the characteristic dimensions of the system(L), i.e. $L \gg \lambda$.

2.2.1 The Basic Equation of Relativistic Hydrodynamics

Standard thermodynamics can explain a static system in global thermodynamical equilibrium, where the intensive parameters(P, T, μ) are constant throughout the volume. But for an expanding system where pressure, temperature etc. vary with space and time. Alone not able to explain how system changes with space-time. Thus we assume the system is in local thermodynamic equilibrium, which means that pressure and temperature are not constant rather are the function of space and time. However the variation is so slow that for any point, one can assume thermodynamic equilibrium in the neighborhood about that point.

In a *fluid rest frame*[1], the assumption of local thermodynamic equilibrium strongly constrains the energy-momentum conservation. The energy-momentum tensor of fluid element in its local rest frame is given by;

$$T_0^{\mu\nu} = diag[\epsilon, -P, -P, -P] \tag{2.1}$$

Isotropy implies that the energy flux T_{i0} and the momentum density T_{0j} vanish in the rest frame of fluid. In addition, it implies that the pressure tensor is proportional to the identity matrix, i.e., $T_{ij} = P\delta_{ij}$, where P is the thermodynamic pressure.

In order to obtain the energy-momentum tensor in a moving frame, one does a Lorentz transformation. To first order in velocity $\vec{v}$, the matrix of a Lorentz transformation is [54, 57]

$$\Lambda = \begin{pmatrix} 1 & v_x & v_y & v_z \\ v_x & 1 & 0 & 0 \\ v_y & 0 & 1 & 0 \\ v_z & 0 & 0 & 1 \end{pmatrix} \tag{2.2}$$

Under a Lorentz transformation, the covariant tensor $T_0^{\mu\nu}$ transforms to

$$T^{\mu\nu} = \Lambda^{\mu}_{\alpha}\Lambda^{\nu}_{\beta}T_0^{\alpha\beta} \tag{2.3}$$

and finally, the energy-momentum tensor for an arbitrary fluid velocity is

$$T^{\mu\nu} = (\epsilon + P)u^{\mu}u^{\nu} - Pg^{\mu\nu} \tag{2.4}$$

[1] The rest frame of a fluid element is the frame in which its momentum vanishes. All thermodynamic quantities associated with a fluid element (for example, ϵ, P, n) are defined in the rest frame. They are, therefore, Lorentz scalars by construction (for the same reason as the mass of a particle is a Lorentz scalar). Local thermodynamic equilibrium implies that the fluid element has isotropic properties in the fluid rest frame.

where ϵ and P is the energy density and pressure respectively, $g^{\mu\nu} \equiv diag(1, -1, -1, -1)$ is the Mankowski metric tensor and u^{μ} is the fluid 4-velocity referred as "collectivity" of the system which can be defined as $u^{\mu} = \gamma(1, \vec{v})$ with $\gamma = 1/\sqrt{1 - \vec{v}^2}$ and $u^{\mu}u_{\mu} = 1$ where $\vec{v}$ is the velocity of fluid element.

The basic equations of relativistic hydrodynamics result from applying constraints of energy-momentum and net baryon number conservations relevant for heavy ion collision at relativistic energies are expressed in Eq. 2.5 and 2.6 respectively.

$$\partial_{\mu} T^{\mu\nu} = 0 \tag{2.5}$$

$$\partial_{\mu} N_B^{\mu} = 0 \tag{2.6}$$

where $T^{\mu\nu}$ is the energy-momentum tensor and $N_B^{\mu} = n_B u^{\mu}$ is the conserved net baryonic current and n_B is baryon number density. For the present work the net baryon number is assumed to be negligible small, so the Eq. 2.5 is the only relevant equation to deal with. In addition to it, the total entropy of and inviscid fluid is conserved through out (S = constant). If we define the entropy current : $s^{\mu} = su^{\mu}$, then the conservation of entropy results in $\partial_{\mu} s^{\mu} = 0$ [57].

Finding the solutions of the hydrodynamic equations become simpler if one assumes azimuthal symmetry and the boost invariance expansion [58] along longitudinal direction. This can be done by making a change in the variables $(t, \vec{r}) = (t, x, y, z) = (\tau, r, \phi, \eta)$, where τ and η can be expressed as;

$$\tau = \sqrt{t^2 - z^2} \tag{2.7}$$

and

$$\eta = \frac{1}{2} \ln \left[\frac{t + z}{t - z} \right] = \tanh^{-1}(z/t) \tag{2.8}$$

The longitudinal boost invariance together with $u^2 = -1$ requires that the fluid velocity be of the form

$$\begin{aligned} u \quad &= \gamma_T(\tau, r)(t/\tau, v_r(\tau, r), z/\tau) \\ &= \gamma_T(M_T \cosh\eta, u_x, u_y, M_T \sinh\eta) \end{aligned} \tag{2.9}$$

where

$$\gamma_T = \sqrt{1 - v_r^2} \quad , \qquad v_r^2 = v_x^2 + v_y^2 \tag{2.10}$$

where v_r is the radial velocity of the fluid element. The assumption of boost invariance and azimuthal asymmetry make all physical quantities like energy densities, temperature, fluid velocities as a function of r and τ. The assumption of azimuthal symmetry will be relaxed while studying elliptic flow.

The perfect-fluid hydrodynamic equations for the stress-energy tensor in the present case may be written in simple form. If we use

$$T^{00} = (\epsilon + P)u^0u^0 - P \tag{2.11}$$

and

$$T^{01} = (\epsilon + P)u^0u^1 \tag{2.12}$$

the hydrodynamic equations are [58]

$$\partial_r T^{00} + \frac{1}{r}\partial_r(rT^{01}) + \frac{1}{\tau}\partial_r(T^{00} + P) = 0 \tag{2.13}$$

and

$$\partial_r T^{01} + \frac{1}{r}\partial_r[r(T^0 + P)v_r^2] + \frac{1}{\tau}T^{01} + \partial_r P = 0 \tag{2.14}$$

2.3 Ideal Hydrodynamical Model

Hydrodynamics introduced in Sec.2.2 is a general framework to describe the space-time evolution of locally thermalized matter for a given equation of state(EoS). In this work, we neglect the effect of dissipation and concentrate on discussion about the ideal hydrodynamical model. The basic ingredients required to solve the ideal hydrodynamic equations are EoS and initial conditions. As the system expands from its initial state, the mean free path between particles within the system increases. At certain stage, the mean free path becomes comparable to the system size then the hydrodynamic description breaks down and the phase space distribution of the particle get fixed by the temperature of the system at this stage. this stage of evolution is called freeze-out state and the corresponding temperature of the system is called thermal freeze-out temperature (T_f). The hydrodynamic evolution stops at the freeze-out point.

2.3.1 Initial Condition

The initial conditions are crucial to the description of space-time evolution. Initial conditions in hydrodynamics may be constrained in the following ways to reproduce the measured final multiplicity. We assume that the system reaches equilibration at a time τ_i (called initial thermalization time) after the collision. The T_i can be related to the measured hadronic multiplicity (dN/dy) by the following relation [59];

$$T_i^3 \tau_i \approx \frac{2\pi^4}{45\zeta(3)} \frac{1}{4a_{eff}} \frac{1}{\pi R_A^2} \frac{dN}{dy}. \tag{2.15}$$

where $R_A \sim 1.1 N_{\rm part}^{1/3}$ is the radius of the system, $\zeta(3)$ is the Riemann zeta function and $a_{eff} = \pi^2 g_{eff}/90$, g_{eff} $(= 2 \times 8 + (\frac{7}{8}) \times 2 \times 2 \times N_c \times N_F)$ is the degeneracy of quarks and gluons in QGP, N_c=number of colors, N_F=number of flavors. The factor '7/8' originates from the difference between the Bose-Einestein and the Fermi-Dirac statistics. T_i depends on the centrality through the multiplicity, dN/dy. The value of dN/dy for various beam energies and centralities can be obtained directly form experiment or calculated using the following relation [60];

$$\frac{dN}{dy} = (1-x)n_{pp}\frac{\langle N_{part}\rangle}{2} + xn_{pp}\langle N_{coll}\rangle \tag{2.16}$$

where n_{pp} is the multiplicity per unit rapidity measured in pp collisions: $n_{pp} = 2.5 - 0.25ln(s) + 0.023ln^2(s)$, the fraction x of n_{pp} is due to "hard' processes, with the remaining fraction (1-x) being "soft" processes. The multiplicity in nuclear collision has then two components: "soft", which is proportional to number of participants, N_{part} and "hard", which is proportional to number of binary collision, N_{coll}.

After the initial thermalization time, τ_i, the system can be treated hydrodynamically. The initial conditions to solve the Eq. 2.13 and 2.14 are given through the energy density and velocity profile,

$$\begin{aligned} \epsilon(\tau_i, r) &= \frac{\epsilon_0}{1+\exp(\frac{r-R_A}{\delta})} \\ v(\tau_i, r) &= 0 \end{aligned} \tag{2.17}$$

where ϵ_0 is the initial energy density which is related to initial (T_i), R_A is the nuclear radius and δ is the diffusion parameter taken as 0.5 fm.

2.3.2 Equation of State(EoS)

The set of hydrodynamic equations are not closed by itself; the number of unknown variable exceeds the number of equations by one. Thus a functional relation between any two variables is required so that the system become deterministic. The most natural course is to look for such relation between the pressure P and the energy density ϵ. Under the assumption of local thermal equilibrium, this functional relation between P, ϵ and n_B is the EoS,

$$P = P(\epsilon, n_B) \tag{2.18}$$

which expresses the pressure as function of energy density, ϵ and baryon density, n_B. This can be obtained by exploiting numerical lattice QCD simulation [21].

Different EoS's (corresponding to QGP vis-a-vis that of hadronic matter) will govern the hydrodynamic flow quite differently. It is thus imperative to understand in what respects the two EoS's differ and how they affect the evolution in space and time. The role of the EoS in governing the hydrodynamic flow lies in the fact that the velocity of sound, $c_s^2 = (\partial P/\partial \epsilon)$ sets an intrinsic scale in hydrodynamic evolution. One can thus write simple parametric form of the EoS: $P = c_s^2 \epsilon$, for baryon free system which is relevant for the present study.

2.3.3 Freeze Out Criteria

The hydrodynamic is valid until $\lambda \leq L$. When the $\lambda > L$, the distribution of the particles are freezes out thermally. To describe this freeze-out prescription, the Cooper-Frye formalism [61] may be used to convert the hydrodynamic picture to particle picture

$$\begin{aligned} E\frac{dN}{d^3p} &= \int_\Sigma f(x,p,t) p_\mu d\sigma^\mu \\ &= \frac{g_h}{(2\pi)^3} \int_\Sigma \frac{p_\mu d\sigma^\mu}{\exp[(E^* - \mu(x))/T_f(x)] \pm 1} \end{aligned} \tag{2.19}$$

where E is the energy, f is the phase space-distribution, g_h is the degeneracy of the particle under consideration, dσ is the normal vector to the freeze-out surface element, E^* is the energy in the co-moving frame, μ is the baryonic chemical potential [2] and

[2]NOTE: Hereafter baryonic chemical potential(μ_B) is denoted as μ.

T_f is the freeze-out temperature assuming isothermal freeze-out hyper-surface Σ. In a co-moving frame, the energy is expressed as $E^* = p^\mu u_\mu$, as $p^\mu u_\mu$ is Lorentz scalar and independent of frame of reference where evaluated and $p^\mu u_\mu$ reduces to p^0 if the fluid velocity is zero. The quantity $p^\mu u_\mu$ for boost invariance can be written as

$$p^\mu u_\mu = \gamma_T \left[m_T \cosh(y-\eta) - v_R P_T \cos\phi\right] \tag{2.20}$$

where $p^\mu = (m_T \cosh y, p_T \cos\phi, p_T \sin\phi, m_T \sinh y)$, $M_T^2 = \sqrt{p_T^2 + m^2}$ is the transverse mass. Contribution from resonance decays should also be included [62]. The T_f is fixed through simultaneous description of p_T spectra for various hadrons in the low p_T region. In the blast wave model, decoupling temperature and radial flow velocity are independent parameters to fit p_T spectra. On the other hand, there is a negative correlation between T_f and average radial flow velocity in the hydrodynamic model: the lower decoupling temperature, the larger average radial flow velocity. The Cooper-Frye formula ensures the energy-momentum conservation on freeze-out hyper-surface Σ as long as the EoS is calculated using the same distribution function. If one puts resonances up to the mass of 2 GeV in the resonance gas model, one should calculate all the contribution of hadrons in the EoS. Otherwise, neglect of the contribution leads to violation of the energy momentum conservation. It should be noted that $p.d\sigma$ term in Eq. 2.19 can be negative. This means the in-coming particles through Σ are counted as a negative number. Although this seems peculiar, this negative contribution is needed for global energy momentum conservation.

The prescription (using Eq. 2.19) described in Sec. 2.3 is used for the comparison of measured single particle spectra of hadrons at freeze-out. However, our main motivation is to study the properties of QGP through the thermal photons and dileptons, which produce through out the space time evolution. So in order to compare the photons and lepton pairs produce from the thermal medium, space-time evolution has to carry out by integration over 4-volume ($d^4x = dxdydzdt = rdrd\phi\tau d\tau d\eta$, is expressed in terms of

$x^\mu = (\tau\cosh\eta, r\cos\phi, r\sin\phi, \tau\sinh\eta)$ where τ and η are defined through the Eq. 2.7 and 2.8.) instead of surface integration which is done for the calculation of hadronic spectra at freeze-out hyper-surface $\Sigma^\mu = (\tau_f\cosh\eta, r\cos\phi, r\sin\phi, \tau_f\sinh\eta)$.

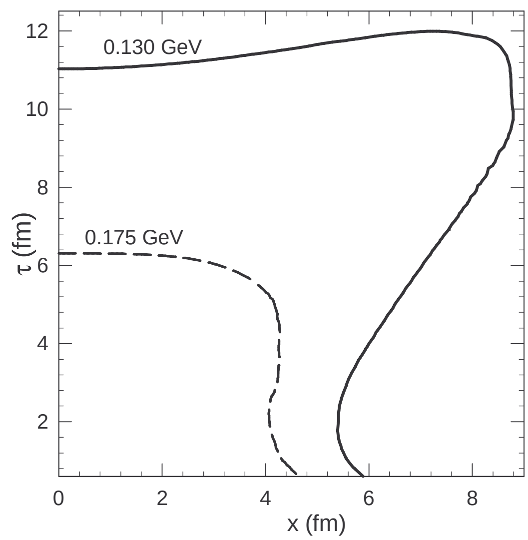

Figure 2.1: Constant temperature contours denoting space-time boundaries of the QGP and hadronic phase. Details of the calculations are described in Chapter- 6

The space-time boundaries of the QGP and hadronic phase are shown in Fig. 2.1 through constant temperature contours corresponding to $T_i = 456$ MeV, $\tau_i = 0.6$ fm, $T_c = 175$ MeV and $T_f = 130$ MeV respectively in $\tau - x$ plane at y = 0 (y denotes the ordinate here). The duration of early QGP phase is $\sim$ 0.6 fm/c at x=0 and lifetime of late hadronic phase is $\sim$ 6-12 fm/c. In the next Chapter we will discuss how thermal contributions from QGP ($T_c \leq T \leq T_i$) and hadronic($T_f \leq T \leq T_c$) can be obtained separately by choosing the phase space appropriately.

Chapter 3

Electromagnetic Radiation - from Partons and Hadrons

3.1 Significance of Electromagnetic Radiations

The main objective of Relativistic Heavy Ion Collisions is to study the transient phase, i.e. *Quark Gluon Plasma(QGP)* which is believed to permeate the early universe a few micro-seconds after the *Big Bang*. Collision between nuclei at ultra relativistic energies produce charged particles either in hadronic or in partonic state depending on the collision energy. Interaction of these charged particles produce electromagnetic(EM) radiation. However, hadrons being strongly interacting objects give snapshot of evolution only from the freeze-out surface. So they have hardly any information about the interior of the plasma. Whereas, EM radiation, *e.g.* the thermal photons and dileptons, from such collision are expected to provide an accurate information about the initial condition and the history of evolution of the plasma while it cools and hadronizes. This is possible since photons interact only through the EM interaction. The EM interaction strength is small compared to that of strong interaction ($\alpha \ll \alpha_s$) and thus dominates the dynamics of nuclear collision processes. Therefore, its mean free path ($\lambda = 1/n\sigma$) is larger than the size of the system. Because of their negligible final-state interactions with the hadronic environment, once produced it brings the electromagnetic particles about to escape unscathed carrying the clean information of all stages of the collision(described in Sec. 1.3). The EM radiations produce all stages of collision process contribute to the measured photon spectra, in principle a careful analysis may be useful to uncover the whole space-time history of nuclear collision. Hence EM radiations - real and the virtual photons (dilepton), are considered as efficient probes to study dynamical evolution of the matter formed in relativistic heavy ion collision [39, 40, 41, 42, 43, 44, 45, 65]. However, as they are emitted continuously, they sense in fact the entire space-time history of the reaction. This expectation has led to an intense and concerted efforts toward the identification of various sources of such radiations. While initially this signals ware treated as *thermometer* of the dense medium created, but later on recent investigations and calculations suggest it might serve qualitatively as *chronometer* [63] and *flow-meter* [64] of HIC.

3.2 Various Sources of EM Radiations

As argued previously that EM radiations emerge out copiously from all stages of collision, so in order to proceed, it is useful to identify various sources of photons and dileptons produced in the HIC. So the "inclusive" photon spectrum coming from such collision in usual sense can be defined as: the unbiased photon spectrum observed in pp, pA or AA collision. This spectrum is built up from a cocktail of various components (discussed below). Depending on their origin, there are two different types of sources which is schematically presented in Fig. 3.1, i.e. "direct photons" and " photons from decay

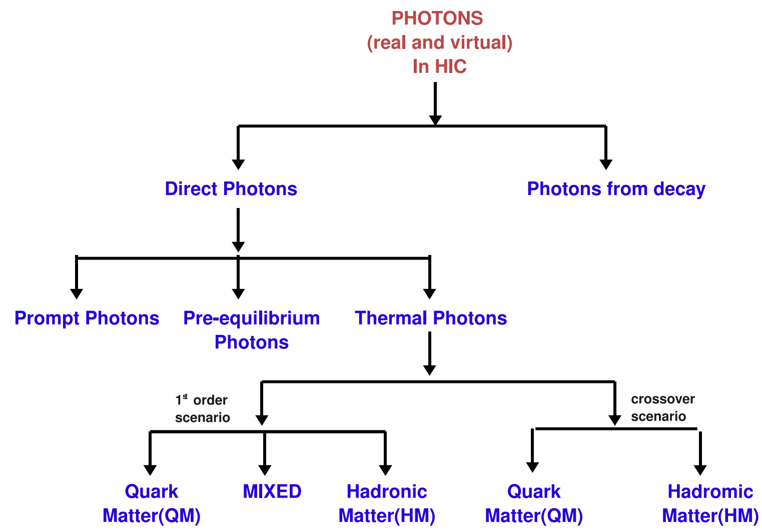

Figure 3.1: Various sources of photons

of hadrons". The term "direct photons" meant for those photons and dileptons which produce directly from collision between the particles. One can subdivide this broad category of "direct photons" into "prompt photons", "pre-equilibrium photons" and "thermal photons" depending on their origin. On the other hand, the decay photons don't come directly from the collision, rather from the decay of hadrons.

3.2.1 (A)Transverse Momentum (p_T) Dependence of EM Radiations:

The EM spectra provided by the experimentalist are mingled with various sources of photons and dileptons and it is difficult to distinguish different sources experimentally. However, real interest lies in the thermal photons and dileptons since it is expected to render an information about the initial condition and the history of evolution of the plasma while it cools and hadronizes. Thus, theoretical models are used with great advantage to identify these sources of photons and their relative importance and characteristics in the spectrum. As indicated in Fig. 3.2, the high p_T part of the spectra is

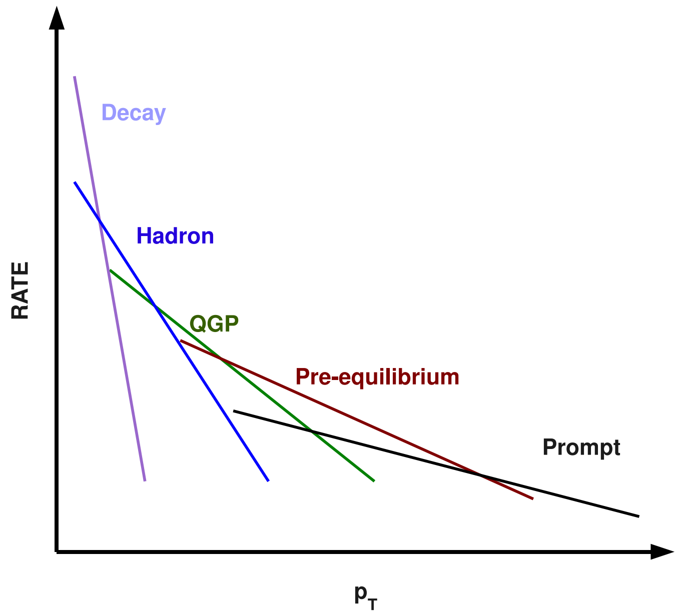

Figure 3.2: Schematic diagram of different sources of photon production in heavy ion collision as function of transverse momentum (p_T).

strongly dominated by prompt contributions and low p_T domain is populated by EM radiations from decay and the thermal photons and dileptons originate from the intermediate p_T. So subtracting out the prompt and decay contributions from the measured inclusive spectra of photons and dileptons, one can get pure contribution coming from the thermalized matter. Theoretically photons and dileptons emerging from QGP and hadronic phase can be calculated separately (will be discussed later). And the calculations based on theory infer that the photons and lepton pairs form hadronic matter dominate the spectrum at lower p_T ($\sim 1-2$ GeV) whereas photons and dileptons form QGP dominate in the intermediate p_T range , i.e. $p_T \sim 2-3$ GeV (depending on the models) [66].

- **Prompt Photons and Dileptons :**

The *prompt* photons and dileptons are produced from the hard collisions between the partons inside the nucleons of the incoming nuclei in early collision stage before the system thermalizes. It is the best understood part of the photons and dileptons production as can be regulated by perturbative QCD technique. The associated spectrum has power law kind of behaviour and dominates at large transverse momentum region (as shown in Fig. 3.2). Large momentum transfer results in small coupling constant which justifies the use of perturbative techniques. However, hadrons take part in experiments rather than partons. In non-perturbative regime, the theoretical calculation of momentum distribution of partons inside hadrons is beyond ones' ability. Inevitably, one must find the platform where the void between what can be measured experimentally and what can be calculated perturbatively can be interconnected. So *factorization method* is the technique where one can interlink the short-distance (perturbative) part with the long-distance (non-perturbative) and expresses as follows [12]:

$$d\sigma = F(\mu, \Lambda_{QCD}) \otimes d\hat{\sigma}(Q, \mu) \tag{3.1}$$

where the $\hat{\sigma}$ can be calculated perturbatively as a function of α_s treating the scattering process of parton interaction. The other factor, $F(\mu, \Lambda_{QCD})$, contains all long distance effects. Although $F(\mu, \Lambda_{QCD})$ depends on α_s in this case become large enough resulting non-perturbative situation and must, therefore, be obtained from data of various type of hard scattering process. The factorization scale μ is an arbitrary parameter. It can be thought of as a scale which separates the long and short-distance physics. Thus a parton emitted with a small transverse momentum, less than the scale μ, is considered part of hadron structure and is absorbed into the parton distribution function.

The prompt photon contributions basically come from (i)Compton scattering ($qg \rightarrow g\gamma$), (ii)quark anti-quark annihilation process ($q\bar{q} \rightarrow g\gamma$) and quark fragmentation ($q \rightarrow q\gamma$) of the partons of the nucleons in colliding nuclei (shown in Fig. 3.3) and can be well described by the techniques of pQCD [67].

The invariant cross section of the reaction($A + B \rightarrow \gamma + anything$) can be written in

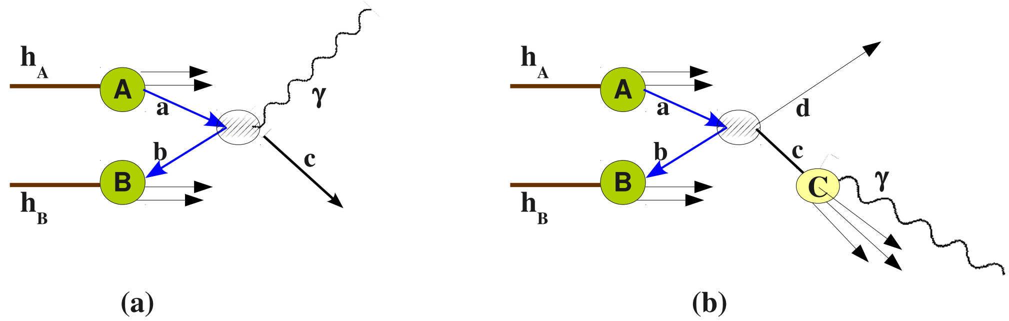

Figure 3.3: The inclusive photon production in collision of particles A and B in partonic level by the direct partonic subprocess and the fragmentation of partons is shown in (a) and (b) respectively.

the factorized form as follows [68]:

$$E_\gamma \frac{d\sigma}{d^3p_\gamma} = \sum_{a,b,c} \int [dx_a dx_b F_1^a(x_a,\mu) F_2^b(x_b,\mu) \times \{E_\gamma \frac{d\hat{\sigma}}{d^3p_\gamma}(a+b\to\gamma)$$
$$+ \int dz_c E_\gamma \frac{d\hat{\sigma}}{d^3p_\gamma}(a+b\to c) D_3^c(z_c,\mu)\}], \tag{3.2}$$

where a, b and c stands for the partons, $F_{1,2}(x,\mu)$ is the parton distribution functions and $D_3(z,\mu)$ is the fragmentation function. In the Eq. 3.2, the leading order cross-sections are considered for the total contribution from the photon productions and has been written in terms of two different terms. The first one expresses the direct partonic process ($ab \to \gamma$ is illustrated in Fig 3.3 (a)), Compton scattering and annihilation processes of quark and anti-quark and the second term represents quark fragmentation process ($ab \to c$ is shown in Fig 3.3 (b)).

The process of high-mass lepton pair emerging from $q\bar{q}$ annihilation in a proton-proton collision is described by *Drell Yan process* [69] (illustrated in Fig. 3.4) and is the best understood part of production of dilepton.

In the naive parton model, the invariant cross-section for producing lepton pair l^+l^-

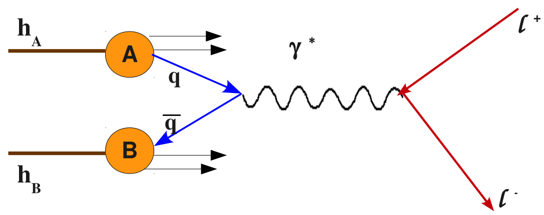

Figure 3.4: The Drell Yan process: $q\bar{q} \rightarrow l^+l^-$

with large invariant mass-squared, $M^2 = (p_{l^+} + p_{l^-})^2 \gg 1\text{GeV}^2$, in the collision of beam A and target B is simply obtained by simply weighing the subprocess invariant cross-section for $q\bar{q} \rightarrow \gamma^* \rightarrow l^+l^-$ with parton distribution functions $f_q(x, M^2)$ and $f_{\bar{q}}(x, M^2)$ extracted from deep inelastic scattering and summing over all quark anti-quark combination in beam and target.

$$E_\gamma \frac{d\sigma_{AB}}{d^3p_\gamma} = \sum_q \int dx_1 dx_2 f_q(x_1, M^2) f_{\bar{q}}(x_2, M^2) E \frac{d\sigma^{\hat{q}}_{DY}}{d^3p} \tag{3.3}$$

where the partonic invariant cross-section for $q+\bar{q} \rightarrow l^+l^-$ is calculated using pQCD [68].

The prompt photons and dileptons from Drell-Yan processes can be estimated from pQCD and the experimental results from pp collisions (at same $\sqrt{s_{NN}}$) may be used to check the validation of the calculation. The production of high p_T photon in A-A collision may be expressed in terms of p-p yield by using the following relation,

$$\frac{dN^{AA}}{d^2p_T dy} = \frac{N_{coll}(b)}{\sigma^{pp}_{in}} \frac{d\sigma^{NN}}{d^2p_T dy} = T_{AA}(b) \frac{d\sigma^{NN}}{d^2p_T dy} \tag{3.4}$$

where, $T_{AA}(b)$ is thickness function, $N_{coll}(b)$ is the number of inelastic nucleon-nucleon collision and σ^{NN}_{in} is the inelastic cross-section of nucleon-nucleon (calculated using pQCD). The $T_{AA}(b)$ and $N_{coll}(b)$ can be calculated using Glauber model [53].

- **Pre-equilibrium Photons and Dileptons :**

The *pre-equilibrium photons and dileptons* are produced in the pre-equilibrium stage where $\tau \leq \tau_i$ (described in Section. 1.3), where τ_i is the thermalization time, i.e., before the thermalization sets in the system. In the present work thermalization time scale at RHIC (τ_i=0.6 fm/c) and LHC (τ_i=0.1 fm/c) energies are taken to be very small. In such scenario the contribution from pre-equilibrium stage will be very small and hence neglected.

- **Thermal Photons and Dileptons :**

At $\tau \geq \tau_i$, the system is produced in QGP phase and with expansion it reverts to hot hadronic gas at a temperature $T \sim T_c$. Thermal equilibrium may be maintained in the hadronic phase until the mean free path remains comparable to the system size. The EM radiations emerge from these thermalized matter (color shaded portion of Fig. 1.8), i.e. from both quark matter (QM) above T_c and hadronic matter (HM) when $T \leq T_c$ is known as *thermal* photons or dileptons.

Thermal photons from the QM arise mainly due to annihilation ($q\bar{q} \rightarrow g\gamma$) and Compton ($q(\bar{q})g \rightarrow q(\bar{q})\gamma$) processes [66, 70, 71]. Later, it was shown that photons from the processes [72]: $gq \rightarrow gq\gamma$, $qq \rightarrow qq\gamma$, $qq\bar{q} \rightarrow q\gamma$ and $gq\bar{q} \rightarrow g\gamma$ contribute in the same order $O(\alpha\alpha_s)$ as Compton and annihilation processes. The relevant reactions and decays for photon production from HM are: (i) $\pi\,\pi \rightarrow \rho\,\gamma$, (ii) $\pi\,\rho \rightarrow \pi\gamma$ (with all possible mesons in the intermediate state [73]), (iii)$\pi\,\pi \rightarrow \eta\,\gamma$ and (iv) $\pi\,\eta \rightarrow \pi\,\gamma$, $\rho \rightarrow \pi\,\pi\,\gamma$ and $\omega \rightarrow \pi\gamma$. [44, 46, 73, 74, 75]. The reactions involving strange mesons: $\pi\,K^* \rightarrow K\,\gamma$,$\pi\,K \rightarrow K^*\,\gamma$, $\rho\,K \rightarrow K\,\gamma$ and $K\,K^* \rightarrow \pi\,\gamma$ [46] are also responsible for the production of thermal photons from hot hadron gas. Contributions from other decays, such as $K^*(892) \rightarrow K\,\gamma$, $\phi \rightarrow \eta\,\gamma$, $b_1(1235) \rightarrow \pi\,\gamma$, $a_2(1320) \rightarrow \pi\,\gamma$ and $K_1(1270) \rightarrow \pi\,\gamma$ have been found to be small [76] for $p_T > 1$ GeV. Like photons, the production of lepton pairs from hot QGP is dominated by $q\bar{q} \rightarrow \gamma^* \rightarrow l^+l^-$ [77, 78, 79] and in the hadronic matter the dominant processes are the decay of light vector mesons (ρ, ω and ϕ); i.e. $\rho \to l^+l^-$, $\omega \to l^+l^-$ and $\phi \to l^+l^-$. [45, 42, 80, 81, 82]

The schematic representation in Fig. 3.2 shows an exponential damping of the thermal photons spectrum at large energy. As the photons from hadronic phase dominate the spectra in low p_T (< 1 GeV), so there is small window around $p_T \sim 2-3$GeV for the detection of contribution from QGP. Disentangling the thermal photons coming out only from QGP phase is not trivial.

• **Photons and Dileptons from Decay :**

The thermal photons are emitted from the hot hadron gas until the freeze out temperature is reached. After the freeze-out of the fireball, photons and dileptons are also produced from the decays of long lived (compared to strong interaction time scale) hadrons and known as "*photons from decay*". For example, photons are produced from the decays like $\pi^0 \to \gamma\gamma$ and $\eta^0 \to \gamma\gamma$ etc. Similarly dileptons are produced from the the process $\pi^0 \to \gamma e^+e^-$, $\eta^0 \to \gamma e^+e^-$ and $\omega \to \gamma e^+e^-$ etc. are commonly known as Dalitz decays. The experimentally measured photon spectra are highly contaminated by the huge background from the decays. This makes the disentanglement of the thermal photon a more challenging task .

WA98 collaboration follows the subtraction method using invariant mass analysis [83] for all photons for each pair p_T bin. The photon-pair combinatorial background is estimated by event mixing and then the decay photon from the real pair spectra is subtracted out. The yield in the π^0 mass peak is extracted to obtain the raw neutral pion p_T spectra. These are then corrected for conversions, for π^0 identification. In addition, ηs' are extracted in a limited transverse momentum range with an analogous procedure. The final inclusive photon spectra are to check for a possible photon excess beyond that form long-lived radiative decays. The background calculations are based on π^0 spectra and measured η/π^0-ratio. The spectral shapes of other hadrons having radiative decays are calculated assuming m_T scaling with yield relative to π^0's taken from the measurement. It should be noted that the measured contribution (from π^0, η) amounts to $\approx 97\%$ of the total photon background.

The major problem while performing invariant mass analysis arises from the accidental (false) photon pairs giving rise to pion mass and it is not possible to distinguish them from the correlated pairs in this method [65]. To overcome this problem, a mixed event analysis [84] procedure has been used successfully. The basic idea of mixed event technique is to compare particle spectrum from one event to the result for particle combinations from different events, which are *a priori* not correlated. As a first step, properly normalized mixed events are constructed by randomly sampling photons from different events. The difference of the invariant mass spectra of the real event and the mixed event then gives the pion and η distributions. Once again the decay photon spectrum is subtracted from the inclusive photon spectrum to get the direct photons.

An alternative approach of separating direct photons from decay background is by measuring the "quasi-real" virtual photons which appear as low mass electron-positron pair. It is assumed that any source of real photons also produces low mass virtual photons which decay into e^+e^- pair. This method is known as internal conversion method [85, 86]. The key advantage of this method is the greatly improved signal to background ratio which is achieved by elimination of the contribution of Dalitz (π^0) decay. The experimentally measured quantity is the ratio of e^+e^- pairs in a particular invariant mass bin and the direct photon spectrum is obtained by multiplying $\gamma^*_{dir}/\gamma^*_{incl}$ to the measured inclusive photon spectrum. Tagging of decay photons is another very useful method used by experimentalists for the subtraction of decay background [87].

Characteristics of Invariant Momentum Distribution and Effect of Flow on It :

The invariant momentum distribution of photons and dileptons produce from a thermal source depends on the temperature (T) of the source through the thermal phase space distributions of the participants of the reaction that produces the photons and dileptons [53]. As a result the p_T spectra of thermal photons and dileptons reflects the temperature of the source through the phase space factor ($e^{-E/T}$). Hence ideally the photons with intermediate p_T values ($\sim 2-3$ GeV, depending on the value of initial temperature) reflect the properties of QGP (realized when $T > T_c$, T_c is the transition temperature). Therefore, one should look into the p_T spectra for these values of p_T for the detection of QGP. However, for an expanding system the situation is far more complex. The thermal phase space factor changes by flow *e.g.* the transverse kick received by low p_T photons due to flow originating from the low temperature hadronic phase (realized when $T < T_c$) populates the high p_T part of the spectra [88]. As a consequence the intermediate or the high p_T part of the spectra contains contributions from both QGP and hadrons. Thus it is not easy task to disentangle the photons coming from pure partonic phase. However, the p_T integrated invariant mass spectra of dilepton may be useful to extract properties of QGP.

3.2.2 (B)Invariant Mass(M) Dependence of EM Radiations:

Being massive, dileptons make situation different from photons. They have two kinematic variables - p_T and M. Out of these two, the p_T spectra is affected by the flow, however, the p_T integrated M spectra remain unaltered by the flow in the system. It should be mentioned here that for M below ρ peak and above ϕ peak dileptons from QGP dominates over its hadronic counterpart (assuming the contributions from hadronic cocktails are subtracted out) if the medium effect of spectral function of the low mass vector mesons are not taken into account. However, the spectral function of low mass vector mesons (mainly ρ) may shift toward lower invariant mass region due to non-zero temperature and density effects. As a consequence the contributions from the decays of ρ mesons to lepton pairs could populate the low M window and may dominate over the contributions from the QGP phase [45, 42, 89]. All these suggests that the invariant mass distribution of dilepton can be used as a clock for HIC and a judicious choice of p_T and M windows will be very useful to characterize the flow in QGP and hadronic phase.

Obtaining the dilepton invariant mass distributions from experimental data is technically very challenging because of the small dilepton-decay branching ratios of ρ, ω, and ϕ mesons as there are many other hadronic sources available those produce leptons. The detector therefore must have an excellent lepton identification capability to detect the dileptons. It must also provide a means to successfully isolate the combinatorial background, where the background caused by an l^+ being erroneously paired up with an l^- from other origin (e.g., a e^+ from $\pi^0 \to \gamma e^+ e^-$ paired up with an e^- from $\gamma^* \to e^+ e^-$ occurring in the same event) [90]. This combinatorial background is found to be very large, specially in the high energy heavy ion collision experiments. The PHENIX experiment (for e^+e^-) at RHIC has reported a signal to background ratio of about 1/100 for minimum bias Au+Au collisions at 200A GeV [90, 91]. To subtract this combinatorial background, methods like event mixing, like-sign pair subtraction are quite useful [92]. However, a broad continuous background due to Dalitz decays still populate the dilepton invariant mass spectrum. The measured distribution is compared with the *hadronic cocktail* (which contains all known sources of l^+l^- pairs produced in the detector acceptance) in order to extract the vector-meson contributions [90].

The measured dilepton spectra can be divided into several phases. Depending on the invariant mass of the emitted dileptons, it can be classified into three distinct regimes (discussed below [42]) and a schematic diagram of dilepton mass distribution is shown in Fig 3.5.

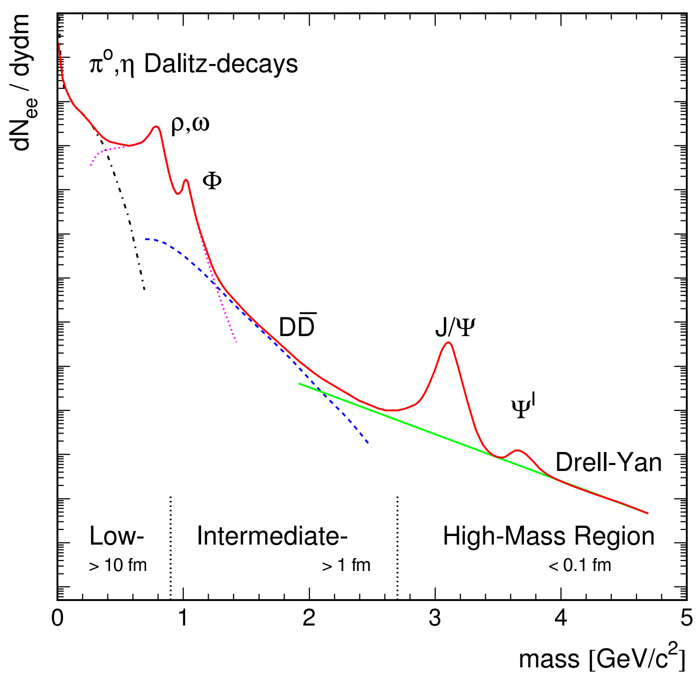

Figure 3.5: Expected different sources of dilepton production in heavy ion collision as function of invariant mass [42].

- **High Mass Region(HMR):**($M \geq M_{J/\Psi}(= 3.1GeV)$, $p_T \sim 3-5GeV$)

  The HMR region corresponds to early pre-equilibrium phase ($\tau < \tau_i$), where the lepton pairs are produced with large invariant mass ($M > 3$ GeV) and the dominant contributions are from the hard scattering between the partons, like Drell Yan annihilation [69]. The final abundance of the heavy quarkonia ($J/\Psi, \Upsilon$) and their contribution to the spectrum is suppressed due to the Debye screening and as a result the bound states are dissolved.

- **Intermediate Mass Region(IMR):** ($M_\phi \leq M \leq M_{J/\Psi}$, $p_T \sim 1-3GeV$)

  Thermalization is achieved in the system after a time scale ($> \tau_i$). In this domain, the dileptons from the QGP are produced from via quark-antiquark annihilation dominates. In this regime, due to higher temperature the continuum radiation from QGP dominates the dilepton mass spectrum and thus this region is important for the detection of QGP. The decays of "open charm "mesons, i.e, pairwise produced $D\bar{D}$ mesons [93] followed by semileptonic decays contribute a large in this domain of M. Although an enhanced charm production is interesting in itself -probably related to the very early collision states - it may easily mask the thermal plasma signal. To some what lesser extent, this also hold true for the lower-mass tail of Drell-Yan production [69]. As the heavy quarks produced in HIC do not get thermalized so their contribution may be estimated from pp collision data with the inclusion of nuclear effects like shadowing etc.. Hence they do not become part of the flowing QGP, then the lepton pairs which originate from the decays of heavy flavors will not contribute to flow [94]. Thus, the lepton pairs produced from the decays of heavy flavors and Drell Yann have been ignored in the present work.

- **Low Mass Region(LMR):**($M \leq M_\phi(= 1.02GeV)$, $p_T < 1GeV$)

  With subsequent expansion and cooling, the QGP converts into a hot hadron gas at the transition temperature, T_c. At later stages, the dileptons are preferentially radiated from hot hadron gas from the decay of (light) vector meson, such as the ρ, ω and ϕ. The low M domain of the lepton pairs are dominated by the decays of ρ. Medium modification of ρ will change the yield in this domain of M. The change of ρ spectral function is connected with the chiral symmetry in the bath, therefore the measurement of low M lepton pairs has great importance to study the chiral symmetry restoration [95] at high temperature and density. Thus the invariant mass of the lepton pair directly reflects the mass distribution of the light vector mesons. This explains the distinguished role that vector mesons in conjunction with their in-medium modifications play for dilepton measurements in HIC.

So far, we have discussed the different sources of photons and dileptons. Usually, the decay contribution is subtracted out from the measured inclusive spectra of photons and dileptons and the hard contribution is controlled by pQCD. As QGP is expected to form in the HIC experiments, so the basic intention of the present study to study the properties of QGP. Therefore, we have emphasized more on the study of thermal photons and dileptons in this dissertation. The detailed study of the emission of thermal photons and dileptons coming from HIC has been carried out in the subsequent sections.

3.3 Formulation of Thermal Emission Rate of EM Radiations

The importance of the electromagnetic probes for the study of thermodynamic state of the evolving matter was first proposed by Feinberg in 1976 [96]. Feinberg showed that the emission rates can be related to the electromagnetic current-current correlation function in a thermalized system. Generally the production of a particle which interacts weakly with the constituents of the thermal bath (the constituents may interact strongly among themselves) can always be expressed in terms of the discontinuities or imaginary parts of the self energies of that particle [97]. In this section, therefore, there is a discussion on how the electromagnetic emission rates (real and virtual photons) is related to the photon spectral function (which is connected with the discontinuities in the interacting propagators) in a thermal system [41], which in turn is connected to the hadronic electromagnetic current-current correlation function [39] through Maxwell equations. It will be shown that the photon emission rate can be obtained from the dilepton emission rate by appropriate modifications.

We begin our discussion with the dilepton production rate which is given by [39, 44, 45]

$$\frac{dN_{l^+l^-}}{d^4xd^4p} \equiv \frac{dR}{d^4p} = L^{\mu\nu}(p)W_{\mu\nu}(p) \ , \tag{3.5}$$

where $L^{\mu\nu}(p)$ is lepton tensor and obtained as

$$\begin{aligned} L^{\mu\nu}(p) &= \frac{(4\pi\alpha)^2}{M^4}\int \frac{d^3p_1}{(2\pi)^3 2p_1^0}\,\frac{d^3q_2}{(2\pi)^3 2q_2^0} Tr\left[(\not{p}_1 - m)\gamma^\mu(\not{p}_2 + m)\gamma^\nu\right]\delta^{(4)}(p - p_1 - p_2) \\ &= -\frac{\alpha^2}{6\pi^3 M^2}\left(g^{\mu\nu} - \frac{p^\mu p^\nu}{M^2}\right) L(M^2) \end{aligned} \tag{3.6}$$

with $p^0_{1,2} = (m^2_{l^\pm} + \vec{q}^{\,2}_{1,2})^{1/2}$ and the factor $L(M^2) = (1 + 2m_l^2/M^2)\sqrt{1 - 4m_l^2/M^2}$ arises from the Dirac spinors (lepton pair) in the final state . $L(M^2) = 1$ by neglecting the rest mass of the leptons ($m_{l^\pm}$ is considered as $m_{e^\pm}$)as compared to their individual 3-momenta $|\vec{p}_1|$, $|\vec{p}_2|$. $M^2 = (p_1 + p_2)^2$ is the total four-momentum square of the pair in the heat bath. The effect of the partonic and hadronic medium is encoded in the tensor $W_{\mu\nu}(p)$. It is obtained from the (thermal) average of the electromagnetic current-current correlation function as

$$W_{\mu\nu}(p) = \int d^4x\, e^{-ipx}\langle j^{em}_\mu(x) j^{em}_\nu(0)\rangle \tag{3.7}$$

$W_{\mu\nu}(p)$ contains the effect of strong interactions and is related to the imaginary part of the retarded current-current correlation function through the following relation;

$$W_{\mu\nu} = (-2) f_{BE}(p_0, T)\mathrm{Im}\Pi^{\mathrm{em}}_{\mu\nu} \tag{3.8}$$

Inserting Eqs. 3.6 and 3.8 into 3.5, and exploiting gauge invariance, $p^\mu \Pi^{em}_{\mu\nu} = 0$, one obtains the general result

$$\frac{dR_{l^+l^-}}{d^4p} = -\frac{\alpha^2}{3\pi^3 M^2}\ f_{BE}(p_0; T)\ \mathrm{Im}\Pi^{\mathrm{em}}(\mathrm{p}_0, \vec{\mathrm{p}}) \tag{3.9}$$

with $f_{BE}(p_0,T) = 1/(e^{p_0/T}-1)$ the Bose distribution function and the imaginary part of the EM current-current correlator is related to EM spectral function .

To obtain the real photon emission rate per unit volume (dR) from a system in thermal equilibrium we note that the dilepton emission rate differs from the photon emission rate in the following way. The factor $e^2L_{\mu\nu}/p^4$ which is the product of the electromagnetic vertex $\gamma^* \rightarrow l^+ l^-$, the leptonic current involving Dirac spinors and the square of the photon propagator should be replaced by the factor $\sum \epsilon_\mu \epsilon^*_\nu (= -g_{\mu\nu})$ for the real (on-shell) photon. Finally the phase space factor $d^3q_1/[(2\pi)^3 E_1]\, d^3q_2/[(2\pi)^3E_2]$ should be replaced by $d^3p/[(2\pi)^3 p_0]$ to obtain

$$dR = -\frac{e^{-\beta p_0}}{2(2\pi)^3}\, g^{\mu\nu}\, W_{\mu\nu}\, \frac{d^3p}{p_0}. \tag{3.10}$$

As in the case of dileptons this expression can be reduced to

$$p_0\frac{dR}{d^3p} = \frac{\alpha}{2\pi^3} g^{\mu\nu}\ f_{BE}(p_0;T)\ \mathrm{Im}\Pi^{\mathrm{em}}_{\mu\nu}. \tag{3.11}$$

The emission rate given above is correct up to order e^2 in electromagnetic interaction but exact, in principle, to all order in strong interaction. However, for all practical purposes one is able to evaluate up to a finite order of loop expansion. Now it is clear from the above results that to evaluate photon and dilepton emission rate from a thermal system we need to evaluate the imaginary part of the photon self energy. The Cutkosky rules at finite temperature or the thermal cutting rules [98, 99, 100] give a systematic procedure to calculate the imaginary part of a Feynman diagram. The Cutkosky rule expresses the imaginary part of the n-loop amplitude in terms of physical amplitude of lower order ($n-1$ loop or lower). This is shown schematically in Fig. (3.6). When the imaginary part of the self energy is calculated up to and including L order loops where L satisfies $x + y < L + 1$, then one obtains the photon emission rate for the reaction x particles $\rightarrow y$ particles $+\gamma$ and the above formalism becomes equivalent to the relativistic kinetic theory formalism [40]. For a reaction $1 + 2 \rightarrow 3 + \gamma$ the photon (of energy E) emission

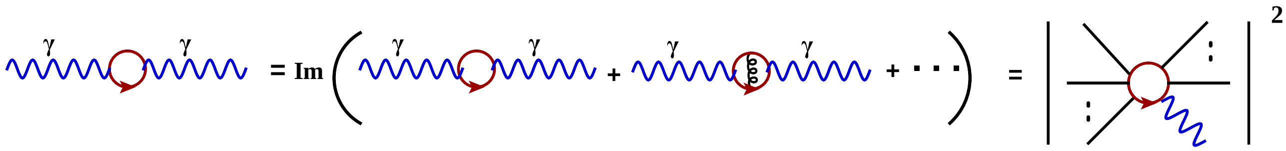

Figure 3.6: Optical Theorem in Quantum Field Theory

rate is given by [73]

$$E\frac{dR}{d^3p} = \frac{\mathcal{N}}{16(2\pi)^7 E}\int_{(m_1+m_2)^2}^{\infty} ds \int_{t_{\min}}^{t_{\max}} dt\,|\mathcal{M}|^2 \int dE_1 \times \int dE_2 \frac{f(E_1)\,f(E_2)\,[1+f(E_3)]}{\sqrt{aE_2^2+2bE_2+c}}, \tag{3.12}$$

where

$$\begin{aligned}
a &= -(s+t-m_2^2-m_3^2)^2 \\
b &= E_1(s+t-m_2^2-m_3^2)(m_2^2-t)+E[(s+t-m_2^2-m_3^2)(s-m_1^2-m_2^2) \\
&\quad -2m_1^2(m_2^2-t)] \\
c &= -E_1^2(m_2^2-t)^2-2E_1E[2m_2^2(s+t-m_2^2-m_3^2)-(m_2^2-t)(s-m_1^2-m_2^2)] \\
&\quad -E^2[(s-m_1^2-m_2^2)^2-4m_1^2m_2^2]-(s+t-m_2^2-m_3^2)(m_2^2-t) \\
&\quad \times(s-m_1^2-m_2^2)+m_2^2(s+t-m_2^2-m_3^2)^2+m_1^2(m_2^2-t)^2 \\
E_{1\min} &= \frac{(s+t-m_2^2-m_3^2)}{4E}+\frac{Em_1^2}{s+t-m_2^2-m_3^2} \\
E_{2\min} &= \frac{Em_2^2}{m_2^2-t}+\frac{m_2^2-t}{4E} \\
E_{2\max} &= -\frac{b}{a}+\frac{\sqrt{b^2-ac}}{a}.
\end{aligned}$$

$\mathcal{N}$ is the overall degeneracy of the particles 1 and 2, $\mathcal{M}$ is the invariant amplitude of the reaction (summed over final states and averaged over initial states), f denotes the thermal distribution functions and s, t, u are the usual Mandelstam variables.

In a similar way the dilepton emission rate for a reaction $a\,\bar{a}\;\rightarrow\;l^+\,l^-$ can be obtained as

$$
\begin{aligned}
\frac{dR}{d^4p} \quad = \quad & \int \frac{d^3p_a}{2E_a(2\pi)^3} f(p_a) \int \frac{d^3p_{\bar{a}}}{2E_{\bar{a}}(2\pi)^3} f(p_{\bar{a}}) \int \frac{d^3p_1}{2E_1(2\pi)^3} \int \frac{d^3p_2}{2E_2(2\pi)^3} \\
& \mid \mathcal{M} \mid^2_{a\bar{a}\to l^+l^-} (2\pi)^4 \delta^{(4)}(p_a + p_{\bar{a}} - p_1 - p_2)\delta^{(4)}(p - p_a - p_{\bar{a}}). \qquad (3.13)
\end{aligned}
$$

where $f(p_a)$ is the appropriate occupation probability for bosons or fermions.

3.4 Emission of Thermal Photons from Heavy Ion Collision

The *thermal* photons emerge just after the system thermalizes ($\tau > \tau_i$) from both QGP due to partonic interactions and hot hadrons (see Fig. 1.8) due to interactions among the hadrons. Now with the formalism given above production of thermal photons from QGP and hot hadronic gas is discussed in the section 3.4.1 and 3.4.2 respectively.

3.4.1 Photons Emission from Quark Gluon Plasma

The contribution from QGP to the spectrum of thermal photons due to annihilation ($q\bar{q} \to g\gamma$) and Compton ($q(\bar{q})g \to q(\bar{q})\gamma$) processes has been calculated in Refs. [66, 70] using hard thermal loop (HTL) approximation [71]. The rate of hard photon emission is then obtained as [66]

$$
E\frac{dR_\gamma^{QGP}}{d^3q} = \sum_f e_f \frac{\alpha\alpha_s}{2\pi^2} T^2\, e^{-E/T} \ln(2.912E/g_s^2T). \qquad (3.14)
$$

where α_s is the strong coupling constant. Later, it was shown that photons from the processes [72]: $gq \to gq\gamma$, $qq \to qq\gamma$, $qq\bar{q} \to q\gamma$ and $gq\bar{q} \to g\gamma$ contribute in the same order $O(\alpha\alpha_s)$ as Compton and annihilation processes (shown in Fig. 3.7). The complete calculation of emission rate from QGP to order α_s has been performed by

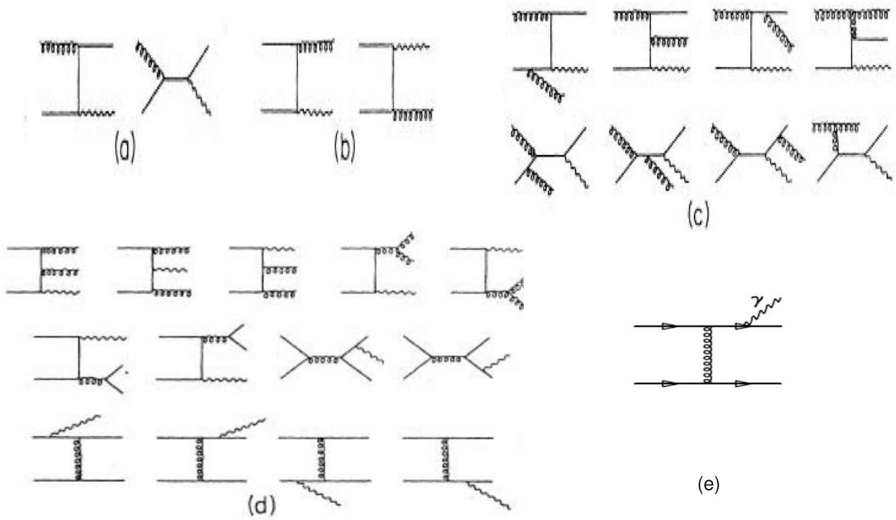

Figure 3.7: Partonic processes for production of photons.

resuming ladder diagrams in the effective theory [101]. In the present work this rate has been used. The temperature dependence of the strong coupling, α_s has been taken from [102].

3.4.2 Photons Emission from Hot Hadronic Gas

For the photon spectra from hadronic phase we consider an exhaustive set of hadronic reactions and the radiative decay of higher resonance states [73, 74, 75].

To evaluate the photon emission rate from a hadronic gas we model the system as consisting of π, ρ, ω and η. The relevant vertices for the reactions $\pi\,\pi \rightarrow \rho\,\gamma$ and $\pi\,\rho \rightarrow \pi\,\gamma$ and the decay $\rho \rightarrow \pi\,\pi\,\gamma$ are obtained from the following Lagrangian [74] (see Fig. 3.8):

$$\mathcal{L} = -g_{\rho\pi\pi}\vec{\rho}^{\mu}\cdot(\vec{\pi}\times\partial_\mu\vec{\pi}) - eJ^{\mu}A_{\mu} + \frac{e}{2}F^{\mu\nu}\,(\vec{\rho}_\mu\,\times\,\vec{\rho}_\nu)_3, \tag{3.15}$$

where $F_{\mu\nu} = \partial_\mu A_\nu - \partial_\nu A_\mu$, is the Maxwell field tensor and J^μ is the hadronic part of

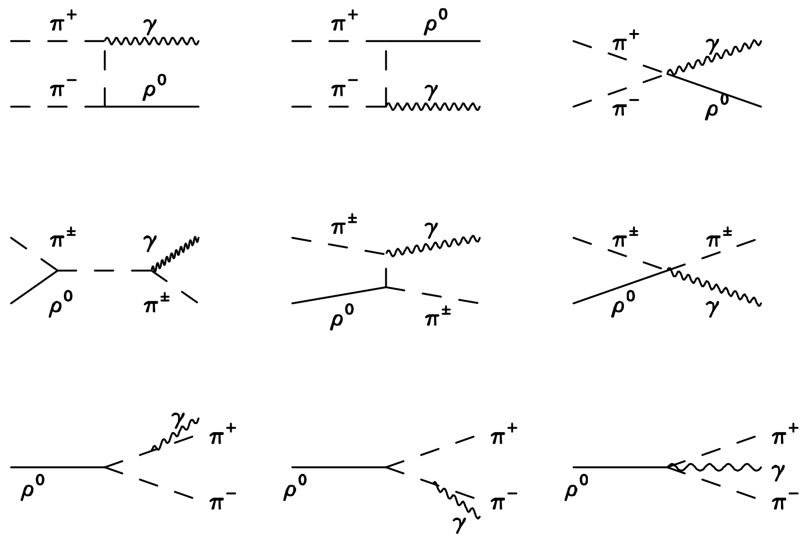

Figure 3.8: Photon producing reactions and decays in hadronic gas.

the electromagnetic current given by

$$J^{\mu} = (\vec{\rho}_{\nu} \times \vec{B}^{\nu\mu})_3 + (\vec{\pi} \times (\partial^{\mu}\vec{\pi} + g_{\rho\pi\pi}\vec{\pi} \times \vec{\rho}^{\mu}))_3 \tag{3.16}$$

with $\vec{B}_{\mu\nu} = \partial_{\mu}\vec{\rho}_{\nu} - \partial_{\nu}\vec{\rho}_{\mu} - g_{\rho\pi\pi}(\vec{\rho}_{\mu} \times \vec{\rho}_{\nu})$.

For the sake of completeness we have also considered the photon production due to the reactions $\pi\,\eta \to \pi\,\gamma$, $\pi\,\pi \to \eta\,\gamma$ and the decay $\omega \to \pi\,\gamma$ using the following interaction:

$$\mathcal{L} = \frac{g_{\rho\rho\eta}}{m_{\eta}}\,\epsilon_{\mu\nu\alpha\beta}\partial^{\mu}\rho^{\nu}\partial^{\alpha}\rho^{\beta}\eta + \frac{g_{\omega\rho\pi}}{m_{\pi}}\,\epsilon_{\mu\nu\alpha\beta}\partial^{\mu}\omega^{\nu}\partial^{\alpha}\rho^{\beta}\pi + \frac{em_{\rho}^2}{g_{\rho\pi\pi}}A_{\mu}\rho^{\mu} \tag{3.17}$$

The last term in the above Lagrangian is written down on the basis of Vector Meson Dominance (VMD) [103, 104]. To evaluate the photon spectra, we have taken the relevant amplitudes for the above mentioned interactions from Ref. [73, 74]. The effects of hadronic form factors [46] have also been incorporated in the present calculation. The reactions involving strange mesons: $\pi\,K^* \to K\,\gamma$, $\pi\,K \to K^*\,\gamma$, $\rho\,K \to K\,\gamma$ and $K\,K^* \to \pi\,\gamma$ [46, 76] have also been incorporated in the present work. Contributions from other decays, such as $K^*(892) \to K\,\gamma$, $\phi \to \eta\,\gamma$, $b_1(1235) \to \pi\,\gamma$, $a_2(1320) \to \pi\,\gamma$ and $K_1(1270) \to \pi\,\gamma$ have been found to be small [76] for $p_T > 1$ GeV.

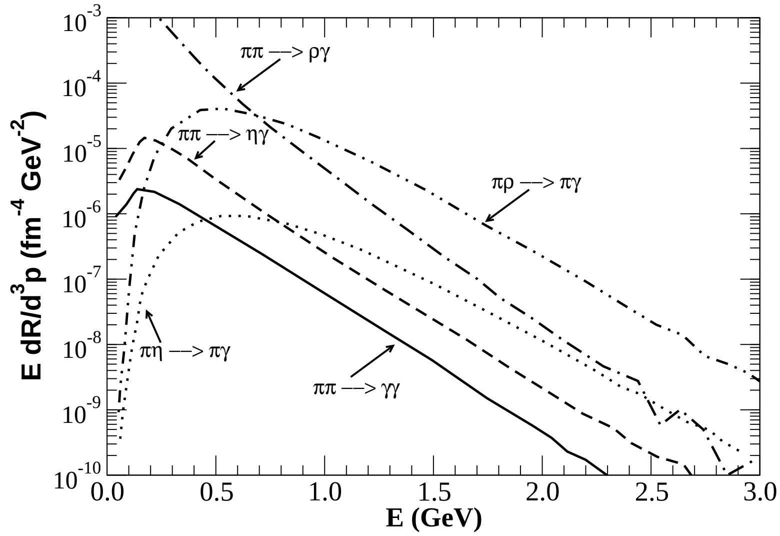

Figure 3.9: The static thermal emission rate for various photon producing hadronic reaction for $T = 200$ MeV [66].

With all photon producing hadronic reaction, the static thermal emission rate of photons for hadronic phase have been evaluated [46, 66, 73, 74, 101] and shown in Fig. 3.9 for $T = 200$ MeV. The reaction involving ρ mesons has dominant contribution. The rate at low photon energy is dominated by reaction with ρ in final state, because these reactions are endothermic with most of the available energy going into rho mass. At high photon energy reactions with the ρ in initial state are dominant because these reactions are because these reactions are exothermic; most of the rho mass is available for the production of high energy photons. Similar remarks can be made concerning reactions involving η mesons, but as the value of $g_{\rho\rho\eta}$ is smaller thus so are the rates. All the isospin combinations for the above processes have properly been implemented.

Emission of Photon from QM vs. HM

In Sec. 3.4.1 and 3.4.2, the static thermal emission rates of high energy photons producing from QGP and hadronic gas have been discussed. In Fig. 3.10, the thermal rates of QGP and hadron is compared at $T = 200$ MeV. However, the results indicate that the thermal rate of production of photons from QGP and hadron gas with energy $\approx\ 1-3$ GeV are similar. Not only in the shape of production curve but also the overall mag-

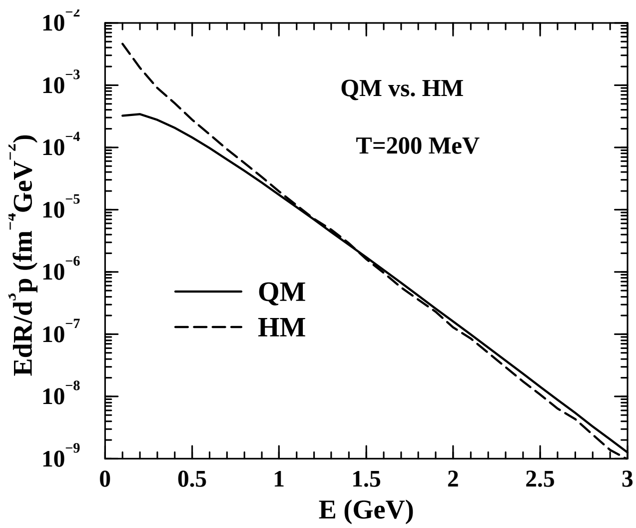

Figure 3.10: Comparison of photon spectrum produce from QGP and hot hadron gas at $T = 200$ MeV

nitude is same. The hadron gas shine as brightly as QGP. The conclusion is that high energy photons make a good " thermometer" for hot hadronic matter created in HIC. The thermal production rate only depend on temperature, so any temperature deduced from the thermally produced photons is nearly independent of the assumption about the phase of matter.

3.4.3 Total Invariant Momentum Spectra of Thermal Photons:

In this section we evaluate photon spectrum from a dynamically evolving system. The evolution of the system is governed by relativistic hydrodynamic. The photon production from an expanding system can be calculated by convoluting the static thermal emission rate with the expansion dynamics, which can be expressed as follows;

$$\frac{dN_\gamma}{d^2p_T dy} = \sum_i \int_i \left[\frac{dR_\gamma}{d^2p_T dy}(E^*, T)\right]_i d^4x \tag{3.18}$$

where the d^4x is the four volume. The energy, E^* appearing in Eq. 3.18 should be replaced by $u^\mu p_\mu$ for a system expanding with space-time dependent four velocity u^μ. Under the assumption of cylindrical symmetry and longitudinal boost invariance, u^μ can be written as;

$$\begin{aligned} u &= \gamma_T(\tau, r)(t/\tau, v_r(\tau, r), z/\tau) \\ &= \gamma_T(M_T \cosh\eta, u_x, u_y, M_T \sinh\eta) \\ &= \gamma_T(M_T \cosh\eta, v_r \cos\phi, v_r \sin\phi, M_T \sinh\eta) \end{aligned} \tag{3.19}$$

where $v_r(\tau, r)$ is the radial velocity, $\gamma_r(\tau, r) = (1 - v_r(\tau, r))^{-1/2}$ and therefore, for the present calculations,

$$u^\mu p_\mu = \gamma_r(M_T \cosh(y - \eta) - v_r p_T \cos\phi) \tag{3.20}$$

For massless photon the factor $u^\mu p_\mu$ can be obtained by replacing M_T in Eq. 3.20 by p_T. For the system produced in QGP phase reverts to hot hadronic gas at a temperature $T \sim T_c$. Thermal equilibrium may be maintained in the hadronic phase until the mean free path remains comparable to the system size. The term "$(dR/d^2p_Tdy)_i = [(...)f_{BE}]$" is the static rate of photon production [1], where i stands for quark matter (QM), mixed phase (M) (in a 1st order phase transition scenario) and hadronic matter (HM) respectively. The p_T dependence of the photon and dilepton spectra originating from an expanding system is predominantly determined by the thermal factor f_{BE}. The total momentum distribution can be obtained by summing the contribution from QM and HM, where the distribution for both the phases can be obtained by choosing the phase space appropriately.

The d^4x integration has been performed by using relativistic hydrodynamics with longitudinal boost invariance [24] and cylindrical symmetry [58] along with the inputs

[1] By conversion of variables $dp_xdp_ydp_z = Jdp_Tdyd\phi$, where $J = Ep_T, \Longrightarrow d^3p/E = 2\pi p_Tdp_T = d^2p_Tdy$.

Table 3.1: The values of various parameters - thermalization time (τ_i), initial temperature (T_i) and hadronic multiplicity dN/dy (the value of dN/dy for various beam energies and centralities are calculated from the Eq. 2.16) - used in the present calculations.

$\sqrt{s_{NN}}$	centrality	$\frac{dN}{dy}$	$\tau_i(fm)$	T_i(MeV)
17.3 GeV	0-06%	700	1.0	200
200 GeV	0-20%	496	0.6	227
	20-40%	226	0.6	203
	min. bias	184	0.6	200

(given in the Table 3.1) as the initial conditions (described in Section 2.3.1) for SPS and RHIC energies.

To estimate dN/dy for RHIC, we have taken $dn_{pp}/dy = 2.43$ and $x = 0.1$ at $\sqrt{s_{NN}} = 200$ GeV. It should be mentioned here that the values of dN/dy (through $N_{\rm part}$ and $N_{\rm coll}$ in Eq. 2.16) and hence the T_i (through dN/dy in Eq. 2.15) depend on the centrality of the collisions. For SPS, dN/dy is taken from experimental data [83]. We use the EoS obtained from the lattice QCD calculations by the MILC collaboration [105]. We consider kinetic freeze out temperature, T_f=140 MeV (here T_f is treated as a parameter) for all the hadrons. The ratios of various hadrons measured experimentally at different $\sqrt{s_{\rm NN}}$ indicate that the system formed in heavy ion collisions chemically decouple at $T_{\rm ch}$ which is higher than T_f which can be determined by the transverse spectra of hadrons [38](here the T_f is treated as a parameter). Therefore, the system remains out of chemical equilibrium from $T_{\rm ch}$ to T_f. The deviation of the system from the chemical equilibrium is taken in to account by introducing chemical potential for each hadronic species. The chemical non-equilibration affects the yields through the phase space factors of the hadrons which in turn affects the productions of the EM probes. The value of the chemical potential has been taken in to account following Ref. [106].

In the subsequent sections, we study the p_T distribution of photons and dileptons. As mentioned before, the relativistic hydrodynamics has been used to describe the space time evolution of the matter formed in HIC. The initial conditions of the hydrodynamics and the static rates are discussed earlier are constrained to reproduce the experimental data available from SPS and RHIC energies. Subsequently, the ratio of p_T spectra of photons and dileptons are used to extract the radial flow velocity (will be discussed in the next chapter).

3.4.4 Results and Discussion on p_T Distributions of Photons

For comparison with direct photon spectra as extracted from HIC two further ingredients are required. With all the ingredients we have reproduced the p_T spectra of direct photon for both SPS and RHIC energies. The prompt photons are normally estimated by using perturbative QCD. However, to minimize the theoretical model dependence here we use the available experimental data from p-p collisions to estimate the hard photon and normalized it to A-A data with $T_{AA}(b)$ for different centrality, i.e. the photon production from A-A collision and p-p collision are related through the following relation,

$$\frac{dN^{AA}}{d^2p_Tdy} = \frac{N_{coll}(b)}{\sigma_{in}^{pp}}\frac{d\sigma^{NN}}{d^2p_Tdy} = T_{AA}(b)\frac{d\sigma^{NN}}{d^2p_Tdy} \tag{3.21}$$

where $N_{coll}(b)$ is taken for the corresponding experiments and the the typical σ_{in}^{pp} (σ_{in}^{pp} 41mb for RHIC and 30mb for SPS).

Photon Spectrum for WA98 Collaboration :

The WA98 photon spectra from Pb+Pb collisions is measured at $\sqrt{s_{NN}} = 17.3$ GeV.

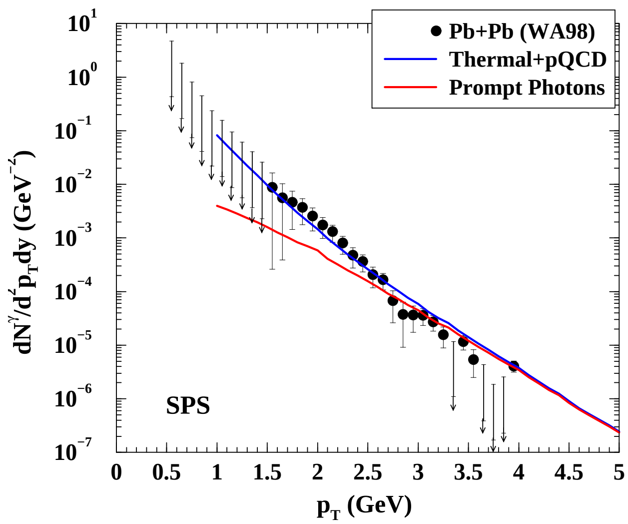

Figure 3.11: Transverse momentum spectra of photon at SPS energy for Pb+Pb collision at mid rapidity [107].

However, no data at this collision energy is available for pp interactions. Therefore, prompt photons for p+p collision at $\sqrt{s_{NN}}$ = 19.4 GeV has been used [108] to estimate the hard contributions for nuclear collisions at $\sqrt{s_{\mathrm{NN}}}$ = 17.3 GeV. Appropriate scaling [83] has been used to obtain the results at $\sqrt{s_{NN}}$ = 17.3 GeV. For the Pb+Pb collisions the result has been appropriately scaled by the number of collisions at this energy (this is shown in Fig. 3.11 as prompt photons). The high p_T part of the WA98 data is reproduced by the prompt contributions reasonably well. At low p_T the hard contributions under estimate the data indicating the presence of a thermal source. The thermal photons with initial temperature = 200 MeV along with the prompt contributions explain the WA98 data well (Fig. 3.11), with the inclusion of non-zero chemical potentials for all hadronic species considered [95, 106, 109]. In some of the previous works [110, 111, 112, 113, 114, 115] the effect of chemical freeze-out is ignored. As a result either a higher value of T_i or a substantial reduction of hadronic masses in the medium was required [110]. In the present work, the data has been reproduced without any such effects.

Photon Spectrum for PHENIX Collaboration :

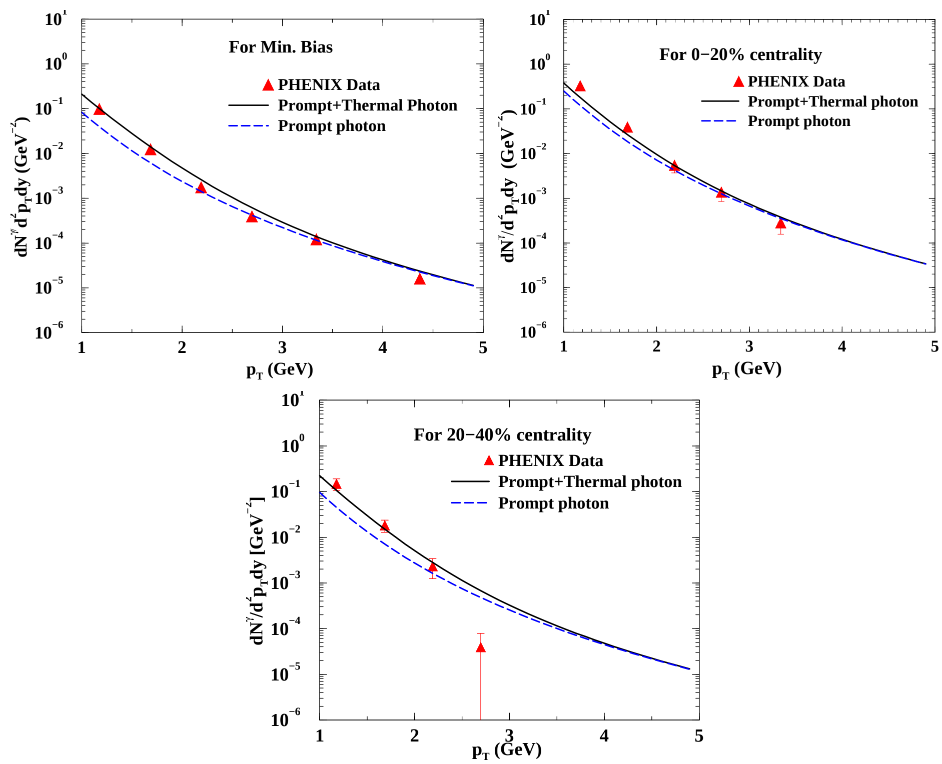

Figure 3.12: Transverse momentum spectra of photons at RHIC energy for Au-Au collision for different centralities at mid-rapidity. [107]

In Fig. 3.12, transverse momentum spectra of photons at RHIC energy for Au-Au collision for three different centralities (0-20 %, 20-40 % and min. bias.) at mid-rapidityi shown, where the red tangles are the direct photon data measured by PHENIX collaboration [85] from Au-Au collision at $\sqrt{s_{NN}} = 200$ GeV, blue dashed line is the contribution of the prompt photons and the black solid line is thermal + prompt photons. For the prompt photon contribution at $\sqrt{s_{NN}} = 200$ GeV, we have used the available experimental data from pp collision and normalized it to Au-Au data with $T_{AA}(b)$ for different centrality [116] (using Eq. 3.21). At low p_T the prompt photons under estimate the data indicating the presence of a possible thermal source. The thermal photons along with the prompt contributions explain the data [85] from Au-Au collisions at $\sqrt{s_{NN}} = 200$

GeV reasonably well. The reproduction of data is satisfactory (Fig. 3.12) for all the centralities with the initial temperature shown in Table 3.1 [117].

3.5 Emission of Thermal Dileptons from Heavy Ion Collision

Unlike real photon, dilepton are massive. Thus dilepton has two kinematic variables, invariant mass (M) and transverse momentum (p_T). Again, the p_T spectra is affected due to flow, whereas the p_T integrated M-spectra remain unaltered by flow. By tuning this two parameters, different stages of expanding fireball can be understood. Dileptons having large M and high p_T are emitted early from the hot zone of the system. On the other hand, those having lower M and p_T produced at later stage of the fireball when the temperature is low. Because of an additional variable, the invariant pair mass M, dileptons have the advantage over real photons [118].

The production of thermal dileptons from QGP (Sec. 3.5.1) and hot hadronic gas (Sec. 3.5.2) is described below.

3.5.1 Dileptons Emission from QGP

Above a critical temperature $T \geq T_c$, , the production of lepton pairs from thermal QM is dominated by the annihilation process of $q\bar{q} \to l^+l^-$. The static thermal emission rate of dilepton from QM is given by ($q\bar{q} \to \gamma^* \to l^+l^-$) [79] (also [77, 78]),

$$\frac{dR_{l^+l^-}}{d^4p} = -\frac{\alpha^2}{12\pi^4} L(M^2) f_{BE} \left(N_c \sum_f e_f^2 \left[1 + \frac{2T}{\vec{p}} ln \left(\frac{n_+}{n_-} \right) \right] \right) \tag{3.22}$$

where N_c (= 3) is the number of colors, e_f is the charge of the quark and $n_{\pm} = 1/\left(e^{(p_0 \pm |\vec{p}|/2T)+1}\right)$

3.5.2 Dileptons Emission from Hot Hadronic Gas

Below T_c, the appropriate degrees of freedom to describe strongly interacting matter are hadrons. In this regime, low M dileptons are produced from the hadronic interactions. In the HM, the hadronic current may be decomposed as

$$\begin{aligned} j^H_\mu &= \frac{1}{2}(\bar{u}\gamma_\mu u - \bar{d}\gamma_\mu d) + \frac{1}{6}(\bar{u}\gamma_\mu u + \bar{d}\gamma_\mu d) - \frac{1}{3}\bar{s}\gamma_\mu s \\ &= j^\rho_\mu + j^\omega_\mu/3 - j^\phi_\mu/3 \end{aligned} \tag{3.23}$$

where vector currents are named by lowest mass hadron ρ^0, ω and ϕ in the corresponding channel. And in analogy with the Eq. 3.7, $W_{\mu\nu}$ can be written as, $W_{\mu\nu} = W^\rho_{\mu\nu} + W^\omega_{\mu\nu}/9 + W^\phi_{\mu\nu}/9$, where $W^V_{\mu\nu} = K_V \rho^V_{\mu\nu}(p_0, \vec{p})$, "V" stands for light vector mesons (ρ^0, ω and ϕ), $\rho^V_{\mu\nu}(p_0, \vec{p})$ is the spectral function which is related to imaginary part of the propagator ($D^V_{\mu\nu}$)and $K_V = F_V^2 m_V^2$, F_V is obtained from the partial decay widths into e^+e^- (F_V=0.156 GeV, 0.046 GeV and 0.079 GeV for ρ^0, ω and ϕ respectively). For HM, the standard rate for lepton pair production(Eq. 3.9) from decays of light vector mesons ρ, ω and ϕ has been considered in [45, 42, 80, 81, 82]. In addition, the spectral function of ρ and ω has been augmented with a continuum contribution given by

$$\frac{dR_{l^+l^-}}{d^4p} = \frac{\alpha^2}{\pi^3} f_{BE} \sum_{V=\rho,\omega} A_v^{cont} \tag{3.24}$$

where the continuum part of the vector mesons spectral functions constrained by experimental data [80, 119] have been included here in the following parametrized form

$$A_\rho^{cont} = \frac{1}{8\pi}\left(1 + \frac{\alpha_s}{\pi}\right)\frac{1}{1 + exp((w_0 - M)/\delta)} \tag{3.25}$$

with ω_0=1.3 (1.1) for ρ (ω) GeV and $\delta = 0.2$ for both ρ and ω. The continuum contribution of the ω contains an additional factor of 1/9. Since the continuum part of the vector meson spectral functions are included in the current work the processes like four pions annihilations [120] are excluded to avoid double counting.

3.5.3 Invariant Mass and Momentum Spectra of Dileptons:

The dileptons can be used as an efficient probe for QGP diagnostics, provided one can subtract out contributions from Drell-Yan process, decays of vector mesons within the life time of the fire ball and hadronic decays occurring after the freeze-out. Like hard photons, lepton pairs from Drell-Yan processes can be estimated by pQCD. The p_T spectra of thermal lepton pair suffer from the problem of indistinguishableness between QGP and hadronic sources unlike the usual invariant mass (M) spectra which shows characteristic resonance peaks in the low M region. The invariant transverse momentum distribution of thermal dileptons (l^+l^-) is given by:

$$\frac{d^2N_{l^+l^-}}{d^2p_Tdy} = \sum_{i=Q,M,H} \int_i \left(\frac{dR_{l^+l^-}}{d^2p_TdydM^2}\right)_i MdMd^4x. \tag{3.26}$$

The invariant transverse mass distribution of thermal dileptons (l^+l^-) is given by:

$$\frac{d^2N_{l^+l^-}}{2MdMdy} = \sum_{i=Q,M,H} \int_i \left(\frac{dR_{l^+l^-}}{d^2p_TdydM^2}\right)_i p_Tdp_Td^4x. \tag{3.27}$$

The limits for integration over p_T and M can be fixed judiciously to detect contributions either from quark matter or hadronic matter. Experimental measurements [85, 121] are available for different M window.

3.5.4 Results and Discussion on p_T Distributions of Dileptons

For the evaluation of invariant momentum and invariant mass distribution of dilepton, we need to fold the static emission rate with the space-time dynamics. The space time dynamics is described by relativistic hydrodynamics. The inputs for the initial condition required to solve the hydrodynamic equations are taken from the Table. 3.1. With all these ingredients the p_T spectra of dileptons for SPS and RHIC energies are calculated.

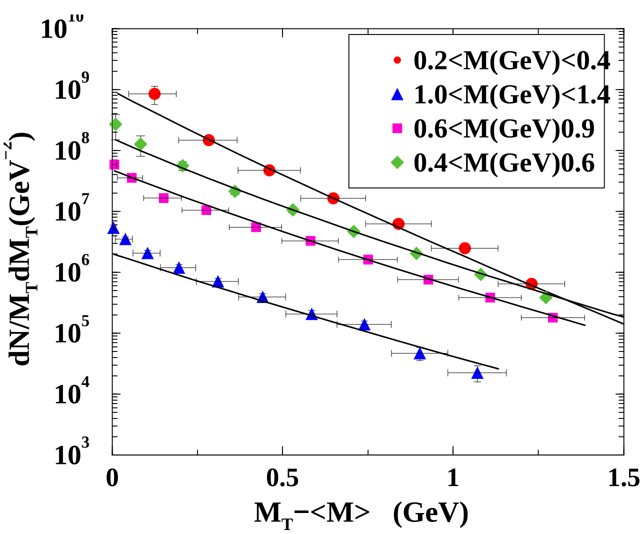

Figure 3.13: Transverse mass spectra of dimuons in In+In collisions at SPS energy. Solid lines denote the theoretical results [107].

The transverse mass distribution of dimuons produced in In+In collisions at $\sqrt{s_{NN}} =$ 17.3 GeV has been evaluated for different invariant mass ranges ([119, 122, 63, 123] for details). The quantity $dN/M_T dM_T$ has been obtained by integrating the production rates over invariant mass windows M_1 to M_2 and M_T is defined as $\sqrt{< M >^2 + p_T^2}$ where $< M >= (M_1 + M_2)/2$. The results are compared with the data obtained by NA60 collaborations [121, 119, 122] at SPS energy (Fig. 3.13). Theoretical results contain contributions from the thermal decays of light vector mesons (ρ, ω and ϕ) and also from the decays of vector mesons at the freeze-out [61, 63] of the system has also been considered. The non-monotonic variation of the effective slope parameter extracted from the M_T spectra of the lepton pair with $\langle M \rangle$ evaluated within the ambit of the present model [123] reproduces the NA60 [121] results reasonably well.

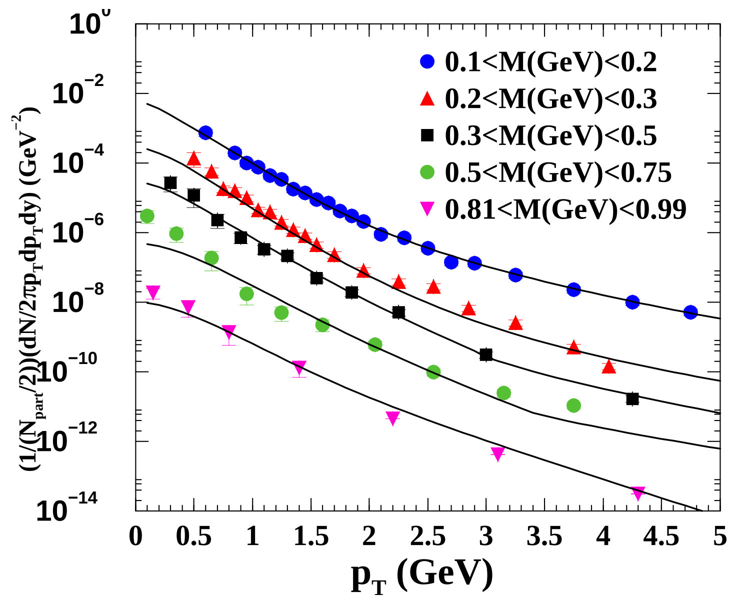

Figure 3.14: Transverse momentum spectra of dileptons for different invariant mass windows for minimum bias Au-Au collisions at RHIC energy [107].

For Au+Au collisions at $\sqrt{s_{NN}}$=200 GeV, we have evaluated the dilepton spectra for different invariant mass bins with the initial condition (min bias) shown in Table 3.1 and lattice QCD equation of state. The results are displayed in Fig. 3.14. The slopes of the experimental data on p_T distribution of lepton pairs for different invariant mass windows measured by the PHENIX collaboration [124] could be reproduced well with the same initial condition that reproduces photon spectra [85]. In fact, the reproduction of data for the mass bins 0.5 <M(GeV)< 0.75 and 0.81 <M(GeV)< 0.99 do not need any normalization factors (Fig. 3.14). For lower mass windows slopes are reproduced well but fail to reproduce the absolute normalization. Therefore, it should be clarified here that the theoretical results shown in Fig. 3.14 for lower mass windows (to be precise for 0.1 <M(GeV)< 0.2, 0.2 <M(GeV)< 0.3 and 0.3 <M(GeV)< 0.5) contain normalization constants 660, 220 and 20 respectively .

3.5.5 Results and Discussion on Invariant Mass Distributions of Dileptons

With the use of Eq. 3.27, we have evaluated the M distribution of lepton pairs originating from QM and HM without medium effects (the invariant mass distribution with medium effect will be discussed in Chapter- 6) on the spectral functions of ρ and ω for RHIC initial conditions. The invariant mass spectra of lepton pairs may be used to extract (i) the

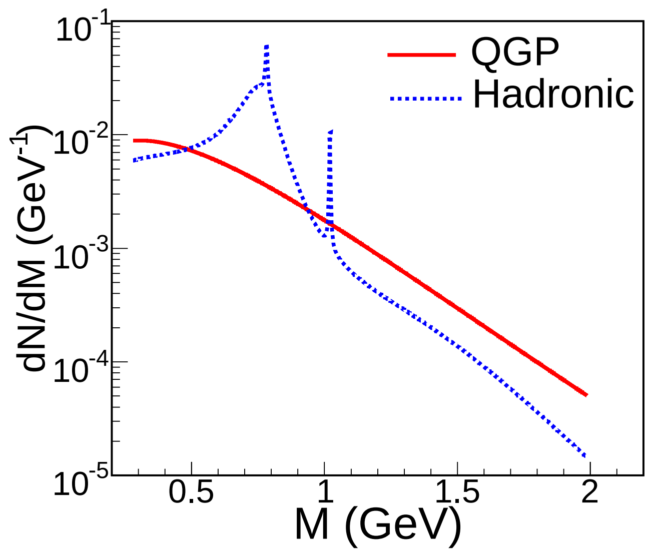

Figure 3.15: Invariant mass distribution of lepton pairs from quark matter (red solid line) and hadronic matter (blue dashed line) [126].

medium effects of the vector meson spectra function, (ii)contributions from the (early) QGP phase by selecting $M > M_\phi$ and (iii) from the (late) hadronic phase ($M \sim m_\rho$). This suggests that the dilepton spectra can be used as a clock for heavy ion collision. As mentioned before, the p_T spectra of the lepton pairs are affected by flow. Therefore, the evolution of flow of the evolving QGP may be estimated by studying the transverse momentum spectra with appropriate selection of invariant mass window. Hence the lepton pairs can also be used as flow-meter [64, 107, 126, 127] for the system formed in relativistic heavy ion collision. The HM dominates in the M $\sim M_\rho$ region whereas QM outshines in M($> M_\phi$) domain. Therefore, these two mass windows are selected to extract the flow parameters of the respective phases. In the present work, two procedures have been proposed to estimate the radial flow of the matter, i.e. (i) ratio of the p_T spectra of thermal photons to dileptons and (ii) HBT radii extracted from the dilepton correlation function.

In this chapter, we are interested only on the p_T distribution of photons and lepton pairs in various M bins. The results will be used in the next Chapter to extract flow for various mass domain from the ratio of the p_T spectra of thermal photons to dileptons. However, it should also be mentioned at this point that for the extraction of the flow the experimental data have been used here. Therefore, the non-reproduction of the absolute normalization of the p_T spectra of lepton pairs for the lower mass windows at RHIC may not affect the extraction of the magnitude of the radial flow. We have studied the Bose-Einstein correlation function(BECF) for lepton pairs in Chapter- 5, and studied the effects of radial flow on the HBT radii extracted from the BECF of lepton pairs. Using the dilepton production from the QGP and hadron (with medium effect of vector meson spectral function), the elliptic flow of dilepton is evaluated (in Chapter- 6).

Chapter 4

Flow from thermal photon and dilepton

4.1 Radial Flow

The hot and dense matter formed in the partonic phase after ultra-relativistic heavy ion collisions expands in space and time owing to high internal pressure. Consequently the system cools and reverts to hadronic matter from the partonic phase. Just after the formation, the entire energy of the system is thermal in nature and with progress of time some part of the thermal energy gets converted to the collective (flow) energy. In other words during the expansion stage the total energy of the system is shared by the thermal as well as collective degrees of freedom. The evolution of the collectivity within the system is sensitive to the EoS. Therefore, the study of the collectivity in the system formed after nuclear collisions will be useful to shed light on the EoS [106, 128, 129, 130, 131] of the strongly interacting system at high temperatures and densities.

4.1.1 Radial Flow of Hadrons

Electromagnetically interacting particles are considered as ideal probes as it provides information throughout the evolution of the fireball. However, the transverse mass spectra $(m_T)(=\sqrt{p_T^2+m_h^2}$ [132]) of hadrons in the low p_T region can provide information about the situation when the thermal system freezes out [27, 131, 133, 134], i.e. the stage when the system disassembles to individual hadrons. Thus the study of the hadronic spectra gives snapshots of the later stages of the nuclear collision dynamics.

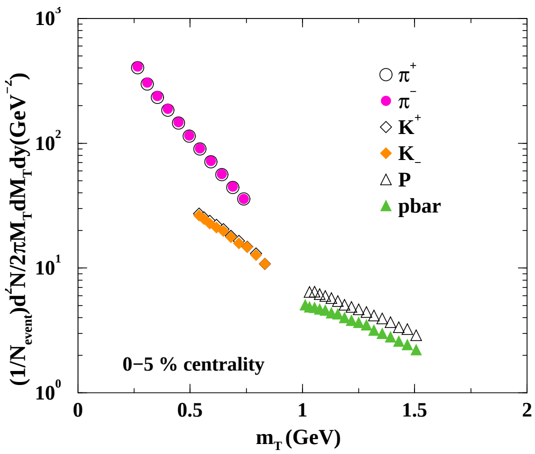

Figure 4.1: m_T spectra of identified hadrons in central Au-Au collision at y=0 (data from [135], replotted)

The collective motion of the hydrodynamically expanding system is reflected through the transverse momentum spectra of the hadrons at the freeze-out point and hence can be extracted from the p_T spectra which predominantly vary with m_T, $\sim \exp(-m_T/T_{eff})$, where T_{eff} effective temperature and the ratio m_T/T_{eff} is larger than 1. The T_{eff} $(= T + m_h v_r^2)$ obtained from the inverse slope of the spectra, where T is the average temperature of the system and v_r is the radial flow velocity. This radial flow affects the particle spectra as compared to static source. In absence of radial flow, the spectra as a function of m_T are identical for all hadrons, but radial flow breaks the identity. It is clear from Fig 4.1, heavier particle are more affected by flow than lighter particles. Due to increase in mass, m_h the respective p_T spectra get more flattened. That is why the spectra of proton is more flattened compared to that of kaon and pion. This is generally considered evidence for transverse flow[1]. The slope of the different particle species (along with the initial thermalization time) affect the effective freeze-out temperature. By varying the initial thermalization, the strength of the final transverse flow that can develop will change. With early thermalization, a larger radial flow builds up and will be reflected in T_{eff}. Again for peripheral collisions the spectra get steeper, due to decrease of average radial velocity as a result of low initial energy density and a shorter lifetime of the reaction zone [27].

4.1.2 Radial Flow of Thermal Photons and Dileptons

As discussed previously in the Sec. 4.1.1, that the average magnitude of radial flow can be extracted from the m_T spectra of the hadrons only at freeze-out surface. However, hadrons being strongly interacting objects can bring the information of the state of the system when it is too dilute to support collectivity, *i.e.*, the parameters of collectivity extracted from the hadronic spectra are limited to the evolution stage where the collectivity ceases to exist. These collective parameters have hardly any information about the interior of the matter. On the other hand, electromagnetic (EM) probes i.e. photons and dileptons are produced and emitted [39, 40, 41, 44, 45, 42] from each space time points. Therefore, estimating radial flow from the EM probes will shed light on the time evolution of the collectivity in the system.

If we suppose the system formed in HIC is thermalized, the pressure is built inside

[1] In the case of central collisions, which have rotational symmetry in the (x,y) plane, transverse flow is also called radial flow

the system. The matter is surrounded by vacuum, so pressure gradient in outward directions is large, huge force $-\vec{\nabla}P$ acts on the system; but this is compensated by the large inertia $\epsilon + p$, resulting in a linear increase of the fluid velocity and collectivity is developed and in turn, the system expands rapidly.

In the next section, we will discuss the extraction radial flow from the ratio of p_T spectra of thermal photon to dilepton (R_{em}).

4.2 Radial Flow from Ratio of Thermal Photon to Dilepton Spectra, $R_{\rm em}$:

In the present section, how the evolution of radial flow is extracted from the analysis of the experimental data on electromagnetic probes measured at SPS and RHIC energies is discussed. The p_T spectra of photons and dileptons which are constrained by the experimental data of the SPS and RHIC energy. With these spectrum, ratio of photon to dilepton spectra is calculated to extract the radial flow, where the model dependences are partially canceled out (for example see [136] for dependancy on T_c on individual spectra as well as on ratio).

The calculations of EM probes from thermal sources depend on the parameters such as; T_i, τ_i, $T_{\rm ch}$, T_f etc, which are not known uniquely. These above mentioned uncertainties have been used in the evaluation of individual single spectra of photon as well as dilepton. In order to overcome the uncertainties and minimize the dependence of thermal sources on these parameters, the importance of the ratio of the transverse momentum spectra of photon to dilepton (R_{em}) has been emphasized in the present study (See Refs. [107, 127, 137, 138]), where the uncertainities are canceled out partially. It may be mentioned here that in the limit of $M \to 0$ the lepton pairs (virtual photons) emerge as real photons. Therefore, the evaluation of the ratio of the p_T spectra of photons to dileptons for various invariant mass bins along with a judicious choice of the p_T and M windows will be very useful to extract the properties of QGP as well as that of hadronic phase. This will be demonstrated in the present work by analyzing WA98 and PHENIX photons (results are shown in Section. 3.4.4) and NA60 and PHENIX dilepton (results are shown in Section. 3.5.4) spectra.

The p_T spectra of photon and dilepton can be parametrized as following;

$$\begin{aligned} \left(\frac{dN}{d^2p_Tdy}\right)_{\gamma} &= A_1\left(\frac{1}{p_T}\right)^{B_1}\exp[-c_1p_T] \;\; ; \quad c_1 = 1/T_{eff_1}, \\ \left(\frac{dN}{d^2p_Tdy}\right)_{l^+l^-} &= A_2\left(\frac{1}{M_T}\right)^{B_2}\exp[-c_2M_T] \;\; ; \quad c_2 = 1/T_{eff_2} \end{aligned} \quad , \tag{4.1}$$

where, $T_{eff1} = T_{av}\sqrt{\frac{1+v_r}{1-v_r}}$ is the blue shifted effective temperature for massless photons and $T_{eff2} = T_{av} + Mv_r^2$, is the effective temperature for massive dileptons. T_{av} is the average temperature and v_r is the average radial flow of the system. The $T_{eff_{1,2}}$ can be obtained by parameterizing the p_T spectra of photons and dileptons (see Sec. 3.4.4 and 3.5.4) respectively with the expressed form of Eq. 4.1. The ratio, R_{em} for different M windows (Figs. 4.2) can be parametrized as follows:

$$R_{em} = A\left(\frac{M_T}{p_T}\right)^{B}\exp[-c(M_T - p_T)] \;\; ; \quad c = 1/T_{eff} \tag{4.2}$$

with different values of T_{eff} for different invariant mass windows. The argument of the exponential in Eq. 4.2 can be written as [127];

$$\begin{aligned} \frac{M_T - p_T}{T_{eff}} &= \frac{M_T}{T_{eff2}} - \frac{p_T}{T_{eff1}} \\ &= \frac{M_T}{T_{av} + Mv_r^2} - \frac{p_T}{T_{av}\sqrt{\frac{1+v_r}{1-v_r}}} \end{aligned} \tag{4.3}$$

As mentioned before some of the uncertainties prevailing in the individual spectra may be removed by taking the ratio, $R_{\rm em}$ of the p_T distribution of thermal photon to dileptons. In the absence of experimental data for both photon and dilepton from the same colliding system for SPS energies, we have calculated the ratio $R_{\rm em}$ for Pb+Pb system, where the initial condition and the EoS are constrained by the measured WA98 photon spectra. The results are displayed in Fig. 4.2(left panel). Also we evaluate the

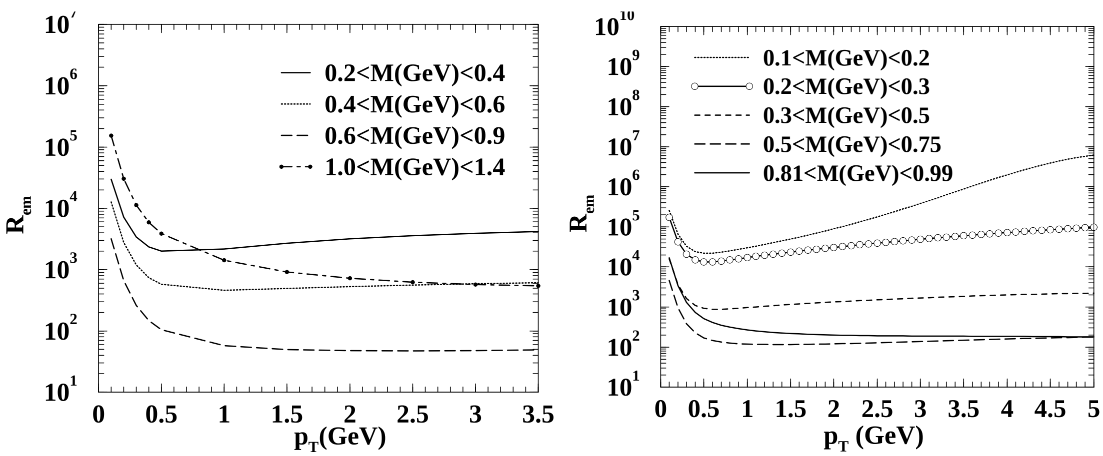

Figure 4.2: Variation thermal photon to dilepton ratio, R_{em} with p_T for different invariant mass windows at SPS energy(left panel)and RHIC energy(right panel) (see text).

ratio of the thermal photon to dilepton spectra constrained by the experimental data from Au+Au collisions measured by PHENIX collaboration. The results for the thermal ratio, $R_{\rm em}$ displayed in Fig. 4.2(right panel) is constrained by the experimental data on the single photon and dilepton spectra. The behavior of $R_{\rm em}$ with p_T for different invariant mass windows which is extracted from the available data is similar to the theoretical results obtained in Ref. [127, 138]. It is observed that the ratio decreases sharply and reaches a plateau beyond $p_T > 1.5$ GeV. This behavior of $R_{\rm em}$ as a function of p_T can be understood as follows: (i) for $p_T >> M$, $M_T \sim p_T$ and consequently $R_{\rm em} \sim$ A giving rise to a plateau at large p_T. The height of the plateau is sensitive to the initial temperature of the system [127, 138]. (ii) For $p_T < M$, $R_{\rm em} \sim exp(-p_T/T_{\rm eff})/p_T^{\rm B}$ indicating a decrease of the ratio with p_T (at low p_T) as observed in the Fig. 4.2.

4.2.1 Variation of Radial Flow with Average Temperature

For a given p_T and M Eq. 4.3 can be written as $v_r = f(T_{av})$. The T_{eff} obtained from the parametrization of ratio at SPS energy are 263 MeV and 243 MeV for M=0.75 and 1.2 GeV respectively. The average flow velocity v_r versus T_{av} have been displayed for M=0.75 GeV and 1.2 GeV in Fig. 4.3.

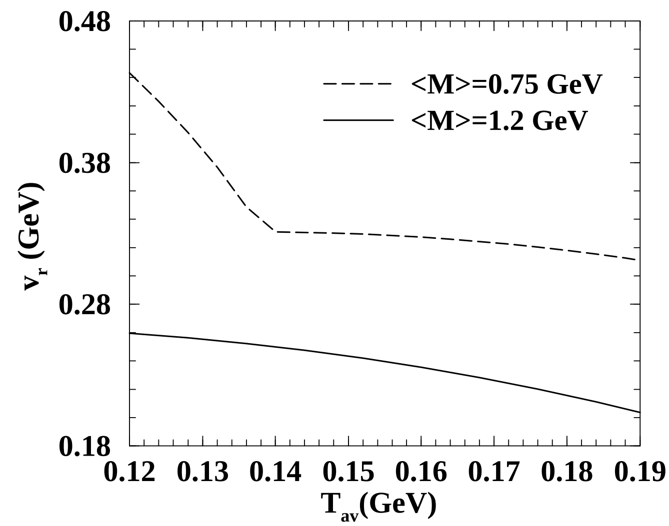

Figure 4.3: The variation of radial flow velocity with average temperature of the system for$< M >= 0.75$ GeV and 1.2 GeV at SPS energy.

The hadronic matter (QGP) dominates the $M \sim 0.75(1.2)$ GeV region. Therefore, these two mass windows are selected to extract the flow parameters for the respective phases [2]. The v_r increases with decreasing $T_{\rm av}$ (increase in time) and reaches its maximum when the temperature of the system is minimum, i.e., when the system attains T_f, the freeze-out temperature. Therefore, the variation of v_r with $T_{\rm av}$ may be treated as to show how the flow develops in the system. The v_r is larger in the hadronic phase

[2]In the mass region $M > 1.2$ GeV, although the contribution from QGP phase domninates, there is good admixture of lepton pairs from the hadronic phase (see Fig.3.15). Therefore, the low T_{av} region in the Fig. 4.3 and 4.4 contain flow from both the phases. The v_r from the higher mass window ($\langle M \rangle$)=1.2 GeV and larger T_{av} corresponds to the v_r from the QM

because the velocity of sound in this phase is smaller, which makes the expansion slower as a consequence system lives longer - allowing the flow to fully develop. On the other hand, v_r is smaller in the QGP phase because it has smaller life time where the flow is only partially developed. In Fig. 4.4 the variation of average transverse velocity with average temperature for RHIC initial conditions is depicted.

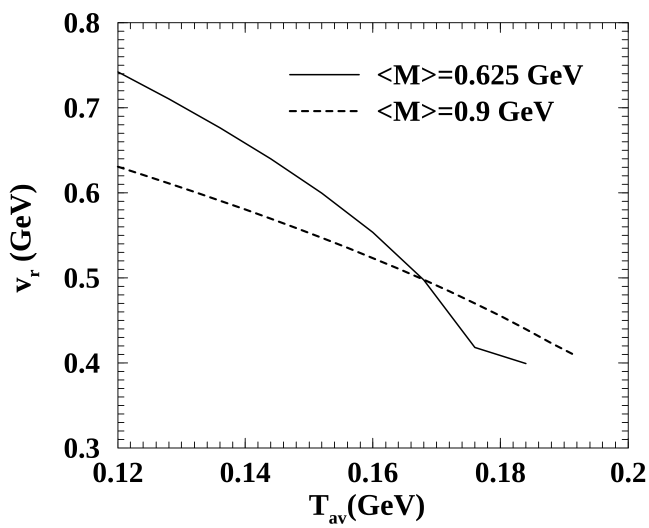

Figure 4.4: The variation of radial flow velocity with average temperature of the system for$< M >$ =0.625 GeV and 0.9 GeV at RHIC energy.

The magnitude of the flow is larger in case of RHIC than SPS because of the higher initial pressure. Because of the larger initial pressure and QGP life time the radial velocity for QGP at RHIC is larger compared to SPS.

4.2.2 Variation of Radial Flow with Invariant Mass

Obtaining T_{eff1} and T_{eff2} from the individual spectra and eliminating T_{av} one gets the variation of v_r with M. Fig. 4.5 (left panel) shows the variation of v_r with M for SPS conditions. The radial flow velocity increases with invariant mass M up to $M = M_\rho$

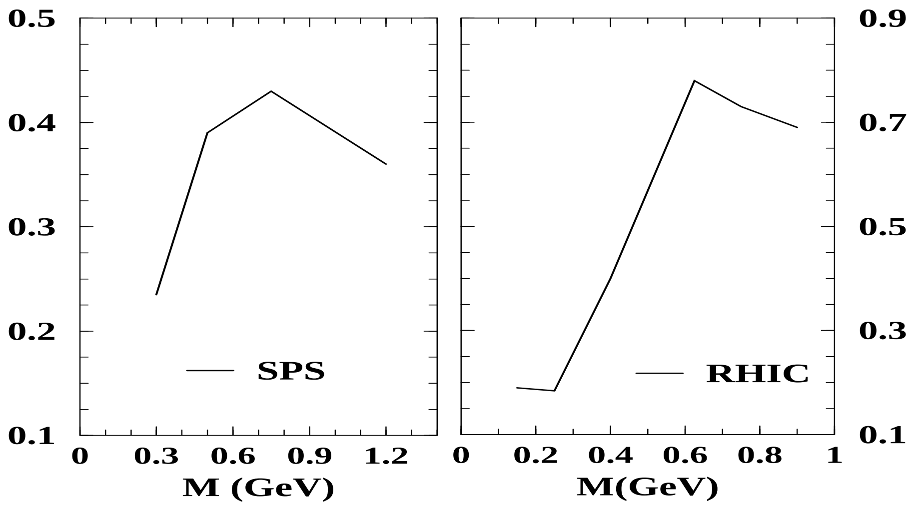

Figure 4.5: The variation of radial flow with invariant mass pairs for SPS (left) and RHIC (right) energies.

then drops. How can we understand this behavior? From the invariant mass spectra it is well known that the low M (below ρ mass) and high M (above ϕ peak) pairs originate from a partonic source [138]. The collectivity (or flow) does not develop fully in the QGP because of the small life time of this phase. Which means that the radial velocity in QGP will be smaller for both low and high M. Whereas the lepton pairs with mass around ρ-peak mainly originate from a hadronic source (at a late stage of the evolution of system) are largely affected by the flow resulting in higher values of flow velocity. In summary, the value of v_r for M below and above the ρ-peak is small but around the ρ peak is large - with the resulting behavior displayed in Fig. 4.5. Similar non-monotonic behavior is observed in case of elliptic flow of photon as a function of p_T [139]. The variation of v_r with M in RHIC (Fig. 4.5 right panel) is similar to SPS, though the values of v_r at RHIC is larger than that of SPS as expected due to higher initial pressure.

It is shown that simultaneous measurements of photon and dilepton spectra in HIC will enable us to quantify the evolution of the average radial flow velocity for the system and the nature of the variation of radial flow with invariant mass indicate the formation of partonic phase at SPS and RHIC energy. The stronger radial flow at RHIC compared to SPS is due to higher initial energy densities and a longer lifetime of the reaction zone.

Some comments on the effect of in-medium effect change of ρ spectral function on R_{em} are in order here. The dilepton emission rate from the hadronic matter will be enhanced in the low M region ($M \leq M_\rho$) due to the broadening of the ρ meson in hot medium. As a consequence, it changes the R_{em} at low M and low p_T ($M \sim 500$ MeV and $p_T \sim 1$ GeV) is significant (R_{em} changes by 50%), but at high p_T the change is negligible. As the dilepton emission in high M region ($M > m_\phi$) doesn't affected due to in medium effect so the R_{em} remains unaltered.

Chapter 5

Two Particle Correlation of Dileptons

5.1 Basic Concepts in Particle Interferometry

Particle interferometry is considered as one of the efficient methods to extract the information of space-time structure of the fireball formed in HIC. The utility of the intensity interferometry with dileptons [126] for extracting fireball properties will be discussed in this chapter. Before discussing dilepton interferometry, the basic physics issues behind the intensity interferometry will be described in the subsequent sections.

5.1.1 HBT Intensity Interferometry

The two particle intensity interferometry, commonly known as Hanbury Brown Twiss (HBT) interferometry, is the technique of studying the correlation between two particles by analyzing the pattern of interference produced by their superposition. This method has been formulated and exploited for the first time in 1950's by Hanbury-Brown and Twiss(HBT) [33] to correlate intensity of electromagnetic(EM) radiation, arriving from extra terrestrial radio-wave sources, and then measures the angular diameter of stars and other astronomical objects. Though it has its origin in astrophysics, but has significant theoretical development and widespread application in HIC. This method is used for the investigation of the spatial and temporal information of the system formed in nuclear collision.

In high energy physics, for the first time this method was introduced by Goldhaber *et al* [34] in 1960 in hadron sector in order to study dynamics and geometry of the system producing two identical pions produced in particle interaction. In the sequel of this work, it was gradually realized that the correlation of identical particles emitted by highly excited nuclei are not only sensitive to the geometry of the system but also to its lifetime.

The study of small relative momentum correlation, a technique also known as HBT interferometry, is one of the efficient way at our disposal to extract the direct experimental information about the spatial as well as temporal size of the particle emitting source created in heavy-ion collision (HIC) from the momentum spectra, by making use of quantum statistical correlation between two identical particles. This effect is popularly known as HBT effect. In HIC, the single particle spectra and two particle correlation are sensitive to certain combination of thermal and collective motion in the source.

5.1.2 A Simple Model of Intensity Interferometry

The intensity interferometry differs from the ordinary amplitude interferometry in the sense that instead of comparing amplitude, it compares the intensities of two waves at two different points. The difference between intensity and conventional amplitude interferometry can be illustrated with the help of Fig. 5.1.

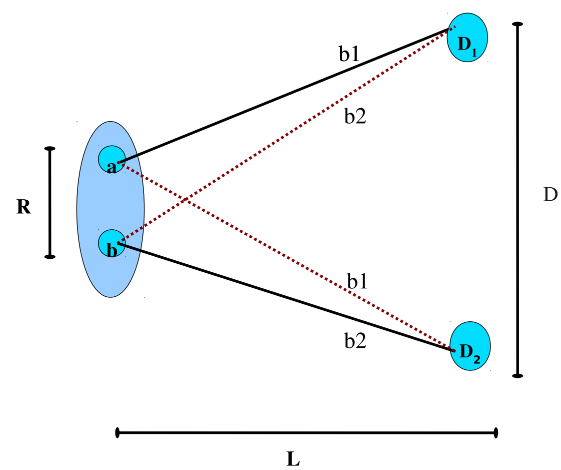

Figure 5.1: The two indistinguishable diagrams that describe the emission of two identical bosons, b_1 and b_2, emerging from the two points a and b, which lie within the emitter volume, and are detected at position D_1 and D_2.

The intensity interferometry can be illustrated through the following ways was done in Ref. [140, 141]. Consider a finite source which emits two indistinguishable particles (same frequency) from position a and b which are a distance R apart from each other. Later they are detected at two different detectors, D_1 and D_2, which are at a distance D from each other. The distance from source to detector is L.

In an amplitude interferometry, the two detectors (D_1 and D_2) acts as two slits through which the emitted particles pass. Then the interference pattern created from the superposition of these two particle wave depend on relative phase of the particle's amplitude as measured at D_1 and D_2. Suppose the source a and b produces a spherical

EM wave of amplitudes $\alpha e^{\left[ik|\vec{r}-\vec{r_a}|+\frac{i\phi_a}{|\vec{r}-\vec{r_a}|}\right]}$, and $\beta e^{\left[ik|\vec{r}-\vec{r_b}|+\frac{i\phi_b}{|\vec{r}-\vec{r_b}|}\right]}$, where ϕ_a and ϕ_b random phases (ignoring polarization). The total amplitude at D_i is

$$A_i = \frac{1}{L}\left(\alpha e^{ikr_{ia}+i\phi_a} + \beta e^{ikr_{ib}+i\phi_b}\right) \tag{5.1}$$

where "i" stands for detector 1 and 2 , r_{ia} distance from source a to detector D_i and then the total intensity at D_i is

$$I_i = A_i A_i^* = |A_i|^2 = \frac{1}{L^2}\left(|\alpha|^2 + |\beta|^2 + \alpha^*\beta e^{i[k(r_{ib}-r_{ia})+\phi_b-\phi_a]} + \alpha\beta^* e^{i[k(r_{ib}-r_{ia})+\phi_b-\phi_a]}\right) \tag{5.2}$$

On averaging over the random phases the later exponential terms average to zero, and the average intensities in the two detector are found as;

$$\langle I_1\rangle = \langle I_2\rangle = \frac{1}{L^2}\left(\langle|\alpha|^2\rangle + \langle|\beta|^2\rangle\right) \tag{5.3}$$

The product of average intensities $\langle I_1\rangle\langle I_2\rangle$ is independent of separation between two detectors. On the other-hand, the average of the product of intensities $I_1 I_2$ is given by,

$$\begin{aligned} \langle I_1 I_2\rangle &= \langle I_1\rangle\langle I_2\rangle + \frac{2}{L^4}|\alpha|^2|\beta|^2\cos(k(r_{1a}-r_{2a}-r_{1b}+r_{2b})) \\ &= \frac{1}{L^4}\left[|\alpha|^4 + |\beta|^4 + 2|\alpha|^2|\beta|^2\{1+\cos(k(r_{1a}-r_{2a}-r_{1b}+r_{2b}))\}\right] \end{aligned} \tag{5.4}$$

Then correlation function can be written as;

$$C = \frac{\langle I_1 I_2\rangle}{\langle I_1\rangle\langle I_2\rangle} = 1 + 2\frac{\langle|\alpha|^2\rangle\langle|\beta|^2\rangle}{\left(\langle|\alpha|^2|\beta|^2\rangle\right)^2}\cos(k(r_{1a}-r_{2a}-r_{1b}+r_{2b})) \tag{5.5}$$

For large separation between the sources and detectors ($L >> R$), $k(r_{1a}-r_{2a}-r_{1b}+r_{2b}) \to k(\vec{r_a}-\vec{r_b}).(\hat{r_2}-\hat{r_1}) = \vec{R}.(\vec{p_2}-\vec{p_1})$, where $\vec{p_i} = K\hat{r_i}$ is the wave vector of light seen in detector i. The correlated signals in Eq. 5.5 varies as a function of the detector separation d on a characteristic length scale $d = \lambda/\theta$, where λ is the wavelength of light, and $\theta = R/L$ is the angular size of the sources as seen from the detectors. Thus by varying separation between the detectors, the apparent angle between two sources can be obtained and with the knowledge of the individual wave vector, the physical size of the source can be known.

The intensity interferometry is closely related to amplitude interferometry which essentially measures the square of the amplitudes, A_1 and A_2 falling on detectors D_1 and D_2.

$$|A_1 + A_2|^2 = |A_1|^2 + |A_2|^2 + (A_1^* A_2 + A_1 A_2^*) \tag{5.6}$$

where the last term is the fringe visibility denoted by V, which is the part of the signal which is sensitive to separation between the emission points. averaged over random variations its square is given by the product of intensities falling on the two detectors.

$$\langle V^2 \rangle = 2\langle |A_1|^2 |A_2|^2 \rangle + \langle A_1^{*2} A_2^2 \rangle + \langle A_1^2 A_2^{*2} \rangle \rightarrow 2\langle I_1 I_2 \rangle \tag{5.7}$$

Since the last two terms of $\langle V^2 \rangle$ vary rapidly and average to zero, $\langle V^2 \rangle$ is proportional to time averaged correlation of product of two intensities.

Instead of two discrete sources, if there is a distribution of sources, $\rho(\vec{r})$, then averaging over distribution, one finds correlation function measures the Fourier transformation of source distribution;

$$C - 1 \sim \left\| \int d^3 r \rho(\vec{r}) \; e^{i(\vec{p_1} - \vec{p_2})\vec{r}} \right\|^2 \tag{5.8}$$

- One important difference between astronomical observation and high energy physics is that star stay fixed, while in HIC, the system evolves in a time scale of 10^{-23} to 10^{-22} sec and thus one has to take the changing geometry into the consideration. So the Fourier transformation of the distribution in both space and time should be taken for good approximation.

- The second important difference is that in astronomy, due to lack of knowledge of the distance between source and detector, one can't measure the actual difference in direction of the wave-vectors of the light in the two detectors, and thus angular size of the sources can be measured as seen from the detectors. In contrast, the wave-vector of the detected particles can be determined in high energy physics, and thus the absolute size of the source can be measured.

5.1.3 Quantum Mechanics of HBT

A classical approach of illustration of intensity interferometry has discussed in the previous Section 5.1.2. To understand it from the quantum mechanical view point, let us consider the following four different processes of emission and detection of two identical bosons (included in Eq. 5.4) and is illustrated in Fig. 5.2

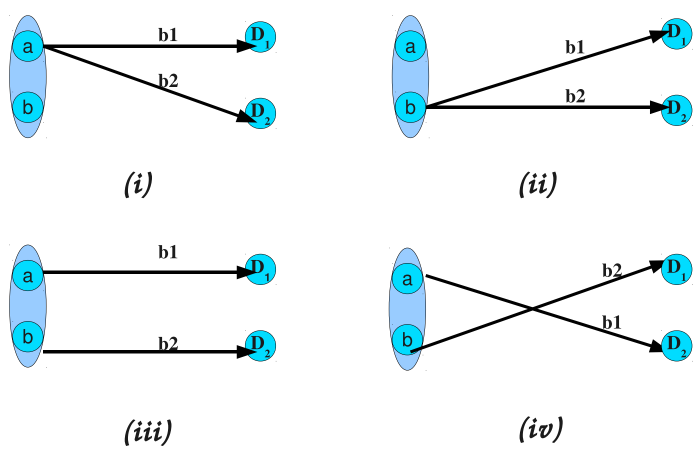

Figure 5.2: Four independent processes of emission and detection of two identical bosons b_1 and b_2.

1. Two identical bosons emitted from source a are detected at D_1 and D_2 (shown in Fig. 5.2(i)).

2. Two identical bosons emitted from source b are detected at D_1 and D_2 (shown in Fig. 5.2(ii)).

3. One boson emitted from source a are detected at D_1 and other form b detected at D_2 (shown in Fig. 5.2(iii)).

4. One boson emitted from source a are detected at D_2 and other form b detected at D_1 (the exchange of previous process) (shown in Fig. 5.2(iv)).

The first two process are distinguishable and do not produce interferometry . They simply corresponds to detection of the sources independently (the $|\alpha|^4$ and $|\beta|^4$ terms in Eq. 5.4). Only later two processes, (*iii*) and (*iv*), which are quantum mechanically coherent give rise to interferometry. [Indeed, if we drop terms proportional to $|\alpha|^4$ and $|\beta|^4$, Eq. 5.5 reduces to $C_2 = 1 + \cos k(r_{1a} - r_{2a} - r_{1b} - r_{2b})$.]

Quantum mechanically, the HBT effect is a consequence of exchage of bosons. As it is well known that in quantum mechanics the interchange of two out of N indistinguishable bosons does not change the wave function describing the multi bosons states $\Psi(1, 2, ..., N) = \Psi(2, 1, ..., N)$. This feature of the Bose-Einestein statistics means that the state Ψ has the symmetric property which leads to an interference term in $|\Psi|^2$ that enhances the production of indistinguishable bosons. HBT interferometry with fermions are also performed in HIC [31, 32, 142]. However, in the present work is confined ti interferometry with bosons only.

5.2 Bose-Einestein Correlation Function(BECF)

5.2.1 Basic Concepts of BECF for Two Identical Particles

Let us first consider a source of discrete emission points, ρ_i, each characterized by a probability amplitude $F_i(r)$ in the 3-vector r_i phase-space [142]

$$F_i(r) = \rho_i \delta^3(r - r_i) \tag{5.9}$$

Next we introduce central assumption pertaining to the Bose-Einestein Correlation (BEC) effect namely, the chaotic or the total incoherence limit, which corresponds to the situation where the phases of production amplitudes wildly fluctuate in every point of space. In this limit all the phase can be set to zero. If $\Psi_{\mathbf{p}}(r)$ is the wave function of the emitted boson, then the total probability $P(\mathbf{p})$ to observe the emission of one particle with a 3-momentum vector $\mathbf{p}$ is given by summing up the contribution from all the i points, that is;

$$P(\mathbf{p}) = \sum_i |\rho_i \psi(r_i)|^2 \tag{5.10}$$

For simplicity we will further use plane wave functions $\Psi_{\mathbf{p}} \propto e^{i(\mathbf{pr}+\phi)}$ where in the incoherent case we can set $\phi = 0$. Next we replace the sum by integral so that

$$P(\mathbf{p}) = \int |\rho(r)|^2 d^3r \tag{5.11}$$

The probability to observe two particles with momenta $\mathbf{p_1}$ and $\mathbf{p_2}$ is

$$P(\mathbf{p_1}, \mathbf{p_2}) = \int |\Psi_{1,2}|^2 |\rho(r_1)|^2 |\rho(r_2)|^2 d^3r_1 d^3r_2 \tag{5.12}$$

where $\Psi_{1,2} = \Psi_{1,2}(\mathbf{p_1}, \mathbf{p_2}, r_1, r_2)$ is two particle wave function.

Taking incoherent plane waves, then for two identical bosons the symmetrized $\Psi_{1,2}$ can be expressed as the following

$$\Psi^s_{1,2} = \frac{1}{\sqrt{2}} \left[e^{i(\mathbf{p_1}r_1 + \mathbf{p_2}r_2)} + e^{i(\mathbf{p_1}r_2 + \mathbf{p_2}r_1)} \right] \tag{5.13}$$

So that

$$\Psi^s_{1,2} = 1 + \cos[((\mathbf{p_1} - \mathbf{p_2}))(r_1 - r_2)] = 1 + cos(\Delta\mathbf{p}\Delta r) \tag{5.14}$$

Now the BEC function, C_2 is constructed as follows;

$$C_2(\mathbf{p_1}, \mathbf{p_2}) = \frac{P(\mathbf{p_1}, \mathbf{p_2})}{P(\mathbf{p_1})P(\mathbf{p_2})} = 1 + \frac{\int d^3r_1 d^3r_2 \cos(\Delta\mathbf{p}\Delta r)|\rho(r_1)|^2|\rho(r_2)|^2}{P(\mathbf{p_1})P(\mathbf{p_2})} \tag{5.15}$$

Assuming that the emitter extension $\rho(r)$ is localized in space then it follows that when $\Delta\mathbf{p} = 0$ the last term of Eq. 5.15 can vary between the values 0 to 1. From Eq. 5.15, one obtains after integration

$$C_2(\Delta\mathbf{p}) = 1 + |\rho(\Delta\mathbf{p})|^2 \tag{5.16}$$

5.2.2 Bose-Einestein Correlation in Heavy Ion Collision

In the previous Section 5.2.1 the BEC function of two identical particles from a given boson emitting source has derived [141, 142]. However, in order to explain the evolving system with changing geometry formed in HIC, the Eq. 5.16 remains unsatisfactory. Since it doesn't allow for a possible time-dependence of emitter and cannot be easily extended to sources with position - momentum correlations.

A sound starting point is provided by Lorentz-invariant one- and two- particle distribution function for each particle species [31].

$$\begin{aligned} P_1(p) &= E\frac{dN}{d^3p} = E\langle \hat{a_p^\dagger}\hat{a_p}\rangle \\ P_1(p_1, p_2) &= E_1E_2\frac{dN}{d^3p_1d^3p_2} = E_1E_2\langle \hat{a_{p1}^\dagger}\hat{a_{p2}^\dagger}\hat{a_{p2}}\hat{a_{p1}}\rangle \end{aligned} \tag{5.17}$$

in terms of creation and destruction operators for on-shell particles with momenta p_i, where $\langle ...\rangle$ denotes an average over the source ensemble. Then the correlation function,

C_2 is defined as the ratio of the Lorentz invariant one- and two- particle inclusive particle spectra (Eq. 5.18).

$$C_2(p_1, p_2) = \frac{P(p_1, p_2)}{P(p_1)P(p_2)} \tag{5.18}$$

For uncorrelated emission and in the absence of final state interactions one can prove [143] a generalized Wick theorem for the factorization of the 2-particle spectrum (Eq. 5.17) and obtains

$$C_2(q, K) = 1 \pm \frac{|\langle \hat{a}^\dagger_{p_1} \hat{a}_{p_2} \rangle|^2}{\langle \hat{a}^\dagger_{p_1} \hat{a}_{p_1} \rangle \langle \hat{a}^\dagger_{p_2} \hat{a}_{p_2} \rangle} \tag{5.19}$$

where $q = p_1 - p_2$ and $K = (p_1 + p_2)/2$ denote the relative and total average momentum of the particle pair respectively , and the $+(-)$ sign applies for bosons (fermions). Note that the second term is positive definite. Thus one obtains

$$C_2(q) = 1 + |\rho(q)|^2 \tag{5.20}$$

We assume a Gaussian distribution for the source density as

$$\rho(r) = \frac{1}{4\pi^2 R^4} \exp(-\frac{r^2}{2R^2}) \tag{5.21}$$

where R is the standard deviation(the Gaussian width). Using Gaussian parametrization, the correlation function, C_2, of Eq. 5.20 can be re-written by using the Fourier transformation of $\rho(r)$ as;

$$C_2(q) = 1 + \exp(-R^2 q^2) \tag{5.22}$$

The equation (Eq. 5.22) is valid only for a fully "chaotic" source. However, experimentally observed correlation function is further suppressed due to several effects such as the partial coherence of the source and pairs comes from resonance decays. For the more realistic "non-chaotic" source, Eq. 5.22 is modified as

$$C_2(q) = 1 + \lambda \exp(-R^2 q^2) \tag{5.23}$$

where λ is commonly referred as "chaotic parameter", which varies from 0 to 1.

In one-dimensional BEC analysis, the C_2 is measured as a function of a Lorentz-invariant relative momentum q_{inv} (q is redefined as q_{inv});

$$C_2(q) = 1 + \lambda_{inv} \exp(-R_{inv}^2 q_{inv}^2) \tag{5.24}$$

with

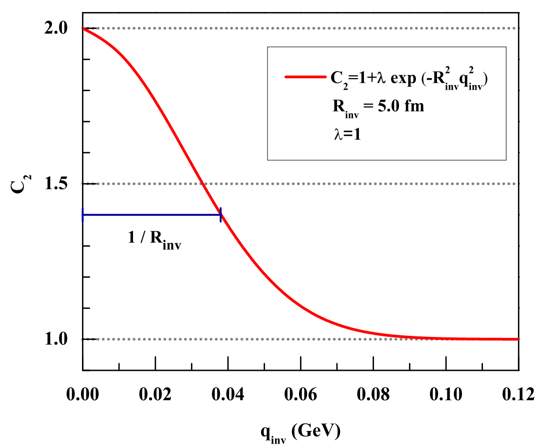

Figure 5.3: One dimensional correlation function as a function of q_{inv} with input parameters, λ_{inv}=1 and R_{inv}=5.0fm

$$q_{inv} = \sqrt{q_0^2 - q_x^2 - q_y^2 - q_z^2} \tag{5.25}$$

where R_{inv} is the one-dimensional HBT radius, which is related to its spatial and temporal sizes as described in Section 5.2.3, and λ_{inv} is the one- dimensional chaotic parameter. $(q_x, q_y, q_z))$ is the relative difference of measured momentum for each direction and q_0 is relative energy difference of pairs ($q_0 = E_1 - E_2$). In this analysis, the particle energy is determined by measured momentum p and m as $E = \sqrt{p^2 + m^2}$. The schematic correlation function as a function of q_{inv} is illustrated in Fig. 5.3.

5.2.3 Parametrization of the Correlation Function and HBT Radii

As mentioned before, the source formed in HIC is not static rather considered to be rapidly expanding. In such a dynamically expanding source, the particle momenta are strongly correlated with their emission points, that is commonly known as "space-momentum correlation". Particles coming out from different space-time point of the evolving fireball have different momentum.

The Bertsch-Pratt (B-P) parametrization [144, 145] of the correlation function has been widely employed to analyze multidimensional HBT radii in earlier BEC analysis. The schematic representation of the parametrization is shown in Fig 5.4. In this rep-

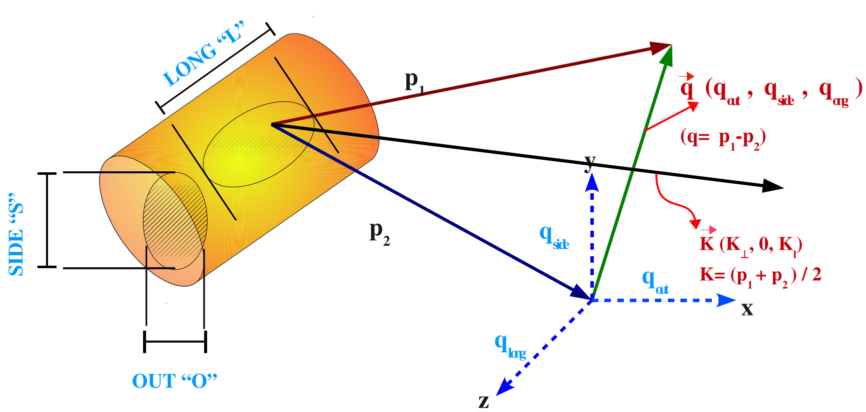

Figure 5.4: The Bertsch-Pratt (“out-side-long“) parametrization.

resentation, the q is the relative momentum difference, $p_1 - p_2$ and K is the average momentum, $K = (p_1 + p_2)/2$, where where p_1 and p_2 are the 4-momenta of the identical particles . According to the parametrization, $\vec{q}$ is decomposed into two components, one along z-direction (parallel to the beam direction) is called q_{long} and the other component q_T is along perpendicular to the beam direction which is further decomposed into q_{out} along outward direction (x-direction), parallel to parallel to $K_T = (p_{1T} + p_{2T})/2$, where

p_{iT} is the transverse momentum of the each particle in pair and q_{side} along side-ward direction (y direction) which is perpendicular to K_T. The q_{out}, q_{side} and q_{long} can be expressed in terms of individual particle momenta as;

$$\begin{aligned}
q_{side} &= \left|\vec{q_T} - q_{out}\frac{\vec{K_T}}{K_T}\right| = \frac{2p_{1T}p_{2T}\sqrt{1-\cos^2(\psi_1-\psi_2)}}{\sqrt{p_{1T}^2+p_{2T}^2+2p_{1T}p_{2T}\cos(\psi_1-\psi_2)}} \\
q_{out} &= \frac{\vec{q_T}.\vec{K_T}}{|K_T|} = \frac{(p_{1T}^2-p_{2T}^2)}{\sqrt{p_{1T}^2+p_{2T}^2+2p_{1T}p_{2T}\cos(\psi_1-\psi_2)}} \\
q_{long} &= p_{1z} - p_{2z} = p_{1T}\sinh y_1 - p_{2T}\sinh y_2 \qquad (5.26)
\end{aligned}$$

Using the B-P parameterization, we can rewrite the correlation function as a function of 4-vector momentum as

$$\begin{aligned}
C_2(q,K) &= 1+\lambda\exp(-R^2(K)q^2) \\
&= 1+\lambda\exp(-R_x^2(K)q_x^2 - R_y^2(K)q_y^2 - R_z^2(K)q_z^2) \\
&= 1+\lambda\exp(-R_{side}^2(K)q_{side}^2 - R_{out}^2(K)q_{out}^2 - R_{long}^2(K)q_{long}^2) \qquad (5.27)
\end{aligned}$$

The quantities R_{side}, R_{out} and R_{long} appearing in Eq. 5.27, are commonly referred to as HBT radii, which is measure of Gaussian widths of source size in q_{side}, q_{out} and q_{long} directions [31].

$$\begin{aligned}
R_{side}^2(K) &= \langle \tilde{y}^2 \rangle \\
R_{out}^2(K) &= \langle (\tilde{x} - v_r\tilde{t})^2 \rangle \\
R_{long}^2(K) &= \langle (\tilde{z} - v_z\tilde{t})^2 \rangle \qquad (5.28)
\end{aligned}$$

Clearly, these HBT radius parameters mix spatial - temporal information on the source in a non-trivial way. The radius corresponding to q_{side} (R_{side}) is closely related to the transverse size of the system, the radius corresponding to q_{out} (R_{out}) measures both the transverse size and duration of particle emission [31, 146, 147]. The ratio, R_{side}/R_{out} will indicate the duration of particle emission [143, 145, 148]. In the dissertation, we will be concentrating on the correlation function of dileptons. As dileptons probe the whole space-time history of the expanding system, thus extracting the radii from its correlation function will decipher the space-dynamics of the source dimension more clearly than that of obtained from hadrons which provide the source dimension at freeze out surface only.

5.3 Dilepton Interferometry- A Tool to Characterize QGP

The main motto of relativistic heavy ion collision is to create and study a state of matter called Quark Gluon Plasma(QGP). Several probes - both EM and hadronic have been proposed for the diagnostics of QGP. Most of the experimental observables for QGP, however, contain mixer contributions from partonic as well as hadronic phase making the detection of QGP very difficult. The study of two particle correlation of hadrons (e.g., pions, kaons, etc.) has been established as a useful tool to obtain information about the size, shape and dynamics of the source. One of the major limitation of carrying out the correlation studies with hadrons appearing at the final state is that the information about the possible early stage of mater is diluted or lost through re-scattering. In contrast to hadrons, two particle intensity interferometry using lepton pairs [126], or photon [149, 150], hence can provide the information on the history of evolution of hot matter efficiently, because EM probes do not re-scatter after its production.

5.3.1 Advantage of Lepton Pairs over Real Photons

In case of EM probes - lepton pairs have advantage over the real photons. The real photons with low transverse momentum (p_T) reflect the temperature of the source as their productions from a thermal source depend on the temperature (T) of the bath through the thermal phase space factors of the participants of the reaction that produces the photon. The thermal phase space factor may be changed by several factors - *e.g.* the transverse kick due to flow received by low p_T photons from the low temperature hadronic phase will mingle with the high p_T photons from the partonic phase, making the task of detecting and characterizing QGP more difficult. For dilepton the situation is, however, different because in this case we have two kinematic variables - out of these two, the p_T spectra of lepton pairs is affected but the p_T integrated invariant mass (M) spectra is unaltered by the flow. Moreover, from Fig. 3.15, it is clear that the p_T integrated M distribution of lepton pairs with $M\,(>\,m_\phi)$ originate from the early time, providing information of partonic phase and pairs with $M\,\leq m_\rho$ are chiefly produced at late times giving information of the hadronic phase. As mentioned before, the study of the p_T integrated M along with p_T distribution of lepton pairs can act as a flow meter and chronometer [63] of the heavy ion collisions. Which suggests that a judicious choice of p_T and M windows will be very useful to characterize the QGP and the hadronic phases separately.

From the experimental point of view, like photon, dilepton interferometry encounters considerable difficulties compared to hadron interferometry due to small yield of the dileptons from the early hot and dense region of the matter and the associated large background primarily from the electro-magnetic decay processes of hadrons at freeze-out. However, recent work demonstrate that it is still possible to carry out experimentally such interferometry studies [149]. With a high statistics data already collected at RHIC in the year 2010 by both STAR and PHENIX collaborations having dedicated detectors (Time-Of-Flight [151] and Hadron Blind Detector [152]) with good acceptance for dilepton measurements, also augurs well for the dilepton interferometry analysis. In this work we present this new proposal for carrying out an experimental measurement of dilepton interferometry at RHIC. We establish through a hydrodynamical model based space-time evolution for central 0-5% Au+Au collisions at $\sqrt{s_{NN}} = 200$ GeV the promise of such a dilepton interferometry analysis will hold out to understand the properties of the partonic phase.

5.3.2 Bose-Einestein Correlation Function for Lepton Pairs

As interferometry of the dilepton pairs actually reflect correlations between two virtual photons, the analysis then concentrates on computing the Bose-Einstein correlation (BEC) function for two identical particles defined as,

$$C_2(\vec{p_1}, \vec{p_2}) = \frac{P_2(\vec{p_1}, \vec{p_2})}{P_1(\vec{p_1})P_1(\vec{p_2})} \tag{5.29}$$

where $\vec{p_i}$ is the three momentum of the particle i and $P_1(\vec{p_i})$ and $P_2(\vec{p_1}, \vec{p_2})$ represent the one- and two- particle inclusive lepton pair spectra respectively and is expressed as following.

$$P_1(\vec{p}) = \int d^4x \; \omega(x, K) \tag{5.30}$$

and

$$P_2(\vec{p_1}, \vec{p_2}) \;\; = \;\; P_1(\vec{p_1})P_1(\vec{p_2}) + \frac{\lambda}{3}\int d^4x_1 d^4x_2 \; \omega(x_1, K)\omega(x_2, K) \; \cos(\Delta x^\mu q_\mu) \tag{5.31}$$

where $K = (p_1 + p_2)/2$, $q_\mu = p_{1\mu} - p_{2\mu} = q_\mu$, $\Delta x_\mu = x_{1\mu} - x_{2\mu}$, $x_{i\mu}$ and $p_{i\mu}$ are four co-ordinates for position and momentum variables respectively and $\omega(x, K)$ is the source function related to the thermal emission rate of lepton pairs per unit four volume, expressed as as follows:

$$\omega(x, K) = \int_{M_1^2}^{M_2^2} dM^2 \, \frac{dR}{dM^2 d^2K_T dy} \tag{5.32}$$

With further simplification, the C_2 can redefined as;

$$C_2(\vec{p_1},\vec{p_2}) = 1 + \frac{\lambda}{3}\frac{[\int d^4x\ \omega(x,K)\cos(\Delta\alpha)]^2 + [\int d^4x\ \omega(x,K)\sin(\Delta\alpha)]^2}{P_1(\vec{p_1})P_1(\vec{p_2})} \tag{5.33}$$

where $\Delta\alpha = \alpha_1 - \alpha_2$, $\alpha_i = \tau M_{iT}\cosh(y_i - \eta) - r p_{iT}\cos(\theta - \psi_i)$, $M_{iT} = \sqrt{p_{iT}^2 + M^2}$ is the transverse mass, y_i is the rapidity, and ψ_i's are the angles made by p_{iT} with the x-axis.

The inclusion of the spin of the virtual photon will reduce the value of $C_2 - 1$ by 1/3. The correlation functions can be evaluated for different average mass windows, $\langle M\rangle$ ($\equiv M_{l^+l^-}$)= $(M_1 + M_2)/2$. The leading order process through which lepton pairs are produced in QGP is $q\bar{q} \to l^+l^-$ [79]. For the low M dilepton production from the hadronic phase the decays of the light vector mesons ρ, ω and ϕ have been considered including the continuum [39, 44, 45, 42, 80]. Since the continuum part of the vector meson spectral functions are included in the current work the processes like four pions annihilations [120] are excluded to avoid double counting.

Table 5.1: Values of the various parameters used in the relativistic hydrodynamical calculations.

Input	RHIC	LHC
dN/dy	1100	2376
T_i	290 MeV	640 MeV
τ_i	0.6 fm	0.1 fm
T_c	175 MeV	175 MeV
T_{ch}	170 MeV	170 MeV
T_{fo}	120 MeV	120 MeV
EoS	2+1 Lattice QCD	2+1 Lattice QCD

For the space time evolution of the system relativistic hydrodynamical model with cylindrical symmetry [58] and boost invariance along the longitudinal direction [24] has been used. The values of the parameters those required for space-time evolution are displayed in Table 5.1. With all these ingredients we evaluate the correlation function

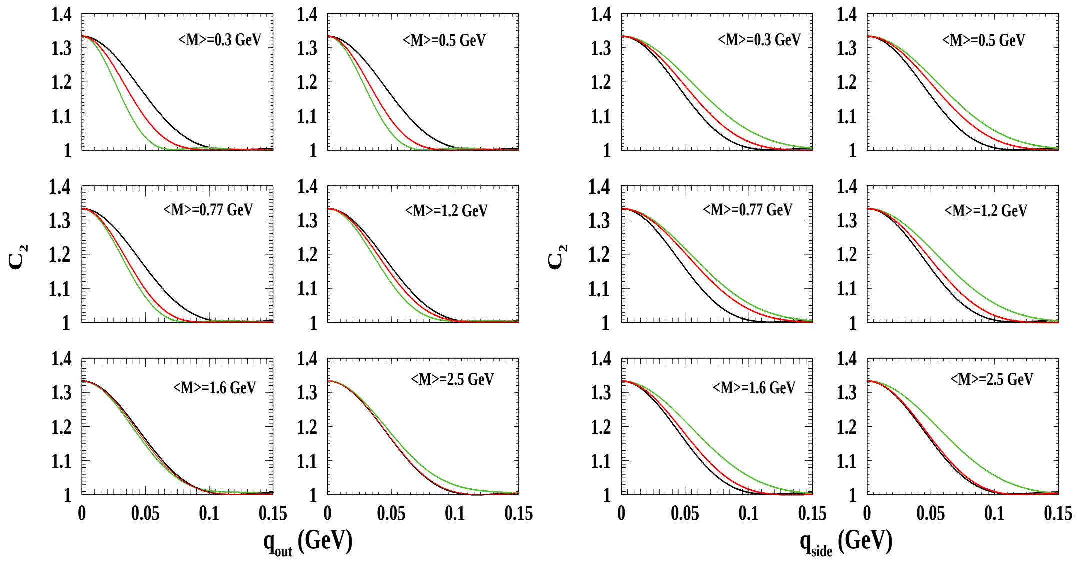

Figure 5.5: The C_2 as function of q_{out} and q_{side} for QGP (green line), hadron (red line), total (black line).

C_2 for 0-5% Au+Au collisions centrality for RHIC at $\sqrt{s_{NN}} = 200$ GeV [153] and Pb+Pb collisions at for LHC at $\sqrt{s_{NN}} = 2.76$ TeV [154] for different invariant mass windows as a function of q_{side} and q_{out} which are related to transverse momenta of individual pair (discussed in Section 5.2.3). Fig. 5.5 shows the BEC function of dilepton pairs for different values of $\langle M\rangle$ as a function of $q_{\rm side}$ and $q_{\rm out}$ for QGP and hadronic gas separately. By choosing appropriate phase space for the QGP and hadron gas and performing the space time integration using the initial condition tabulated in the Table. 5.1, the C_2 for different phase has been evaluated. We have evaluated the C_2 for $\langle M\rangle$ =0.3, 0.5, 0.7, 1.2, 1.6 and 2.5 GeV. In Fig. 5.6 the results for only three values of $\langle M\rangle$ corresponding to low and high mass which are expected to be dominated by radiations from QGP ($\langle M\rangle \sim 1.6$ GeV) and hadronic phase ($\langle M\rangle \sim 0.77$ GeV) respectively are displayed.

In Fig. 5.6, we plot the C_2 as function of q_{side} and q_{out} for RHIC initial conditions as tabulated in Table. 5.1. A clear difference of dilepton pair mass dependence of the BEC studied as a function of q_{side} is observed for the contributions from different M

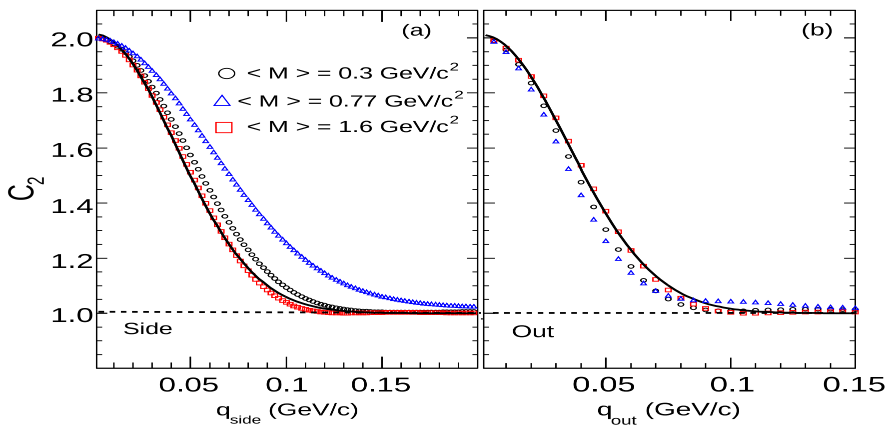

Figure 5.6: Correlation function for dilepton pairs as a function of q_{side} ((a), for $p_{1T} = p_{2T} = 2$ GeV and $\psi_2 = 0$) and q_{out} ((b), for $\psi_1 = \psi_2 = 0$ and $p_{1T} = 2$ GeV) for three values of $\langle M \rangle$ [126]. The solid lines shows the parameterization of C_2 using Eq. 5.27.

domains.The differences are however small when BEC is studied as a function of q_{out}.

5.4 Source Dimension

The source dimensions can be obtained by parameterizing the calculated correlation function of the dilepton pairs with the empirical (Gaussian) form:

$$C_2 = 1 + \lambda \exp(-R_i^2 q_i^2). \tag{5.34}$$

where the subscript i stand for *out* and *side* and λ (= 1/3 here) represents the degree of chaotic of the source. The deviation of λ from 1/3 will indicate the presence of non-thermal sources. A representative fit to the correlation functions are shown in Fig. 5.6 (solid lines). While the radius ($R_{\rm side}$) corresponding to q_{side} is closely related to the transverse size of the system and considerably affected by the collectivity, the radius ($R_{\rm out}$) corresponding to q_{out} measures both the transverse size and duration of particle emission [31, 146, 147]. The extracted $R_{\rm side}$ and $R_{\rm out}$ for different $\langle M \rangle$ are shown in

Fig. 5.7 and 5.8 respectively.

5.4.1 Variation of R_{side} with $\langle M \rangle$

The variation of R_{side} for QGP, hadronic and QGP + hadronic phase is obtained from the respective C_2 in that phase with an appropriate selection of phase space in space-time integration. The Fig. 5.7 shows non-monotonic dependence of $R_{\rm side}$ on M, starting from a value close to QGP value (indicated by the dashed line) it drops with increase in M finally again approaching the QGP value for $\langle M \rangle > m_\phi$.

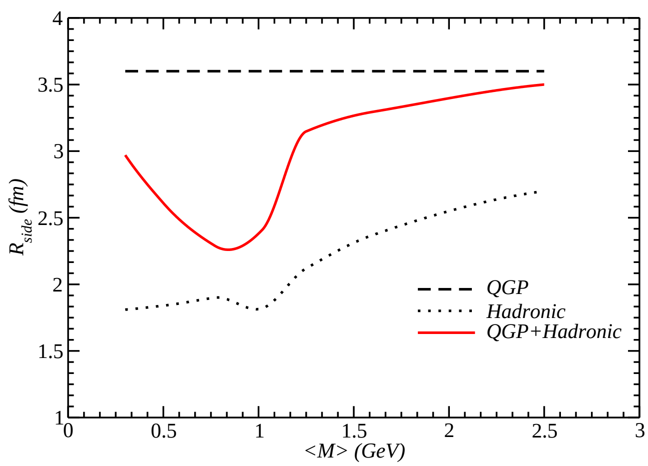

Figure 5.7: R_{side} is evaluated with $p_{1T} = p_{2T} = 2$ GeV and $\psi_2 = 0$ as a function of $\langle M \rangle$ for RHIC energy. The dashed, dotted and the solid line indicate the HBT radii for the QGP, hadronic and total dilepton contributions from all the phases respectively.

It can be shown that $R_{side} \sim 1/(1 + E_{\rm collective}/E_{\rm thermal})$ [145]. In the absence of radial flow, $R_{\rm side}$ is independent of $q_{\rm side}$. With the radial expansion of the system a rarefaction wave moves toward the center of the cylindrical geometry as a consequence the radial size of the emission zone decreases with time. Therefore, the size of the emission zone is larger at early times and smaller at late time. The high $\langle M \rangle$ regions are dominated by the early partonic phase where the collective flow has not been developed fully *i.e.*

the ratio of collective to thermal energy is small hence the source has larger R_{side}. In contrast, the lepton pairs with $M \sim m_\rho$ are emitted from the late hadronic phase where the size of the emission zone is smaller due to larger collective flow giving rise to a smaller R_{side}. The ratio of collective to thermal energy for such cases is quite large, which is reflected as a dip in the variation of R_{side} with $\langle M \rangle$ around the ρ-mass region (Fig. 5.7). Thus the variation of R_{side} with M can be used as an efficient tool to measure the collectivity in various phases of matter. The dip in R_{side} at $\langle M \rangle \sim m_\rho$ is due to the contribution dominantly from the hadronic phase. We observe that by keeping the ρ and ω contributions and setting radial velocity, $v_r = 0$, the dip in R_{side} vanishes, confirming the fact that the dip is caused by the radial flow of the hadronic matter. Therefore, the value of R_{side} at $\langle M \rangle \sim m_\rho$ may be used to estimate the average v_r in the hadronic phase.

5.4.2 Variation of R_{out} with $\langle M \rangle$

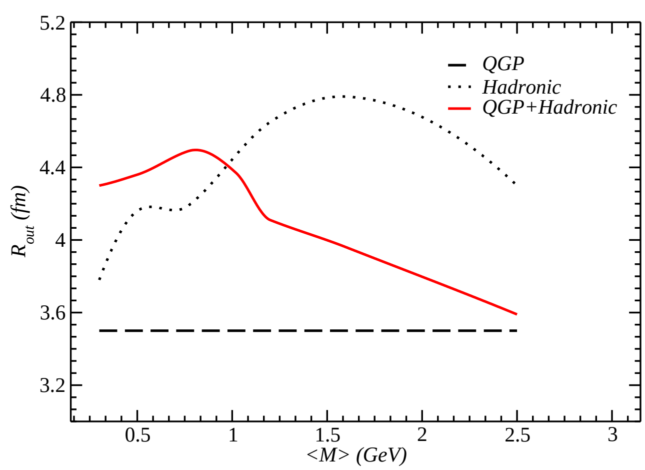

Figure 5.8: R_{out} is evaluated with $\psi_1 = \psi_2 = 0$ and $p_{1T} = 2$ as a function of $\langle M \rangle$ for RHIC. The dashed, dotted and the solid line indicate the HBT radii for the QGP, hadronic and total dilepton contributions from all the phases respectively.

The R_{out} probes both the transverse dimension and the duration of emission and unlike R_{side} it does not remain constant even in the absence of radial flow. As a result its variation with M is complicated. The values R_{out} for different phase are obtained in a similar fashion as followed for obtaining the R_{side} values for the different phases. The large M regions are populated by lepton pairs from early partonic phase where the effect of flow is small and the duration of emission is also small - resulting in smaller values of R_{out}. For lepton pair from $M \sim m_\rho$ the flow is large which could have resulted in a dip as in R_{side} in this M region. However, R_{out} probes the duration of emission too which is large for hadronic phase because the expansion is slower in this phase for the EoS used in the present work. The velocity of sound which controls the rate of expansion and hence the duration of the phase has larger value in hadronic phase than in the partonic phase. Thus resulting in the larger R_{out} in the hadronic phase than that of in partonic phase. The larger duration compensates the reduction of R_{out} due to flow in the hadronic phase resulting is a bump in R_{out} in this region of M (Fig. 5.8).

Both R_{side} and R_{out} approach QGP values for $\langle M \rangle \sim 2.5$ GeV implying dominant contributions from partonic phase.

5.4.3 Comparison of HBT Radii with Different Collision Energies

Now we study the sensitivity of the HBT radii on the different collision energy. The R_{side} and R_{out} extracted from the C_2's evaluated for 0-5% centrality in Au+Au collisions for RHIC at $\sqrt{s_{NN}} = 200$ GeV [153] and Pb+Pb collisions for LHC at $\sqrt{s_{NN}} = 2.76$ TeV [154] for different invariant mass windows as a function of q_{side} and q_{out} are shown in Fig. 5.9. The change of R_{side} with $\langle M \rangle$ for RHIC and LHC is qualitatively similar but quantitatively different. The smaller values of R_{side} for LHC is due to the larger radial expansion which can be understood from the fact that the quantity $E_{\text{collective}}/E_{\text{thermal}}$ is larger at LHC than RHIC. So, the dip in the R_{side} variation at LHC is below than that

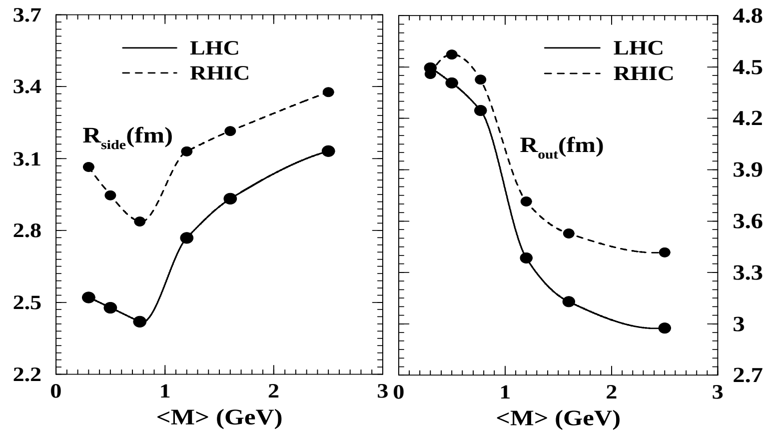

Figure 5.9: R_{side}(left panel) is evaluated with $p_{1T} = p_{2T} = 1$ GeV and $\psi_2 = 0$ and R_{out}(right panel) is evaluated with $p_{1T} = 1$ GeV and $\psi_1 = \psi_2 == 0$ as a function of $\langle M \rangle$ for RHIC (dashed line) and LHC (solid line) energies.

of at RHIC confirming a larger flow at LHC than RHIC. As the $R_{\rm out}$ probes both the transverse size and the duration of emission. From the previous discussion in Sec. 5.4.2, the larger duration compensates the reduction of $R_{\rm out}$ due to flow resulting is a bump in $R_{\rm out}$ for $M \sim m_\rho$. Though the duration of particle emission is more at LHC compared to RHIC (shown in Fig. 5.13), the larger flow (corresponds to smaller size) at LHC [127] than that of RHIC compensates other factor (like duration of emission) which has an enhancing effect on $R_{\rm out}$. So the value $R_{\rm out}$ at LHC is smaller than that of RHIC.

Radial Flow from HBT Radii

According to the discussion given in the Section 5.4, $R_{\rm side}$ is independent of $q_{\rm side}$ in the absence of radial flow. R_{side} is related to radial flow as following;

$$R_{side}(M) = \frac{\mathcal{K}}{\langle p_T(M) \rangle} \quad ; \quad \langle P_T(M) \rangle = T_{av} + M v_r^2 \tag{5.35}$$

The values of $R_{side}(M)$ is obtained for different $\langle M \rangle$ windows (shown in Fig. 5.7). The higher mass, i.e. $\langle M \rangle = 2.5$ GeV, corresponds to the initial stage of collision where the flow is not developed fully. So assume for $\langle M \rangle = 2.5$, $v_r = 0$ and $T = T_i$ the value of $\mathcal{K} = T_i \times R_{side}|_{\langle M \rangle = 2.5}$. Once we know the value of $\mathcal{K}$, we can calculated the $\langle p_T(M) \rangle$ $(= \mathcal{K}/R_{side}(M))$ The variation of $\langle p_T \rangle$ with $\langle M \rangle$ has displayed in Fig. 5.10.

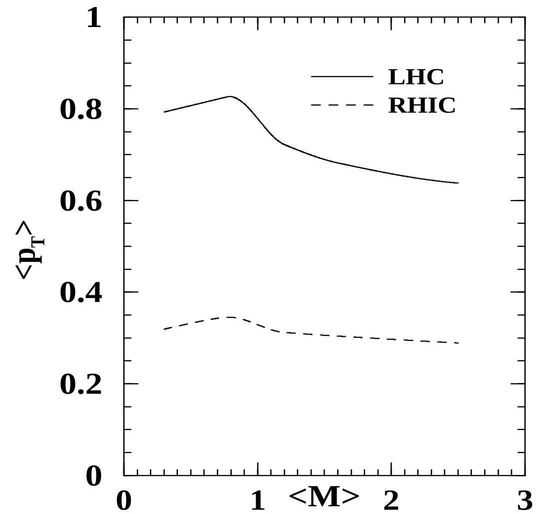

Figure 5.10: variation of $\langle p_T \rangle$ as function of M(See Eq. 5.35).

The high $\langle M \rangle$ regions are dominated by the early partonic phase where the collective flow has not been developed fully hence show smaller $\langle p_T \rangle$. In contrast, due to larger collective flow for the lepton pairs with $M \sim m_\rho$, emitted from the late hadronic phase, $\langle p_T \rangle$ is larger. The larger value of $\langle p_T \rangle$ around the ρ-mass region is due to the contribution of large flow in the hadronic phase. Thus the variation of $R_{\rm side}$ with M(Fig. 5.7) can be used as an efficient tool to measure the collectivity in various phases of matter.

5.4.4 Sensitivity of HBT Radii on p_{iT}

In this section, the sensitivity of the HBT radii for different values of the individual transverse momentum of the pairs is described. In Fig. 5.11, the variation of R_{side} and

R_{out} with $\langle M\rangle$ are shown for $p_{1T} = 1$ and 2 GeV. The lepton pairs coming from higher p_T and high mass region enable us to quantify the size of hotter zone. As mentioned befor, the p_T contains the effect of flow as well as thermal motion. Hence the larger R_{side} at $M \sim M_\rho$ for p_T=2 GeV is associated with longer flow and hence smaller source size. The observed bump in R_{out} (Fig. 5.11, right) is resulted from the fact that it contains both the size of the system as well as the duration of dilepton emission as discussed earlier.

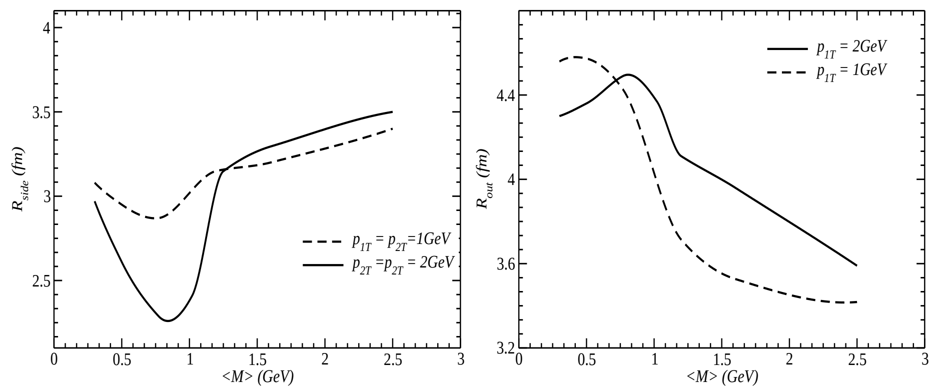

Figure 5.11: Left panel of figure shows R_{side} as a function of $\langle M\rangle$ which is evaluated with $p_{1T} = p_{2T}$ =1 and 2 GeV and $\psi_2 = 0$ and similarly R_{out} as a function of for $\psi_1 = \psi_2 = 0$ and p_{1T}=1 and 2 GeV $\langle M\rangle$. The p_{1T}=1 and 2 GeV results are shown as dashed line and solid line respectively.

5.4.5 Duration of Particle Emission from HBT Radii

The HBT radii, $R_{\rm out}$ and $R_{\rm side}$, provide the information of average source size. However, in the ratio, $R_{\rm out}/R_{\rm side}$ some of the uncertainties associated with the space time evolution get canceled out. The quantity, $R_{\rm out}/R_{\rm side}$ gives the duration of particle emission [143, 145, 148] for various domains of M. The difference between $R^2_{side}(K)$ and $R^2_{out}(K)$ at non-zero in K is then only due to the explicit K-dependence in Eqs. 5.28, i.e. the term $v_r\langle t^2\rangle$. This implies that the explicit K-dependence dominates if the emission duration is sufficiently large or if the position-momentum correlations in the source are sufficiently weak,

$$R^2_{diff} = R^2_{out}(K) - R^2_{side}(K) = v_r \langle t^2 \rangle \tag{5.36}$$

In this case, the difference between these two HBT radius parameters gives direct access to the average emission duration $\langle t^2 \rangle$ of the source and allows to partially disentangle the spatial and temporal information contained in Eqs. 5.28.

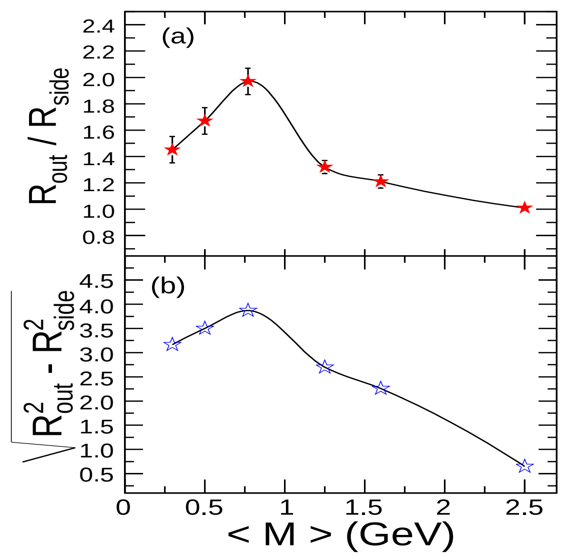

Figure 5.12: The ratio R_{out}/R_{side} and the difference $\sqrt{R^2_{out} - R^2_{side}}$ as a function of $\langle M \rangle$.

Figure 5.12 shows the R_{out}/R_{side} and the difference $\sqrt{R^2_{out} - R^2_{side}}$ as a function of $\langle M \rangle$ for Au+Au collisions at $\sqrt{s_{NN}} = 200$ GeV. Both show a non-monotonic dependence on $\langle M \rangle$. The smaller values of both the quantities, particularly at high mass region, reflect the contributions from the early partonic phase of the system. The peak around ρ-meson mass reflects dominance of the contribution from hadronic phase as discussed before. Fig. 5.13 shows a comparative study of the above two quantities (the ratio and the difference of R_{out} and R_{side}) for RHIC and LHC energies. The reflect a larger life time of thermal system for LHC than RHIC.

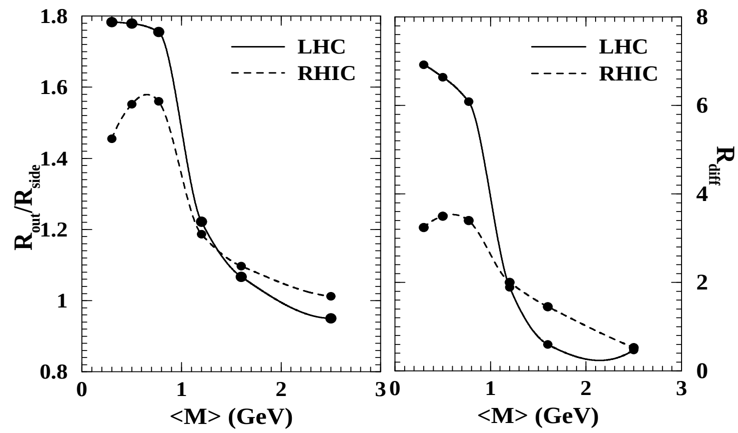

Figure 5.13: The ratio R_{out}/R_{side} (left panel) and the difference $\sqrt{R^2_{out} - R^2_{side}}$ (right panel) as a function of $\langle M \rangle$ for RHIC (dashed line) and LHC (solid line) energies is shown.

Some comments on the effects of in-medium effect change of ρ spectral function on R_{side} and R_{out} are in order here. The dilepton emission rate from the hadronic matter may change ue to the broadening of the ρ meson in hot medium in low mass domain ($M \leq M_\rho$). Such chages in the emission rate may alter the values of R_{out} and R_{side} in the region $M \leq M_\rho$. We have checked that the values of R_{side} and R_{out} change by 10% for $M \sim 500$ MeV but their values in the high M region ($M \geq M_\phi$) remain unaltered.

5.5 Experimental Challenges

Now we discuss two experimental challenges in such studies, i.e. probability to get two pairs and possibility of dilution of signal due to addition of random pairs.

5.5.1 Probability to Get Two Lepton Pairs

In this section, a rough estimation of the probability of getting two lepton pairs at RHIC and LHC energy has been evaluated. Thus the number of events has been predicted to perform the interferometry with lepton pair in a given p_T an M window.

RHIC :

We quote some numbers from the PHENIX measurements, keeping in mind that the situation will further improved by increasing the luminosity as well as collision energy. The number of events can be computed from the luminosity ($\mathcal{L}$), the in-elastic cross-section (σ) and the run time ($\mathcal{T}$) of the machine as,

$$N_{\rm event} = \mathcal{L} \times \sigma \times \mathcal{T} \tag{5.37}$$

For RHIC, the luminosity, $\mathcal{L}$ is of the order of $50 \times 10^{27}/\mathrm{cm}^2$.sec and σ=40 mb. If RHIC runs for 12 weeks then the number of events, $N_{\rm event} = 1.45 \times 10^{10}$. For the M, $810 \leq M(MeV) \leq 990$, the differential number $(dN/2\pi p_T dp_T dy)$ measured by PHENIX collaboration in Au+Au collisions [124] at $\sqrt{s_{\rm NN}} = 200$ GeV is give by (Fig.3.15):

$$\frac{dN}{2\pi p_T dp_T dy} \mid y = 0 = \frac{N_{part}}{2} \times 1.29 \times 10^{-7} \tag{5.38}$$

for the p_T bin 1-1.8 GeV. Therefore, the (differential) number of pairs in the above range of p_T and M is $\sim 1.45 \times 10^{10} \times \frac{N_{part}}{2} \times 1.29 \times 10^{-7} \sim \frac{N_{part}}{2} \times 1870$. Similarly for M, $500 \leq M(MeV) \leq 750$, the measured value of the above quantity is:

$$\frac{dN}{2\pi p_T dp_T dy} \mid_{y=0} = \frac{N_{part}}{2} \times 2.235 \times 10^{-7} \tag{5.39}$$

for the p_T bin 1.4-1.8 GeV. This indicates that the (differential) number of pairs in this kinematic domain is $\sim 1.45 \times 10^{10} \times \frac{N_{part}}{2} \times 2.235 \times 10^{-7} \sim \frac{N_{part}}{2} \times 3240$.

For 0-10 % centrality the number of participants for Au-Au collisions at $\sqrt{s_{NN}}$=200 GeV is about 330. The number of lepton pairs in the p_T range 1.4-1.5 GeV is $\sim 5.3 \times 10^5$ for the M window 0.5-0.75 GeV. For 12 weeks of runtime the number of events estimated with the current RHIC luminosity is $\sim 1.45 \times 10^{10}$. Then the number of pairs produced per event is $\sim 3 \times 10^{-5}$ in the kinematic range mentioned above. The probability to have two pairs of dileptons is $\sim 10^{-9}$. Therefore, roughly 10^9 events are required to make the HBT interferometry with lepton pairs possible.

It is expected that further increase in luminosity at RHIC by a factor 2 beyond the years 2012 to about 10^{28} cm^{-2} s^{-1} may be a motivating factor for such measurements. The increase in production at Large Hadron Collider (LHC) may also provide a reason to pursue such measurements.

LHC :

We compute the number of events (using Eq. 5.39) for a run time, $\mathcal{T}$=12 weeks of the LHC with $\mathcal{L} = 50 \times 10^{27}/(\text{cm}^2.\text{sec})$ and σ=60 mb, we get $N_{event} \sim 2 \times 10^{10}$. As an example for $\langle M \rangle$ =500 MeV and $p_T = 1$ GeV, the value of (dN/d^2p_Tdy) for Pb+Pb collision at $\sqrt{s_{NN}}$=2.76 TeV is $\sim 0.138 \times 10^{-3}$. Therefore, the total (for 2×10^{10} number of events) differential number of pairs in the above range of p_T and M is $\sim 2 \times 10^{10} \times 0.138 \times 10^{-3} \sim 2.7 \times 10^6$. Similarly for the $\langle M \rangle$ =1.02 GeV and p_T=1 GeV, the total (differential) number of pairs is $\sim 2 \times 10^6$. In this domain of p_T and M the number of pairs produced per event is $\sim 10^{-4}$. Therefore, the probability to get two pairs is 10^{-8}, Therefore, roughly 10^8 events will be necessary to perform the interferometry with lepton pairs in this region of p_T and M.

5.5.2 Possibility of Dilution of Signal Due to Random Pairs

The possibility of dilution of signal due to addition of random pairs, which one may encounter in the analysis of experimental data is discussed below. We have added some " mixture" to the dilepton source with exponential energy distribution, *i.e.* we have replaced ω by $\omega + \delta\omega$ where $\delta\omega$ has exponential energy (of the pair) dependence and weight factor is as large as that of ω itself. Then we find that the resulting change in the HBT Radii is negligibly small. This can be understood from the fact that the C_2 (Eq. 5.29) can be written as:

$$\begin{aligned} C_2 \quad &= 1 + \frac{\int d^4x_1\omega(x_1,P)\cos(\alpha_1)\int d^4x_2\omega(x_2,KP)\cos(\alpha_2)}{\int d^4x\omega(x,\vec{p_1})\int d^4x\omega(x,\vec{p_2})} \\ &+ \frac{\int d^4x_1\omega(x_1,P)\sin(\alpha_1)\int d^4x_2\omega(x_2,K)\sin(\alpha_2)]}{\int d^4x\omega(x,\vec{p_1})\int d^4x\omega(x,\vec{p_2})} \end{aligned} \tag{5.40}$$

where

$$\begin{aligned} \alpha_1 &= \tau_1 M_{1T}\cosh(y_1-\eta_1) - r_1 p_{1T}\cos(\theta_1-\psi_1) - \tau_1 M_{2T}\cosh(y_2-\eta_1) + r_1 p_{2T}\cos(\theta_1-\psi_2) \\ \alpha_2 &= \tau_2 M_{2T}\cosh(y_2-\eta_2) - r_2 p_{2T}\cos(\theta_2-\psi_2) - \tau_2 M_{1T}\cosh(y_1-\eta_2) + r_2 p_{1T}\cos(\theta_2-\psi_1) \end{aligned}$$

It is clear that the expression for C_2 contains quadratic power of the source function both in the numerator and denominator. Therefore, changes in the source function will lead to some sort of partial cancellation (complete cancellation is not possible because source function appears in the numerator and the denominator inside the integral with different dependent variables, P or p_i).

Chapter 6

Elliptic Flow of Thermal Dileptons

6.1 Introduction

The recent results obtained from RHIC and LHC provide compelling evidence of formation of dense partonic matter. It has been claimed that the dense matter formed at RHIC and LHC acts like a strongly coupled plasma with almost perfect fluid behavior [155]. Out of several signatures of QGP, elliptic flow in non-central collision is one of the most important observable which provides strong evidence of the existence of collectivity - which if exists in the partonic phase - may persist after the transition into hadronic phase. The large azimuthal anisotropy $v_2(p_T)$ [27, 28, 29, 30] of particle emission with respect to reaction zone obtained from non-central collision at RHIC and LHC suggests that collectivity developed at early stage of the collision. Thus elliptic flow is considered as early time phenomenon. The strong elliptic flow, together with detailed dependence on particle mass and p_T , is well described by hydrodynamics [27].

6.2 Elliptic Flow

The azimuthal momentum distribution can be expanded into Fourier series as ;

$$\frac{dN}{d\phi} = \frac{N}{2\pi}\left[1 + 2v_1\cos(\phi) + 2v_2\cos(2\phi)\right] \tag{6.1}$$

$$v_n = \frac{\int d\phi \cos(n\phi)\frac{dN}{d\phi}}{\int d\phi \frac{dN}{d\phi}} \tag{6.2}$$

where ϕ is the azimuthal angle of momentum between produced particle w.r.t reaction plane and v_n's are the Fourier coefficient of n-th harmonic. Because of symmetry around y-axis (see Fig. 6.1) the sine term vanishes. The first and second harmonics, v_1 an v_2, are called directed and elliptic flow parameters respectively. Elliptic flow, v_2 measures

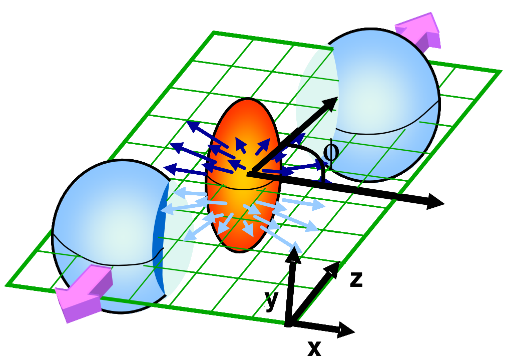

Figure 6.1: Elliptic flow in a non central collision.

the azimuthal correlation of produced particle with respect to the reaction plane. From geometric consideration, the initial reaction zone formed in a non-central nuclear collision between two spherical nucleus is anisotropic. The asymmetry of this elliptic zone is described by the spatial eccentricity, which is defined as

$$\varepsilon_x = \frac{\langle y^2 - x^2\rangle}{\langle y^2 + x^2\rangle} \tag{6.3}$$

The $\langle ... \rangle$ denotes the average over the transverse plane with the number density of the participants as a weighting function

$$\langle ... \rangle = \int dxdy...n_{part}. \tag{6.4}$$

It is assumed that due to the strong interaction and high collision rate among the constituent particles, the system quickly reaches local thermal equilibrium. Assuming local thermal equilibrium the state of the system can described by the thermodynamic variables such as energy density, pressure and temperature etc. The initial azimuthal anisotropy of the reaction zone results in a asymmetric pressure gradient. Thus the expansion takes at a higher rate along the short axis of the elliptic zone compared to the direction of the longer axis. The asymmetry in the fluid velocity is described by

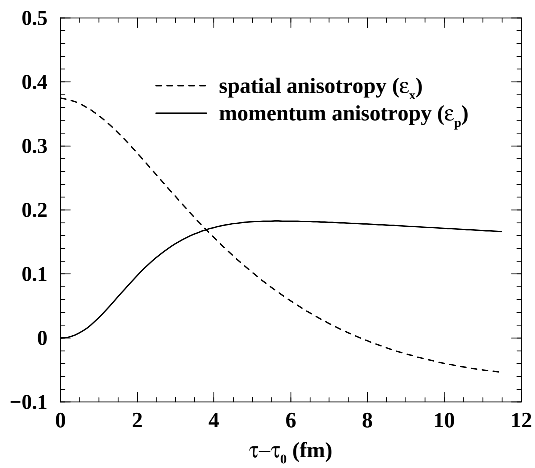

Figure 6.2: Variation of spatial anisotropy and momentum anisotropy as function proper time.

momentum anisotropy which is analogous to spatial anisotropy and is defined as

$$\varepsilon_p = \frac{\int dxdy(T^{xx} - T^{yy})}{\int dxdy(T^{xx} + T^{yy})} \tag{6.5}$$

where T^{xx} and T^{yy} are the spatial component of the energy momemtum tensor, $T^{\mu\nu}$. In Fig. 6.2, we display the spatial and momentum anisotropy. Because of the transverse expansion, the spatial anisotropy decreases and momentum anisotropy increases with time. In a hydrodynamic model elliptic flow coefficient, v_2 is proportional to ε_p. Thus the increasing momentum anisotropy leads to a increased v_2.

6.3 Hadron Elliptic Flow

Most of the studies with the elliptic flow have done with the hadrons [27, 28, 29, 30]. Figure 6.3 shows the rest mass dependance of the differential $v_2(p_T)$, at low p_T which rises and saturates at higher p_T.

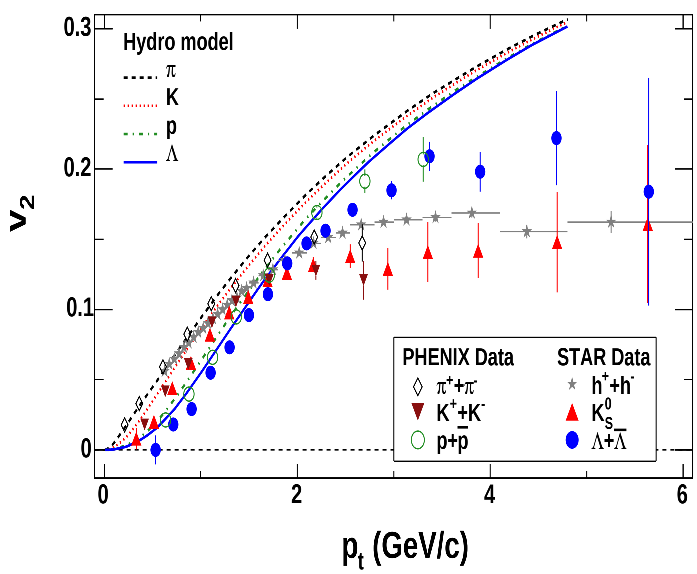

Figure 6.3: The differntial elliptic flow of identified hadrons from STAR collaboration [29] with hydro predictions from the Ref. [27]

A mass ordering for hadronic elliptic flow has been predicted by hydrodynamics [27]. For a given p_T, v_2 obtained is smaller for the heavier particles, such as proton and Λ, compared to lighter pions and kaons. $v_2(p_T)$ of hadrons obey a clear mass ordering in the range of $p_T \sim 1 - 2GeV$. As radial flow builds up in the collision, the heavier particles gain more momentum than lighter ones, which is responsible for m_T scale breaking

(Section. 4.1.1). At low p_T regime, the reduction of $v_2(p_T)$ is due to the flattening of p_T spectra for massive particles. The measured elliptic flow matches the upper limit of ideal hydrodynamics for large range of impact parameters and transverse momenta ($p_T < 1.5 \sim 2$GeV). The hydrodynamics constrained to both dynamical evolution as well as thermalization time of the collision. The fireball must experience an early thermalization, to match the large $v_2$observed experimentally. Without early thermalization, the initial spatial eccentricity will reduce and not contribute to elliptic flow. With large thermalization, i.e. $\tau_i > 1$fm/c, the hydrodynamics will not be able to reproduce the measured single particle spectrum and hadronic elliptic flow. Since the early dynamics of a heavy-ion collision reflects a strongly interacting non-perturbative ideal fluid in the QGP phase, its often given the name "sQGP" for "strongly coupled quark gluon plasma".

6.4 Elliptic Flow of Thermal Dilepton

In contrast to hadrons, which are predominantly emitted from the freeze-out surface of fireball, the the observables of electromagnetically interacting particles (real photons and dileptons) are considered as more direct and penetrating probes to span the entire space-time profile of the expanding fireball and also provide information about pristine stage of the matter produced in HIC. In this regard, estimating flow using photons and dilepton is more beneficial (described in Sec 4.1.2). The v_2 of real photons and dileptons [139, 156, 157, 158] have been evaluated for RHIC energies and shown that it can be used as effective probes to extract the properties of the partonic plasma. The sensitivity of the v_2 of lepton pairs on EoS has been elaborated in [158] for RHIC collision conditions. The lepton pairs are produced from each space time point of the system and hence the study of v_2 of lepton pairs will shed light on the time evolution of collectivity in the system [107, 159]. The radial flow alters the shape of the p_T spectra of dileptons - it kicks the low p_T pairs to the higher p_T domain, making the spectra flatter. Therefore, the presence of large radial flow may diminish the magnitude of v_2 at low p_T [27] and this effect will be larger when the radial flow is large i.e. in the hadronic phase which corresponds to lepton pairs with $M \sim m_\rho$.

It has been argued that the anisotropic momentum distribution of the hadrons can bring the information on the interaction of the dense phase of the system [130] despite the fact that the hadrons are emitted from the freeze-out surfaces when the system is too dilute to support collectivity. Therefore, a suitable dynamical model is required to extrapolate the final hadronic spectra backward in time to get the information about the early dense phase. Such an extrapolation is not required for lepton pairs because they are emitted from the entire space-time volume of the system. Therefore, the v_2 of lepton pairs provide information of the hot and dense phase directly. The v_2 of dileptons can also be used to to test the validity and efficiency of the extrapolation required for hadronic v_2. We will also see below that the p_T integrated M distribution of lepton pairs with $M\,(>\,m_\phi)$ originate from the early time, providing information of the partonic phase and pairs with $M\,\leq\,m_\rho$ are chiefly produced later from the hadronic phase. Therefore, the p_T integrated M distribution of lepton pairs may be used as a chronometer [63] of the heavy ion collisions. On the other hand, the variation of v_2 with p_T for different M windows may be used as a flow-meter [64].

The elliptic flow of dilepton, v_2, can be defined as

$$v_2(p_T, M) = \langle cos2\phi \rangle = \frac{\sum_{i=Q,H} \int cos(2\phi) \left(\frac{dN^{\gamma*}}{d^2p_T dM^2 dy}|_{y=0}\right)_i d\phi}{\sum_{i=Q,H} \int \left(\frac{dN^{\gamma*}}{d^2p_T dM^2 dy}|_{y=0}\right)_i d\phi} \tag{6.6}$$

where the $\sum$ stands for summation over Quark Matter(QM) and Hadronic Matter(HM) phases. The quantity $dN/d^2p_T dM^2 dy|_{y=0}$ appearing in Eq. 6.6 can be obtained from the dilepton production per unit four volume, dN/d^4pd^4x in a thermalized medium by integrating over the space-time evolution of the system (described in Sec.3.5). The dN/d^4pd^4x for lepton pairs for QGP and hadrons are discussed in Sec. 3.5.1 an 3.5.2 respectively . For the present study, we have taken low mass dilepton production from HM the decays of thermal light vector mesons namely ρ, ω and ϕ have been considered. The change of spectral function of ρ due to its interaction with π, ω, a_1, h_1 (see [81] for details) and baryons [160] have been included in evaluating the production of lepton pairs from HM. For the ω spectral function the width at non-zero temperature is taken from Ref [161] and medium effects on ϕ is ignored here. The continuum part of the spectral function of ρ and ω have also been included in dilepton production rate [45, 80]. In the present work dileptons from non-thermal sources [162] *e.g.* from the Drell-Yan process and decays of heavy flavours have been ignored in evaluating the elliptic flow of lepton pairs from thermal partons and hadrons. The model employed in the present work leads to a reasonably good agreement with NA60 dilepton data [121] for SPS collision conditions [123] (although there is a small discrepancy in the low mass window).

To evaluate v_2 from Eq. 6.6 one needs to integrate the fixed temperature production rate given by Eq. 3.9 over the space time evolution of the system - from the initial QGP phase to the final hadronic freeze-out state through a phase transition in the intermediate stage. The space-time evolution is done over the 4-volume, which is defined as d^4x $(= \tau d\tau\, dx\, dy\, d\eta)$ is expressed in terms of $x^\mu = (\tau, x, y, \eta)$ where τ and η are defined through the Eq. 2.7 and 2.8. We assume that the matter is formed in QGP phase with zero net baryon density in Pb+Pb collision at $\sqrt{s_{\rm NN}} = 2.76$ TeV. The energy of the lepton pair (p_0) should be replaced by its value in the co-moving frame of the expanding system which is given by Eq.2.20. The EoS required to close the hydrodynamic equations is constructed by complementing Wuppertal-Budapest lattice simulation [21] with a hadron resonance gas comprising of all the hadronic resonances up to mass of 2.5 GeV [30, 163]. The necessary initial conditions to solve the hydrodynamic equations is $T_i = 456$ MeV, the value of the temperature corresponding to the maximum of the initial energy profile for 30-40% centrality at $\sqrt{s_{\rm NN}}$ =2.76 TeV, with $\tau_i = 0.6$ fm/c, the thermalization time. The transition temperature, T_c for quark hadron conversion is taken as 175 MeV. The system is assumed to get out of chemical equilibrium at $T = T_{ch} = 170$ MeV [106]. The kinetic freeze-out temperature $T_F = 130$ MeV is fixed from the p_T spectra of the produced hadrons at the same collision energy of Pb+Pb system. The EoS and the values of the parameters mentioned above are constrained by the p_T spectra (for $0-5\%$ centrality) and elliptic flow (for $10-50\%$ centrality) of charged hadrons [30] measured by ALICE collaboration [164].

6.4.1 Results and Discussion

In Fig. 6.4 we depict the constant temperature contours corresponding to $T_c = 175$ MeV and $T_f = 130$ MeV in the $\tau - x$ plane (at zero abscissa) indicating the boundaries for the QM and HM phases respectively.

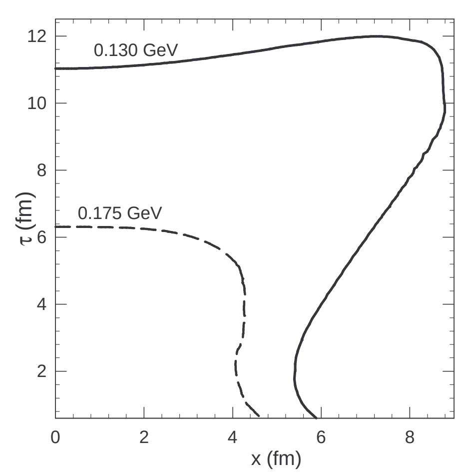

Figure 6.4: Constant temperature contours denoting space-time boundaries of the QGP and hadronic phase.

The life time of the QM phase ~ 6 fm/c and the duration of the HM is$\sim 6-12$ fm/c. Throughout this work by early and late will approximately mean the duration of the QM and HM respectively.

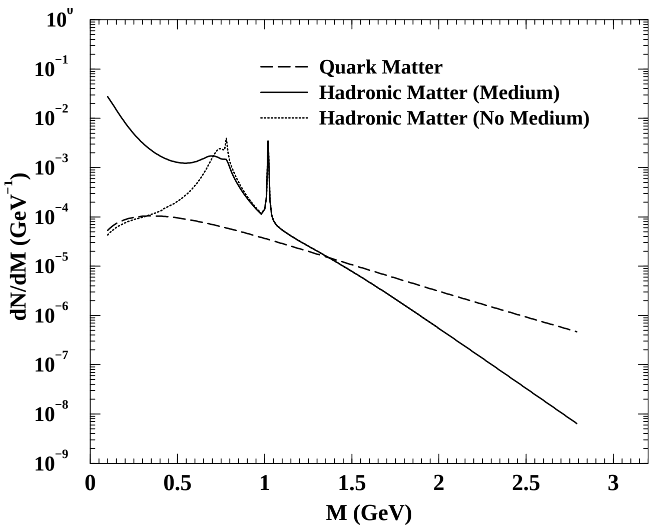

Figure 6.5: Invariant mass distribution of lepton pairs from quark matter and hadronic matter [125].

With all the ingredients mentioned above we evaluate the p_T integrated M distribution of lepton pairs originating from QM and HM (with and without medium effects on the spectral functions of ρ and ω). The results are displayed in Fig. 6.5 for the initial conditions and centrality mentioned above. We observe that for $M > M_\phi$ the QM contributions dominate. For $M_\rho \leq M \leq M_\phi$ the HM shines brighter than QM. For $M < M_\rho$, the HM (solid line) over shines the QM due to the enhanced contributions primarily from the medium induced broadening of ρ spectral function. However, the contributions from QM and HM become comparable in this region of M if the medium effects on ρ spectral function is ignored (dotted line). Therefore, the results depicted in Fig. 6.5 indicate that a suitable choice of M window will enable us to unravel the contributions from a particular phase (QM or HM).

To further quantify these issues we evaluate the following quantity:

$$F = \frac{\int' \left(\frac{dN}{d^4xd^2p_TdM^2dy}\right) dxdyd\eta\tau d\tau d^2p_TdM^2}{\int \left(\frac{dN}{d^4xd^2p_TdM^2dy}\right) dxdyd\eta\tau d\tau d^2p_TdM^2} \tag{6.7}$$

where the M integration in both the numerator and denominator are performed for selective M windows from M_1 to M_2 with mean M defined as $\langle M\rangle = (M_1 + M_2)/2$. The prime in $\int'$ in the numerator indicates that the τ integration in the numerator is done from $\tau_1 = \tau_i$ to $\tau_2 = \tau_i + \Delta\tau$ with progressive increment of $\Delta\tau$, while in the denominator the integration is done over the entire lifetime of the system. In the Fig. 6.6, F is

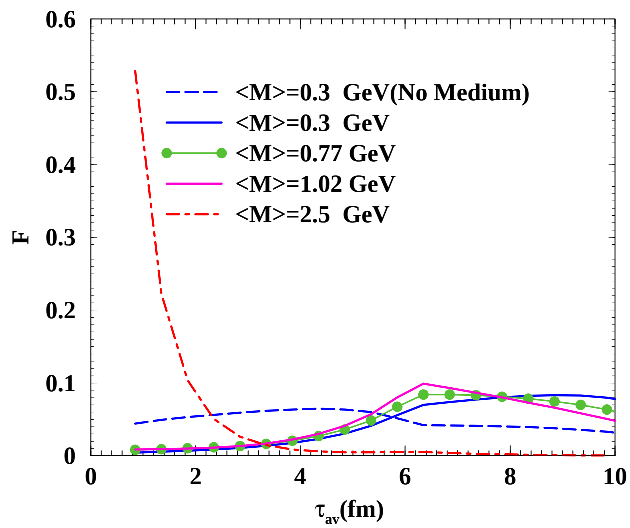

Figure 6.6: Fractional contribution of lepton pairs for various invariant mass windows as a function of average proper time (see text for details) [125].

plotted against $\tau_{\rm av}(= (\tau_1 + \tau_2)/2)$. The results substantiate the fact that pairs with high $\langle M\rangle \sim 2.5$ GeV originate from QM ($\tau_{\rm av} \leq 6$ fm/c, QGP phase) and pairs with $\langle M\rangle \sim 0.77$ GeV mostly emanate from the HM phase ($\tau_{\rm av} \geq 6$ fm/c). The change in the properties of ρ due to its interaction with thermal hadrons in the bath is also visible through F evaluated for $\langle M\rangle \sim 0.3$ GeV with and without medium effects. This clearly indicates that the $\langle M\rangle$ distribution of lepton pairs can be exploited to extract collectivity of different phases of the evolving matter.

The Fig. 6.7 (left pannel) shows the differential elliptic flow, $v_2(p_T)$ of dileptons

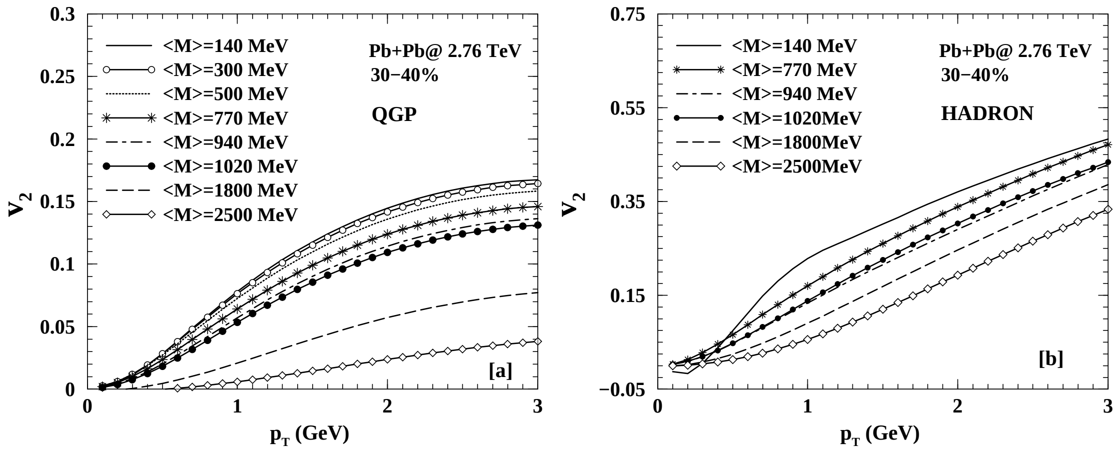

Figure 6.7: Elliptic flow of quark matter(left pannel) and hadronic matter(right pannel) as function of p_T for various mass windows.

arising from various $\langle M \rangle$ domains in quark matter. Similarly the right pannel of Fig. 6.7 shows the differential elliptic flow, $v_2(p_T)$ of dileptons arising from various $\langle M \rangle$ domains from hadronic matter. The individual v_2 for QM and HM is obtained by doing a integration over specific invariant masses (M) window as well as space time integration over the regime where $T_c < T(\tau, x, y) < T_i$ and $T_f < T(\tau, x, y) < T_c$ respectively . The v_2 is small at low p_T and gradually increase and attains large value around $p_T \sim 2{-}3GeV/c$. Also there is clear mass ordering has been observed for $v_2(p_T)$ for QM, i.e., v_2 decreases with increase in M. This is because dileptons come from high M region, $M > M_\phi$, come mostly from hot partonic phase where the fluid velocity is not strong to support the collectivity but the spatial eccentricity of the source is large. On the other hand dileptons that come from low M region, M below ϕ peak dominantly come from late hadronic matter where the collectivity is strong and the spatial asymmetry dissolve into momentum asymmetry.

Fig. 6.8 shows the differential elliptic flow, $v_2(p_T)$ of dileptons arising from various $\langle M \rangle$ domains. We observe that for $\langle M \rangle = 2.5$ GeV v_2 is small for the entire p_T range because these pairs arise from the early epoch (see Fig. 6.6) when the flow is not de-

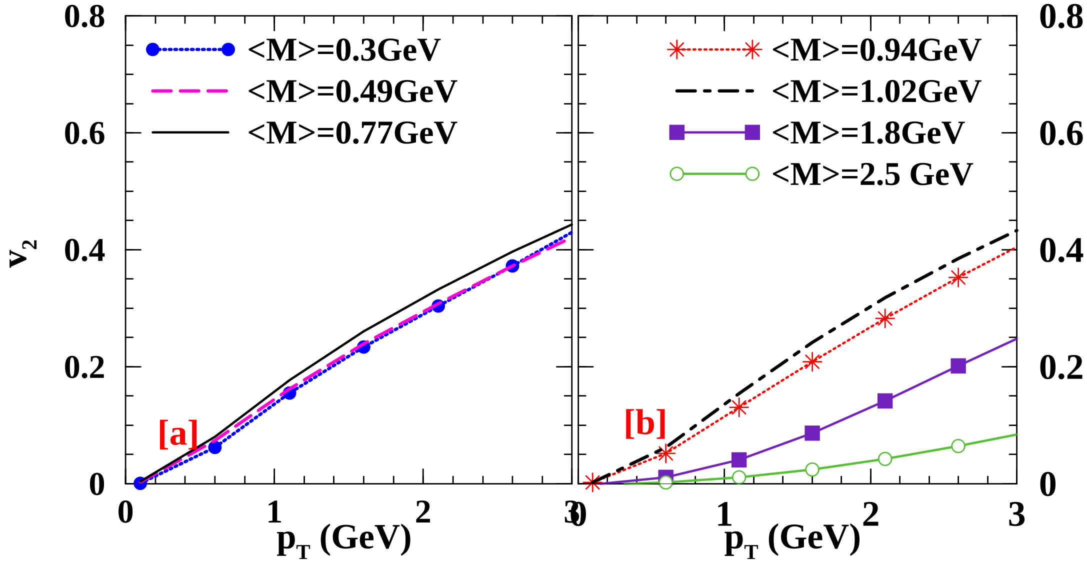

Figure 6.8: Total elliptic flow as function of p_T for various mass windows.

veloped entirely. However, the v_2 is large for $\langle M \rangle = 0.77$ GeV as these pairs originate predominantly from the late hadronic phase when the flow is fully developed.

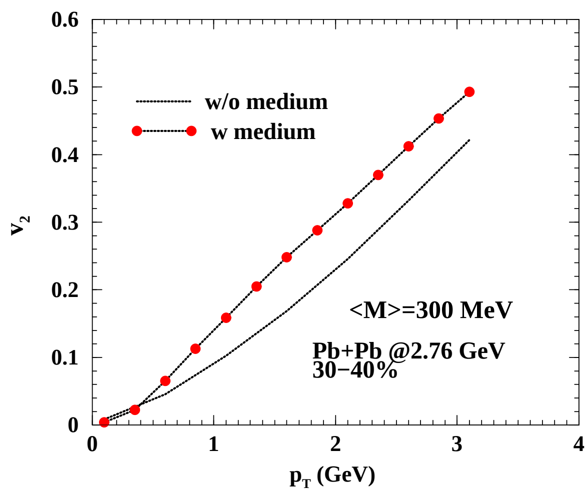

Figure 6.9: The fig displays the effect of the broadening of ρ spectral function on the elliptic flow for $\langle M \rangle = 300$ MeV.

It is also interesting to note that the medium induced enhancement of ρ spectral function provides a visible modification in v_2 for dileptons below ρ peak. The Fig. 6.9 shows the comparison between $v_2(p_T)$ of dilepton at $\langle M \rangle$=300 MeV with and without medium effects.

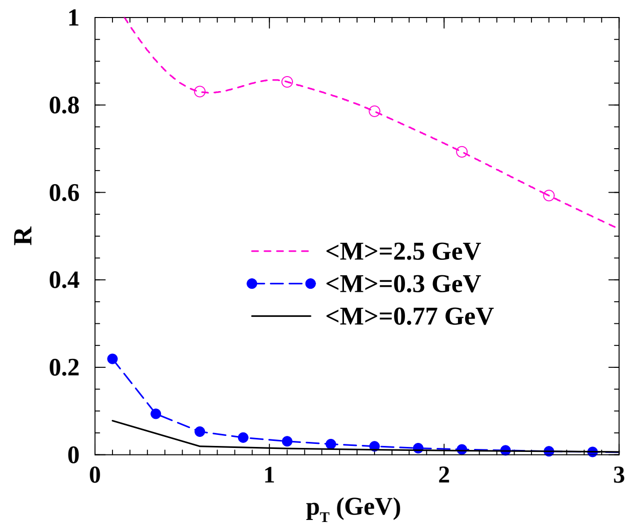

Figure 6.10: shows the variation of R_Q (see text) with p_T for ¡M¿ = 0.3 GeV, 0.77 GeV and 2.5 GeV

In Fig. 6.10 we depict the variation of R_Q with p_T for $\langle M\rangle = 0.3$ GeV (line with solid circle) 0.77 GeV (solid line) and 2.5 GeV (line with open circle). The quantity R_Q (R_H) is defined as

$$R_Q = v_2^{\rm QM}/(v_2^{\rm QM} + v_2^{\rm HM}) \quad \left(R_H = v_2^{\rm HM}/(v_2^{\rm QM} + v_2^{\rm HM})\right) \tag{6.8}$$

where $v_2^{\rm QM}$ and $v_2^{\rm HM}$ are the elliptic flow of QM and HM phases respectively. The results clearly illustrate that v_2 of lepton pairs in the large $\langle M\rangle(= 2.5$ GeV) domain (open circle in Fig. 6.10) originate from QM for the entire p_T range considered here. The value of R_Q is large in this domain because of the large (negligibly small) contributions from QM (HM) phase. $f_{\rm QM}$ is large here. It is also clear that the contribution from QM phase to the elliptic flow for $\langle M\rangle(= 0.77$ GeV) is very small (solid line in Fig. 6.10). The value of R_H for $\langle M\rangle = 0.77$ GeV is large (not shown in the figure). The v_2 at the (late) hadronic phase (either at ρ or ϕ peak) is larger than the (early) QGP phase (at $\langle M\rangle = 2.5$ GeV, say) for the entire p_T range considered here. Therefore, the p_T integrated values of v_2 should also retain this character of v_2 at the corresponding values of $\langle M \rangle$. It is also important to note that the differential elliptic flow, $v_2(p_T)$ obtained here at LHC is larger than the values obtained at RHIC [157, 158] for all the invariant mass windows. The value of R_H for $\langle M \rangle = 0.77$ GeV is large (not shown in the figure).

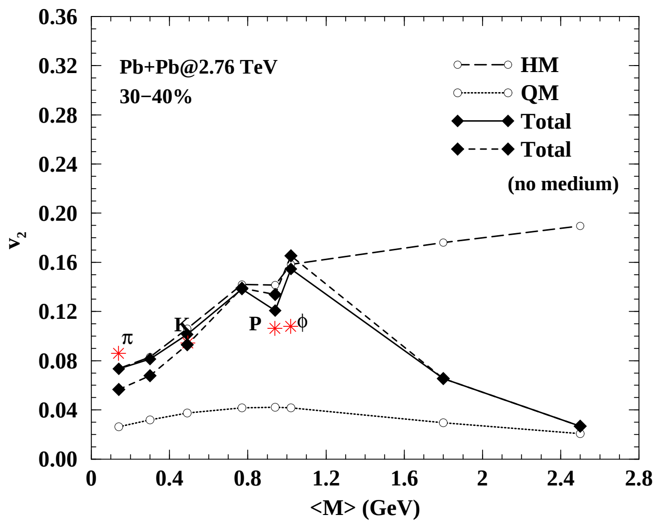

Figure 6.11: (Color online) Variation of dilepton elliptic flow as function of $\langle M \rangle$ for QM, HM (with and without medium effects) and for the entire evolution. The symbol $*$ indicates the value of v_2 for hadrons *e.g.* π, kaon, proton and ϕ.

The v_2 at the HM phase (either at ρ or ϕ peak) is larger than its value in the QGP phase (at $\langle M \rangle = 2.5$ GeV, say) for the entire p_T range considered here. Therefore, the p_T integrated values of v_2 should also retain this character at the corresponding values of $\langle M \rangle$, which is clearly observed in Fig. 6.11 which displays the variation of $v_2(\langle M \rangle)$ with $\langle M \rangle$. The v_2 ($\propto \epsilon_p$) of QM is small because of the small pressure gradient in the QGP phase. The v_2 resulting from hadronic phase has a peak around ρ pole indicating the full development of the flow in the HM phase. For $\langle M \rangle > m_\phi$ the v_2 obtained from the combined phases approach the value corresponding to the v_2 for QGP. Therefore, measurement of v_2 for large $\langle M \rangle$ will bring information of the QGP phase at the earliest time of the evolution. It is important to note that the p_T integrated $v_2(\langle M \rangle)$ of lepton pairs with $\langle M \rangle \sim m_\pi, m_K$ is close to the hadronic v_2^π and v_2^K (symbol $*$ in Fig. 6.11) if the thermal effects on ρ properties are included. Exclusion of medium effects give lower v_2 for lepton pairs compared to hadrons. The fact that the v_2 of the (penetrating) lepton pairs are similar in magnitude to the v_2 of hadrons for ($\langle M\rangle \sim m_\pi, m_K$, $m_{\rm proton}$ etc), it ascertains that the anisotropic momentum distribution of hadrons carry the information of the HM phase with duration $\sim 6-12$ fm/c (Fig. 6.2). We also observe that the variation of $v_2(\langle M\rangle)$ with $\langle M\rangle$ has a structure similar to dN/dM vs M. As indicated by Eq. 6.6 we can write $v_2(\langle M\rangle) \sim \sum_{i=QM,HM} v_2^{\rm i} \times f_{\rm i}$, where f_i is the fraction of QM or HM from various space-time regions. The structure of dN/dM is reflected in $v_2(\langle M\rangle)$ through f_i. We find that the magnitude of $v_2(\langle M\rangle)$ at LHC is larger than its value at RHIC [157, 158].

In conclusion, we have evaluated the v_2 of dileptons originating from the Pb+Pb collisions at $\sqrt{s_{NN}} = 2.76$ TeV for $30-40\%$ centrality. Our study shows that $v_2(M)$ provides useful information on the collective motion of the evolving QCD matter formed in high energy heavy-ion collisions. The present work indicates that experimental observation of the reduction of $v_2(M)$ with increasing M beyond ϕ mass would reflect the presence of small momentum space anisotropy through small collective motion in the partonic phase. We observe that $v_2(\langle M\rangle)$ of the penetrating probe (lepton pairs) for $\langle M\rangle = m_\pi$ and m_K is similar to the hadronic v_2^π and v_2^K when the medium induced change in the ρ spectral function is included in evaluating the dilepton spectra. Since the medium effects is large during the dense phase of the system, therefore, this validates the statement that the hadronic v_2 carry the information of the early dense phase of the collisions. Our study also establishes the fact that the invariant mass dependence of dilepton v_2 can in principle act as a clock for the space time evolution of the system formed in HIC.

Chapter 7

Summary and Discussion

The search of QGP has been the major driving force behind research activities in the field of heavy ion collision for the last three decades. The motivation of the present work is to study the signature of formation of quark gluon plasma and its properties. The hot and dense matter expected to be formed in the partonic phase after ultra-relativistic heavy ion collisions dynamically evolve in space and time due to high internal pressure. Consequently the system cools and reverts to hadronic matter from the partonic phase. Just after the formation, the entire energy of the system is thermal in nature and with progress of time some part of the thermal energy gets converted to the collective (flow) energy. In other words, during the expansion stage the total energy of the system is shared by the thermal as well as the collective degrees of freedom. The evolution of the collectivity within the system is sensitive to the Equation of State (EoS). Therefore, the study of the collectivity in the system will be useful to shed light on the EoS and on the nature of the transition that may take place during the evolution process.

It is well known that the average magnitude of radial flow at the freeze-out surface can be extracted from the transverse momentum (p_T) spectra of the hadrons. However, hadrons being strongly interacting objects can bring the information of the state of the system when it is too dilute to support collectivity *i.e.* the parameters of collectivity extracted from the hadronic spectra are limited to the evolution stage where the collectivity ceases to exist. These collective parameters have hardly any information about the interior of the matter. On the other hand electromagnetic (EM) probes, *i.e.* photons and dileptons are produced and emitted from each space time points. Therefore, estimating radial flow from the EM probes will shed light on the time evolution of the collectivity in the system.

The photon and dilepton spectra measured at SPS and RHIC energies by different experimental collaborations have been analyzed to understand the evaluation of collectivity in the system. The initial conditions of the evolving matter required to calculate the photon and dilepton spectra have been constrained to reproduce the measured multiplicity in these collisions. The EoS, the other crucial input to the calculations has been taken from lattice QCD calculations. The deviation of the hadronic phase from chemical equilibrium is taken in to account by introducing non-zero chemical potential for each hadronic species.

The invariant momentum distribution of photons produced from a thermal source depends on the temperature (T) of the source through the thermal phase space distributions of the participants of the reactions that produce photon. As a result the p_T spectra of photon reflects the temperature of the source. Hence ideally the photons with intermediate p_T values ($\sim 2-3$ GeV, depending on the value of initial temperature) reflect the properties of QGP (realized when $T > T_c$, T_c is the transition temperature). Therefore, one should look into the p_T spectra for these values of p_T for the detection of QGP. However, for an expanding system the situation is far more complex. The thermal phase space factor changes due to several factors *e.g.* the transverse kick received by low p_T photons due to flow originating from the low temperature hadronic phase (realized when $T < T_c$) populates the high p_T part of the spectra. As a consequence the intermediate or the high p_T part of the spectra contains contributions from both QGP and hadrons.

For dilepton the situation is, however, different because in this case we have two kinematic variables - out of these two, the p_T spectra is affected by the flow, however, the p_T integrated invariant mass (M) spectra is unaltered by the flow in the system. Moreover, for M below ρ peak and above ϕ peak dileptons from QGP dominates over its hadronic counterpart (assuming the contributions from hadronic cocktails are subtracted out and medium effects on the vector meson spectral function are ignored). The invariant mass spectra of lepton pairs may be used in principle to extract (i) the medium effects of the vector meson spectral function, (ii)contributions from the (early) QGP phase by selecting $M > M_\phi$ and (iii) from the (late) hadronic phase. This suggests that the dilepton spectra can be used as a clock for heavy ion collision. As mentioned before, the p_T spectra of the lepton pairs are affected by flow. Therefore the evolution of flow of the evolving QGP may be estimated by studying the transverse momentum spectra with appropriate selection of invariant mass window. Hence the lepton pairs can also be used as flow meter [107, 126, 127] for the system formed in relativistic heavy ion collision. In the present work, two procedures have been proposed to estimate the radial flow of the matter, i.e. (i) ratio of the p_T spectra of thermal photons to dileptons and (ii) HBT radii extracted from the dilepton correlation function.

The calculations of EM probes from thermal sources depend on the parameters like initial temperature (T_i), thermalization time (τ_i), chemical freeze-out temperature ($T_{\rm ch}$), kinetic freeze-out temperature (T_f) etc, which are not known unambiguously. To minimize the dependence of thermal sources on these parameters the importance of the ratio of the transverse momentum spectra of photon to dilepton has been considered in order to partially overcome the above mentioned uncertainties. It may be mentioned here that in the limit of $M \to 0$ the lepton pairs (virtual photons) emerge as real photons. Therefore, the evaluation of the ratio of the p_T spectra of photons to dileptons for various invariant mass bins along with a judicious choice of the p_T and M windows will be very useful to extract the properties of QGP as well as that of hadronic phase. This is demonstrated in the present work by analyzing WA98 and PHENIX photons and NA60 and PHENIX dilepton spectra. It is shown that simultaneous measurements of photon and dilepton spectra in heavy ion collisions will enable us to quantify the evolution of the average radial flow velocity for the system and the nature of the variation of radial flow with invariant mass will indicate the formation of partonic phase.

Experimental measurements of two-particle intensity interferometry has been established as a useful tool to characterize the space-time evolution of the heavy-ion reaction. For the case of dileptons, such an interferometry needs to be carried out over dilepton pairs, theoretically representing a study of the correlations between two virtual photons. Although, the dilepton production rate is down by a factor of α compared to real photon, the analysis involving lepton pairs has been successfully used to get direct photon yields at RHIC. In contrast to hadrons, two-particle intensity interferometry of dileptons, like photons, which have almost no interactions with the surrounding hadronic medium hence can provide information on the history of the evolution of the hot matter very efficiently.

In this work, we present a new proposal for carrying out an experimental measurement of dilepton interferometry both for RHIC and LHC. We establish through a hydrodynamical model based space-time evolution the promise of such a dilepton interferometry analysis will be useful to understand the properties of the partonic phase. We have evaluated the correlation function, C_2 for two dilepton pairs for various invariant mass domains and extracted the HBT radii, i.e. R_{side} and R_{out} as a function of M. These HBT radii show a non-monotonic dependence on the invariant mass, reflecting the evolution of collective flow in the system which can be considered as a signal of the QGP formation in heavy ion collisions. The M dependence of the R_{out}/R_{side} and $\sqrt{R_{out}^2 - R_{side}^2}$ which can be experimentally measured could be used to characterize the source properties at various instances of the evolution.

Elliptic flow is proposed as an useful tool to characterize Quark-Gluon Plasma. Comparison of measured v_2 calculated using relativistic hydrodynamic and transport approaches have lead to several important results. The most important of these is the small shear viscosity to entropy ratio of the QGP compared to other known fluids. The mass ordering of v_2 of identified hadrons, clustering of v_2 separately for baryons and mesons at intermediate p_T are considered as signatures of partonic coalescence as a mechanism of hadron production. In contrast to hadrons, which are predominantly emitted from the freeze-out surface of fireball, the electromagnetically interacting particles (real photons and lepton pairs) are considered as penetrating probes which can carry information from the hot interior of the system. Therefore, the analysis of v_2 of lepton pairs and photons can provide information of the pristine stage of the matter produced in HIC. The lepton pairs are produced from each space time point of the system and hence the study of v_2 of lepton pairs will shed light on the time evolution of collectivity in the system.

It has been argued that the anisotropic momentum distribution of the hadrons can bring the information on the interaction of the dense phase of the system despite the fact that the hadrons are emitted from the freeze-out surfaces when the system is too dilute to support collectivity. For hadrons, a suitable dynamical model is required to extrapolate the final hadronic spectra backward in time to get the information about the early dense phase. Such extrapolation is not required for lepton pairs because they are emitted from the entire space-time volume of the system. Therefore, the v_2 of lepton pairs provide information of the hot and dense phase directly. The v_2 can also be used to reassert the conclusion that hadronic v_2 can be used as a probe of early dense phase. It is well known that the p_T integrated M distribution of lepton pairs with $M\,(>\ m_\phi)$ originate from the early time, providing information of partonic phase and pairs with $M\ \leq\ m_\rho$ are chiefly produced at late times giving information of the hadronic phase. Therefore, the study of the p_T integrated M distribution of lepton pairs can act as a chronometer of the heavy ion collisions. On the other hand, the variation of v_2 with p_T for different M windows may be used as a flow meter.

We have evaluated the v_2 of dileptons originating from the Pb+Pb collisions at $\sqrt{s_{NN}} = 2.76$ TeV for $30-40\%$ centrality. Here, the (2+1) dimensional hydrodynamical model has been used for space-time dynamics. The dilepton emission rate used for the evaluation of v_2 of dilepton includes the medium effect on the spectral function of the vector mesons. However, the spectral function of low mass vector mesons (mainly ρ) may shift toward lower invariant mass region due to non-zero temperature and density effects. As a consequence the contributions from the decays of such vector mesons to lepton pairs could populate the low M $(< M_\rho)$ window and may dominate over the contributions from the QGP phase.

The differential elliptic flow, $v_2(p_T)$ has been evaluated for different invariant mass windows. We found an increasing trend of v_2 with p_T. Our study shows that $v_2(M)$ provides useful information on the collective motion of the evolving QCD matter formed in high energy heavy-ion collisions. Our calculation indicates that a reduction of $v_2(M)$ with increasing M beyond ϕ mass would reflect the presence of small momentum space anisotropy through modest collective motion in the QM phase. We observe that $v_2(\langle M\rangle)$ of the penetrating probe (lepton pairs) for $\langle M\rangle = m_\pi$ and m_K is similar to the hadronic v_2^π and v_2^K when the medium induced change in the ρ spectral function is included in evaluating the dilepton spectra. The medium effects are large during the dense phase of the hadronic system, therefore, this validates the findings that the hadronic v_2 carry the information of the dense part of the hadronic phase. Our study also establishes the fact that the invariant mass dependence of dilepton v_2 can in principle act as a clock for the space time evolution of the system formed in HIC.

Some comments on the initial conditions used in this work are in order here. For the results presented here, different initial conditions have been used. In the chapter-3, the main focus is to describe the available experimental data of p_T spectra of photon and dilepton at SPS and RHIC energies. So the initial conditions taken in this chapter are constrained to specific collision energy, centrality and final multiplicity. These set of initial conditions are also used in chaper-4, where the p_T spectra of photon and dilepton which reproduce the experimental data are used to evaluate the ratio (R_{em}) and quantify the radial flow. For the analysis of HBT radii (in chapter-5) we have used different set of initial condition for RHIC and LHC energies which is for most cental collision. Again, for the evaluation of v_2 of dilepton, the inital condition is taken for LHC energies for a peripheral collision (30-40 % centrality). Therefore, in summary, the initial conditions have been made to vary to suit different collision centralities and beam energies.

Bibliography

[1] Steven Weinberg, *The First Three Minutes: A Modern View of the Origin of the Universe*, Basic Books, 1977, [ISBN: 0-465-02437-8].

[2] E. W. Kolb and M. S. Turner, *The Early Universe*, Westview Press, 1990

[3] J. C. Collins and M. J. Perry, Phys. Rev. Lett. **34** (1975) 1353.

[4] G. Baym and S. A. Chin, Phys. Lett. B **62** (1976) 241.

[5] E. Witten, Phys. Rev. D **30** (1984) 272.

[6] D. J. Gross and F. Wilczek, Phys. Rev. Lett. **30** (1973) 1343; H. Politzer, Phys. Rev. Lett. **30** (1973) 1346;

[7] t"Hooft and M. Veltman, Nucl. Phys. B**44** (1972) 189 - 213 t' Hooft (1972) Unpublished, Nucl. Phys. B **254** (1985) 11

[8] G. Sterman *et. al.*, Rev. Mod. Phys. **67** (1995) 157-248.

[9] T. Muta, *Foundations of Quantum Chromodynamics: An Introduction to Perturbative Methods in Gauge Theorie*, World Scientific, Singapore, 1998.

[10] M. E. Peskin and D. V. Schroeder, *An Introduction to Quantum Field Theory*, Addison-Wesley Pub., 1995.

[11] C. N. Yang and R. L. Mills, Phys. Rev. **96** (1954) 191.

[12] R. K. Ellis, W. J. Stirling and B. R. Webber, *QCD and Collider Physics*, Cambridge University Press, 1996

[13] L. D. Faddeev and V. N. Popov, Phys. Lett. B25 (1967) 29

[14] K. Wilson, Phys. Rev. D **10** (1974) 2445

[15] S. Bethke, Nucl. Phys. Proc. Suppl. **121** (2003) 74.

[16] M. A. Stephanov, PoS **LAT2006** (2006) 024, [arXiv: hep-lat/0701002].

[17] B. Muller, *The Physics of Quark Gluon Plasma*, Springer, Heidelberg, 1985.

[18] R. C. Hwa and X. N. Wang (ed.), *Quark Gluon Plasma*, Vol. I II, World Scientific, Singapore, 1990, 1995.

[19] L. D. McLerran and B. Svetitsky, Phys. Lett B **98** (1981) 195.

[20] F. Karsch, Nucl. Phys. A **698** (2002) 199 [arXiv:hep-ph/0103314].

[21] S. Borsanyi *et al.* JHEP **1011** (2010) 077 arXiv: 1007.2580 [hep-lat]

[22] M. M. Aggarwal *et. al.* [STAR Collaboration], arXiv: hep-lat/0701002; S. Gupta, X. Luo, B. Mohanty, H. G. Ritter and Nu Xu, Science **332** (2011) 1525-1528.

[23] T. Sakaguchi [PHENIX Collaboration], PoS C **POD2009** (2009) 055 [arXiv:0908.3655 [hep-ex]].

[24] J. D. Bjorken, Phys. Rev. D **27** (1983) 140.

[25] A. Andronic, P. Braun-Munzinger , J. Stachel , Nucl. Phys. A **772** (2006) 167-199

[26] J. Y. Ollitrault Phys. Rev. D **46** (1992) 229245

[27] P. Huovinen,P. F. Kolb, U. W. Heinz, P. V. Ruuskanen, and S. A. Voloshin Phys. Lett. B **503** (2001) 58; T. Hirano and M. Gyulassy Nucl Phys. **A 769** (2006) 273

[28] P. F. Kolb, U. W. Heinz, P. Huovinen, K. J. Eskola and K. Tuominen, Nucl. Phys. A **696**, 197 (2001); P. F. Kolb, J. Sollfrank, P. V. Ruuskanen and U. W. Heinz, Nucl. Phys. A **661**, 349 (1999); P. F. Kolb, J. Sollfrank and U. W. Heinz, Phys. Rev. C **62**, 054909 (2000); ibid., Phys. Lett. B **459**, 667 (1999).

[29] J. Adams *et al.* [STAR Collaboration], Phys. Rev. Lett. **92** (2004) 052302; ibid. Phys. Rev. C **72** (2005) 14904.

[30] V. Roy and A. K. Choudhuri, Phys. Lett. B**703** (2011) 313-317, arXiv:1103.2870 [nucl-th]

[31] U. A. Widemann and U. Heinz, Phys. Rept. **319** (1999) 145.

[32] U. Heinz and B. V. Jacak, Annu. Rev. Nucl. Part. Sci. **49** (1999) 52979.

[33] R. Hanbury Brown and R. Q. Twiss, Nature **178** (1956) 1046.

[34] G. Goldhaber,S. Goldhaber, W. Lee and A. Pais, Phys. Rev. Lett., **3** (1959) 181; ibid., Phys. Rev. **120** (1960) 300

[35] F. Abe *et al.* , Phys. Rev. D **48** (1993) 998 [CDF Collaboration].

[36] M. Gyulassy, P. Levai and I. Vitev, Nucl. Phys. B **571** (2000) 197; ibid., Phys. Rev. Lett. **85** (2000) 5535.

[37] H. Zhang, J. F. Owens, E. Wang and X. N. Wang, Phys. Rev. Lett. **98** (2007) 212301 [arXiv:nucl-th/0701045].

[38] I. Arsene *et al.* (BRAHMS Collaboration), Nucl. Phys. A **757** (2005) 1; B. B. Back *et al.* (PHOBOS Collaboration), Nucl. Phys. A **757** (2005) 28; J. Adams *et al.* (STAR Collaboration), Nucl. Phys. A **757** (2005) 102; K. Adcox *et al.* (PHENIX Collaboration), Nucl. Phys. A **757** (2005) 184.

[39] L. D. McLerran and T. Toimela, Phys. Rev. D **31** (1985) 545.

[40] C. Gale and J. Kapusta, Phys. Rev. **C35**, (1987) 2107.; Nucl. Phys. B **357** (1991) 65.

[41] H. A. Weldon, Phys. Rev. D **42** (1990) 2384.

[42] R. Rapp and J. Wambach, Adv. Nucl. Phys. **25** (2000) 1.

[43] R. Rapp, J. Wambach and H. van Hees, arXiv:0901.3289 [hep-ph].

[44] J. Alam, S. Raha and B. Sinha, Phys. Rep. **273** (1996) 243.

[45] J. Alam, S. Sarkar, P. Roy, T. Hatsuda and B. Sinha, Ann. Phys. **286** (2001) 159.

[46] S. Turbide, R. Rapp and C. Gale, Phys. ReV. C **69** (2004) 014903.

[47] T. Matsui and H. Satz, Phys. Lett. **B 178** (1986) 416

[48] M. Asakawa and T. Hatsuda, Phys. Rev. Lett. **92** (2004) 012001

[49] R. Rapp, D. Blaschke and P. Crochet Prog. Part. Nucl. Phys. **65** (2010) 209;

P. Braun-Munzinger and J. Stachel, arXiV: Nuclth/0901.2500; L. Kluberg and H. Satz ,arXiV: Nuclth/0901.3831.

[50] J. Rafelski, B. Müller, Phys. Rev. Lett. **48** (1982) 1066 ; J. Rafelski, Nucl. Phys. **A 418**,(1984) 215.

[51] Giorgio Torrier, J. Phys. G: Nucl. Part. Phys. **36** (2009) 064007

[52] T D Lee, Rev. Mod. Phys. **47** (1975) 267

[53] C. Y. Wong, *Introduction of High Energy Heavy Ion Collisions*, World Scientific, Singapore, 1994.

[54] L.. D. Landau, and E. M. Lifshitz, *Fluid Mechanics*, Addison-Wesley, Reading, Mass., 1959.

[55] T. Hirano, N. van der Kolk and A. Bilandzic, Lect. Notes Phys. **785** (2010) 139 [arXiv:0808.2684 [nucl-th]].

[56] J. Y. Ollitrault, Eur. J. Phys. **29** (2008) 275 [arXiv:0708.2433 [nucl-th]].

[57] S. Weinberg, The Astronomical Journal **168** (1971) 175-194.

[58] H. Von Gersdorff, L. D. McLerran, M. Kataja and P. V. Ruuskanen, Phys. Rev. D **34** (1986) 794.

[59] R. C. Hwa and K. Kajantie, Phys. Rev. D **32** (1985) 1109.

[60] D. Kharzeev and M. Nardi, Phys. Lett. **B 507** (2001) 121.

[61] E. Cooper and G. Frye, Phys. Rev. D **10** (1974) 186.

[62] J. Solfrank, P. Koch and U. Heinz, Phys. Lett. B **252**(1990) 256; Z. Phys. C **52** (1991) 593

[63] H. van Hees and R. Rapp, Nucl. Phys. A **806**, 339 (2008) [arXiv:0711.3444 [hep-ph]].

[64] R. Rapp, Acta Phys. Polon. B **42** (2011) 2823

[65] R. Chatterjee, L. Bhattacharya and D. K. Shrivastava, Lect. Notes Phys. **785** (2010) 219

[66] J. Kapusta, P. Lichard, and D. Seibert, Phys. Rev. D **44**(1991)2774 ; ibid. Phys. Rev. D **47** (1993) 4171 [Erratum].

[67] L. E. Gordon and W. Vogelsang, Phys. Rev. D **50** (1994) , 1901 .

[68] R.D. Field, *Application of Perturbative QCD*, Addison-Wesley Pub. Company, N.Y. 1989.

[69] S. D. Drell and T. M. Yan, Phys. Rev. Lett. **25** (1970) 316; [Erratum-ibid. **25** (1970) 902]; ibid., Annals Phys. **66** (1971) 578; ibid., Annals Phys. **281** (2000) 450.

[70] R. Bair, H. Nakkagawa, A. Niegawa, and K. Redlich, Z. Phys. C **53**, 433(1992).

[71] E. Braaten and R. D. Pisarski, Nucl. Phys. B **337** (1990) 569; ibid **339** (1990) 310.

[72] P. Aurenche, F. Gelis, R. Kobes, and H. Zaraket, Phys. Rev. D **58** (1998) 085003.

[73] S. Sarkar, J. Alam, P. Roy , A. K. Dutt-Mazumder, B. Dutta-Roy, B. Sinha, Nucl. Phys. A **634** (1998) 206.

[74] P. Roy, S. Sarkar, J. Alam and B. Sinha, Nucl. Phys. A **653** (1999) 277.

[75] J. Alam, P. Roy and S. Sarkar, Phys. Rev. C **71** (2005) 059802.

[76] K. L. Haglin, J. Phys. G **30** L27 (2004).

[77] T. Altherr and P. V. Ruuskanen, Nucl. Phys. B **380** (1992) 377.

[78] M. H. Thoma and C. T. Traxler, Phys. ReV. D **56** (1997) 198.

[79] J. Cleymans, J. Fingberg and K. Redlich, Phys. Rev. D **35** (1987) 2153; K. Dusling and I. Zahed, Phys. Rev. C **80**, 014902 (2009).

[80] E. V. Shuryak, Rev. Mod. Phys. **65** (1993) 1.

[81] S.Ghosh, S. Mallik and S. Sarkar, Eur. Phys. J. C **70** (2010) 251; S.Ghosh, S. Sarkar and J. Alam, Eur. Phys. J. C **71**, 176 (2011).

[82] G.E. Brown and M. Rho, Phys. Rep. **269** (1996) 333.

[83] M.M. Aggarwal *et al.* (WA98 Collaboration), Phys. Rev. Lett. **85** (2000) 3595.

[84] S. S. Adler *et al.*, Phys. Rev. C **76**, (2007) 034904.

[85] A. Adare *et al.* (PHENIX collaboration), Phys. Rev. Lett. **104** (2010) 132301

[86] S. Bathe, [PHENIX Collaboration], Eur. Phys. J. C **49**, 225 (2007).

[87] T. Dahms *et al.*, Eur. Phys. J. **C49** (2007) 249.

[88] J. Alam, D. K. Srivastava, B. Sinha and D. N. Basu, Phys. Rev. D **48** (1993) 1117.

[89] J. Ruppert, C. Gale, T. Renk, P. Lichard and J. I. Kapusta, Phys. Rev. Lett. **100**, 162301 (2008).

[90] R. S. Hayano and T. Hatsuda, Rev. Mod. Phys. **82** (2010) 2949

[91] S. Afanasiev *et al.*, [PHENIX Collaboration], arXiv:0706.3034 [nucl-ex].

[92] A. Toia [PHENIX Collaboration], Nucl. Phys. **A774** (2006) 743; *ibid.*, Eur. Phys. J. **C49** (2007) 243 (2007).

[93] S. Gavin, P. L. McGaughey, P. V. Ruuskanen and R. Vogt, Phys. Rev. C **54** (1996) 2606 [arXiv:hep-ph/9604369].

[94] H. van Hess and R. Rapp, J. Phys. G **35** (2008) 054001 .

[95] R. Rapp, Nucl. Phys. A **661**, 33 (1999) [hep-ph/9907342]; R. Rapp and J. Wambach, Eur. Phys. J. A **6**, 415 (1999) [hep-ph/9907502].

[96] E. L. Feinberg, Nuovo Cim. **34 A** (1976) 39.

[97] M. Le Bellac, *Thermal Field Theory*, Cambridge University Press, 1996.

[98] A. Das, *Finite Temperature Field Theory*, World Scientific, Singapore, 1997.

[99] R. Kobes and G. Semenoff, Nucl Phys. **B260** (1985) 714; **B272**, (1986) 329.

[100] F. Gelis, Nucl. Phys. **B508**, (1997) 483.

[101] P. Arnold, G.D. Moore, and L.G. Yaffe, J. High Energy Phys. **0111** (2001) 057; ibid. **0112** (2001) 009; ibid. **0206** (2002) 030.

[102] O. Kaczmarek and F. Zantow, Phys. Rev D **71** (2005) 114510.

[103] J. J. Sakurai, *Currents and Mesons*, The University of Chicago Press, Chicago, 1969.

[104] R. K. Bhaduri, *Models of Nucleon - From Quarks to Soliton*, Addison-Wesley Pub., 1988.

[105] C. Bernard *et al.*, Phys. Rev. D **75** (2007) 094505.

[106] T. Hirano and K. Tsuda, Phys. Rev. C **66** (2002) 054905.

[107] P. Mohanty, J. K. Nayak, J. Alam and S. K. Das, Phys. Rev. C **82** (2010) 034901.

[108] D. L. Adams *et al.*, (E704 Collaboration), Phys. Lett. B **345** (1995) 569.

[109] T. Renk, J. Phys. G **30** (2004) 1495; ibid., Phys. Rev. C **71** (2005) 064905 ;

[110] J. Alam, S. Sarkar, T. Hatsuda, T. K. Nayak and B. Sinha, Phys. Rev. C **63** (2001) 021901 (R); J. Alam, P. Roy, S. Sarkar and B. Sinha, Phys. Rev. C **67** (2003) 054901.

[111] D. K. Srivastava and B. Sinha, Phys. Rev. C **64**, (2001) 034902.

[112] P. Huovinen, P. V. Ruuskanen and S. S. Rasanen, Phys. Lett. B **535** (2002) 109.

[113] K. Gallmeister, B. Kämpfer and O. P. Pavelenko, Phys. Rev. C **62** (2000) 057901.

[114] F. D. Steffen and M. H. Thoma, Phys. Lett. B **510**, 98 (2001).

[115] R. Chatterjee, D. K. Srivastava and S. Jeon, Phys. Rev. C **79**, 034906 (2009).

[116] S. S. Adler *et al.* (PHENIX collaboration), Phys. Rev. Lett. **91** (2003) 072301.

[117] F. M. Liu, T. Hirano, K. Werner and Y. Zhu, Phys. Rev. C **79** (2009) 014905.

[118] I. Tserruya, Nucl. Phys. A590 (1995) 127c

[119] H. van Hees and R. Rapp, Phys. Rev. Lett. **97**, 102301 (2006) [hep-ph/0603084].

[120] P. Lichard and J. Jura, hep-ph/0601234.

[121] R. Arnaldi *et al.* [NA60 Collaboration], Phys. Rev. Lett. **96**, 162302 (2006); ibid., Phys. Rev. Lett. **100**, 022302 (2008).

[122] R. Rapp, G. Chanfray and J. Wambach, Nucl. Phys. A **617**, 472 (1997) [hep-ph/9702210].

[123] J. K. Nayak, J. Alam, T. Hirano, S. Sarkar and B. Sinha, arXiv:0902.0446 [nucl-th].

[124] A. Toia [PHENIX Collaboration], J. Phys. G **35** (2008) 104037, A. Adare *et al.* [PHENIX Collaboration] ,Phys. Rev. C **81**, 034911 (2010).

[125] P. Mohanty et. al., Phys. Rev. C **85** (2012) 031903 (R).

[126] P. Mohanty, J. Alam and B. Mohanty, Phys. Rev. C **84**, (2011) 024903; P. Mohanty, J. Alam and B. Mohanty, Nucl. Phys. A **862** (2011) 301-303. Payal Mohanty, Jan-e Alam, PoS**(WPCF2011)040**, (2012), arXiV : 1202.2189[Nucl-th].

[127] J. K. Nayak and J. Alam, Phys. Rev. C **80** (2009) 064906.

[128] E. Schnedermann, J. Sollfrank and U. Heinz, Phys. Rev. C **48** (1993) 2462.

[129] C. M. Hung and E. Shuryak, Phys. Rev. C **57** (1998) 1891.

[130] P. Huovinen and P. V. Ruuskanen, Ann. Rev. Nucl. Part. Sci. **56** (2006) 163.

[131] D. A. Teaney, arXiv:0905.2433 [nucl-th]. D. Teany, J. Lauret and E. V. Shuryak Nucl-th/0110037

[132] T. Csorgo and B. Lorstad, Phys. Rev. C **54**, 1390 (1996)

[133] J. Cleymans and K. Redlich, Phys. Rev. C **60** (1999) 054908

[134] J. Solfrank, P. Huovinen, M. Kataja, P. V. Ruuskanen, M. Prakash and R. Venugopalan, Phys. Rev. **C 55** (1997) 392

[135] J. Adams *et al.* [STAR Collaboration], Phys. Rev. Lett. **92** (2004) 112301

[136] J. K. Nayak, J. -eAlam, S. Sarkar and B. Sinha, J. Phys. G **35** (2008) 104161

[137] B. Sinha, Phys. Lett. B **128** (1983) 91.

[138] J. K. Nayak, J. Alam, S. Sarkar and B. Sinha, Phys. Rev. C **78** (2008) 034903.

[139] R. Chatterjee, E. S. Frodermann, U. W. Heinz and D. K. Srivastava, Phys. Rev. Lett. **96** (2006) 202302.

[140] D. H. Boal, C. K. Gelbke and B. K. Jenninig, Rev. Mod. Phys. **62** (1990) 553

[141] G. Baym, Acta Phys. Polon. B**29** (1998) 1839

[142] G. Alexander, Rept. Prog., Phys.**66** (2003) 481-522

[143] S. Chappman, P. Scotto and U. Heinz, Phys. Rev. Lett. **74**, 4400 (1995).

[144] G. Bertsch and G. E. Brown Phys. Rev. C **40** (1989) 1830

[145] S. Pratt, Phys. Rev. Lett. **53** (1984) 1219; ibid., Phys. Rev. **D 33** (1986) 1314.

[146] U. Heinz and B. V. Jacak, Ann. Rev. Nucl. Part. Sci. **49**, 529 (1999);

T. Csörgo and B. Lörstad, Phys. Rev. C **54**, 1390 (1996);

B. R. Schlei and N. Xu, Phys. Rev. C **54** (1996) R2155 .

[147] D. H. Rischke and M. Gyulassy, Nucl. Phys. A **608** (1996) 479 .

[148] M. Herrmann and G. F. Bertsch, Phys. Rev. C **51** (1995) 328.

[149] D. Peressounko, Phys. Rev. C **67** (2003) 014905

[150] Y. M. Sinyukov, Nucl. Phys. A **498** (1989) 151

J. Alam *et al.*, Phys. Rev. C **67** (2003) 054902;

S. A. Bass *et al.*, Phys. Rev. Lett. **93** (2004) 162301.

[151] B. Bonner *et al.*, Nucl. Inst. and Meth. in Physics Research A **508** (2003) 181.

[152] A. Kozlov *et al.*, Nucl. Inst. and Meth. in Physics Research A **523** (2004) 345.

[153] A. Adare *et al.*, Phys. Rev. Lett. **98** (2007) 172301.

[154] B. Abelev *et al.* [The ALICE Collaboration] Phys. Rev. Lett. **105**(2010) 252301 .

[155] R. Averbeck [PHENIX Collaboration], J. Phys. G **35** (2008) 104115. R. A. Lacey *et al.*, Phys. Rev. Lett. **98** (2007) 092301 L. P. Csernai, J. I. Kapusta and L. D. McLerran, Phys. Rev. Lett. **97** (2006) 152303

[156] H. van Hees, C. Gale and R. Rapp, Phys. Rev. C **84**, 054906 (2011) [arXiv:1108.2131 [hep-ph]].

[157] R. Chatterjee, D. K. Srivastava, U. W. Heinz and C. Gale, Phys. Rev. C **75**, 054909 (2007) R. Chatterjee, D. K. Srivastava, U. W. Heinz and C. Gale, Phys. Rev. C **75**, 054909 (2007)

[158] J. Deng, Q. Wang, N. Xu and P. Zhuang Phys.Lett. B **701**, 581 (2011)

[159] T. Renk and J. Ruppert, Phys. Rev. C **77**, 024907 (2008).

[160] V. L. Eletsky, M. Belkacem, P. J. Ellis and J. I. Kapusta, Phys. Rev. C **64** (2001) 035202

[161] R. A. Schneider and W. Weise, Phys. Lett. B **515**, 89 (2001)

[162] H. van Hess and R. Rapp, J. Phys. G **35**, 054001 (2008).

[163] B. Mohanty and J. Alam, Phys. Rev. C **68**, 064903 (2003).

[164] K. Aamodt *et al.* [ALICE Collaboration], Phys. Rev. Lett. **106**, 032301 (2011); Phys. Lett. **B 696**, 30 (2011); arXiv:1011.3914 [nucl-ex]